Carbon diffusion behavior in bulk zirconium and zirconia of the used fuel claddings by multi-scale simulations

Yu Xu

NNT : 2015SACLS199

THESE DE DOCTORAT
DE
L'UNIVERSITE PARIS-SACLAY
PREPAREE A
L'UNIVERSITE PARIS-SUD

ÉCOLE DOCTORALE 576
Particules, Hadrons, Énergie, Noyau, Instrumentation, Imagerie, Cosmos et Simulation (PHENIICS)

Spécialité de doctorat : Aval du cycle nucléaire, radioprotection et radiochimie

Par

Mme Yu XU

Etude de la diffusion du carbone dans le zirconium et la zircone en volume des gaines de combustible usées par simulations multi-échelles

Thèse dirigée par Eric Simoni, présentée et soutenue à Orsay, le 10 décembre 2015 :

Composition du Jury :

M. Garrido Frederico	Professeur, Université Paris Sud	Président
Mme Dufaure Corinne	Professeur, Université Toulouse	Rapporteur
M. Legris Alexandre	Professeur, Université Lille	Rapporteur
M. Roques Jérôme	Maître de conférences, Université Paris Sud	Examinateur
M. Domain Christophe	Ingénieur de recherche, EDF R&D	Examinateur
Mme Pinard Nathalie	Maître de conférences, IPNL	Examinateur
Mme Cochin Florence	Manager R&D Déchets MAVL, AREVA NC	Invité

Etude de la diffusion du carbone dans le zirconium et la zircone en volume des gaines de combustible usées par simulations multi-échelles

Dans le cadre de la gestion des déchets nucléaires, les coques et embouts des gaines de combustibles sont coupés, compactés et empilés dans les colis CSD-C (Colis Standards de Déchets Compactés). Actuellement entreposés à la Hague, ces déchets seront stockés en milieu géologique profond dans des alvéoles en béton. Ces déchets MA-VL contiennent des RN d'intérêt dont le carbone-14 qui provient de l'activation neutronique de l'azote-14 et de l'oxygène-17 présents dans le Zircaloy oxydé. L'objectif de cette thèse, qui est menée en collaboration avec EDF et AREVA, est de répondre à la question du devenir et du comportement du carbone-14 dans ZrO_2 et Zr-métal. Cette thèse consistera à utiliser la simulation numérique, au moyen de la Théorie de la Fonctionnelle de la Densité (DFT), afin de modéliser le comportement du carbone-14 dans les CSD-C.

Les simulations sont effectuées avec une approche multi-échelles :

1) A l'échelle atomique, nous avons optimiséles modèles atomiques permettant dereprésenter la phase hexagonale de Zr et les différentes phases de ZrO_2. Par l'identification des différents sites d'insertion possibles pour l'atome de carbone, deux types de sites interstitiels possibles ont été caractérisés: le site Basal Tétragonal déformé noté, site BT_d, et le site Octahedrique, noté que site O. Le site BT_d est moins stable que le site O par 1,45 eV. Pour C dans la phase monoclinique, huit types de sites interstitiels possibles pour l'atome de carbone ont été caractérisés. Les énergies de formation pour l'atome de carbone en substitution à un atome d'oxygène ou de zirconium ont été calculées pour comparer les stabilités relatives de l'atome carbone. La modélisation des différents chemins d'énergie minimale, associés à la migration d'un atome de carbone d'un site à un autre, nous permettra d'obtenir la trajectoire du carbone par mécanismes interstitiels et lacunaires.

2) A l'échelle macroscopique, les simulations par l'approche Kinetic Monte-Carlo (KMC) dans ZrO_2 monoclinique pure et Zr pure ont été réalisées en utilisant les probabilités de saut. A partir des simulations KMC à des températures différentes, la trajectoire du carbone ainsi que le coefficient de diffusion (en fonction de la température) ont été

calculés. Il est constaté que l'énergie d'activation effective est 2.02 eV pour la diffusion du carbone dans zirconium, ce qui correspond au chemin de migration avec l'énergie la plus basse: site O →siteBT_d →siteBT_d (n fois)→site O →siteBT_d ... (par rapport au chemin site O →site O). Le coefficient de diffusion du carbone dans les cristaux de Zr pur, à la température de stockage (environ 50 °C) est calculé pour être très faible (~ 10^{-34} cm^2/s). Par conséquent, ces premières investigations montrent qu'il sera très difficile pour un atome de carbone de diffuser dans un cristal parfait de Zr dans les conditions de stockage. D'après les simulations macroscopiques Monte-Carlo cinétique pour l'atome carbone dans la zircone monoclinique, on a constaté qu'il est très difficile pour cet atome de diffuser par un mécanisme interstitiel (avec une énergie d'activation effective de 1,19 eV). Le coefficient de diffusion du carbone dans la phase Zr monoclinique, à la température de stockage (environ 50 °C) est calculée pour être très faible (~ 10^{-22} cm^2/s).A titre d'exemple, un atome de carbone présent au centre d'une couche d'oxyde de 50μm aura besoin de 10^{11} ans pour la quitter.

Carbon diffusion behavior in bulk zirconium and zirconia of the used fuel claddings by multi-scale simulations

General Introduction

Chapter 1:Methodologies

Chapter 2:Carbon diffusion in bulk zirconium

Chapter 3:Carbon Diffusion in the bulk monoclinic zirconia

Conclusion

General Introduction

Introduction

In a pressurized water reactor (PWR), the core contains fuel assemblies that are cooled by water circulated using powered pumps. PWRs contain between 150-200 fuel assemblies. In each fuel assembly, there are about 264 rods placed in a square array. For the 4 meter tall rod, the fuel consists of uranium dioxide and MOX (uranium and plutonium oxide) which are loaded in 272 pellets.

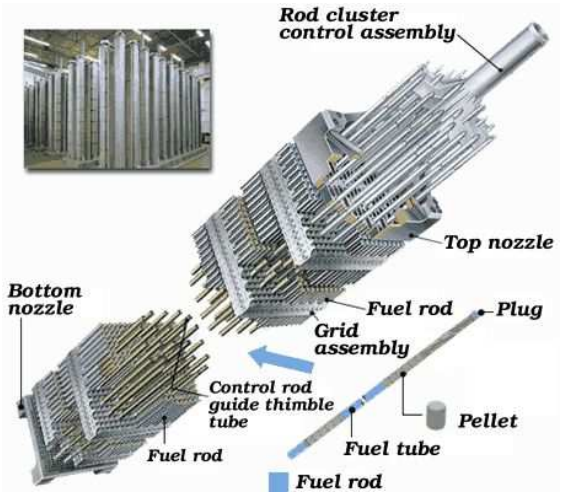

Figure 1: Schematic view of PWR fuel assembly (Mitsubishi Nuclear Fuel)

The fuel rods' claddings are made of zirconium alloys (such as zircaloy-4) which is principally zirconium. The composition of zircaloy-4 is controlled with the weight percent listed in Table 1. The zirconium has a hexagonal close packed structure (α – Zr) which is stable until 800 °C. The composition elements' characterization and their crystallographic structures in the zirconium matrix have been described in the case of Zy-4 [X. Y. Meng 1985].

Element	Content (wt %)
Zr	97.37-98.17
Sn	1.2-1.7
Fe	0.18-0.24
Cr	0.07-0.13
O	0.09-0.16
C	0.008-0.027

Table 1: Composition of zircaloy-4 in the fuel cladding (cladding of ASTM B353)

The formation of oxide layer and ^{14}C

Since there is water outside the claddings, the oxidation reaction with the zirconium forms an oxide layer which is zirconia (tetragonal and monoclinic phases).

$$Zr + 2H_2O \rightarrow ZrO_2 + 2H_2 \quad (1)$$

The oxide process of the zirconium claddings has been studied in several projects [P. Bouvier 2000, L. Gosmain 2001, C. Roy 1970, F. Garzarolli 1991, J. S. Moyal 2000, E. A. Garcia 1999]. The thickness of the oxide layer is function of time [L. Gosmain 2001]. For the 570 µm thickness cladding, the oxide layer is about 50 µm after 6 nuclear fuel cycles [Bossis et al., 2005] (Figure 2). At the storage temperature (max around 50° C), the stable zirconia structure is monoclinic zirconia which will be chosen in this work for later calculations [E. C. Subarao 1974, H. Boysen 1991].

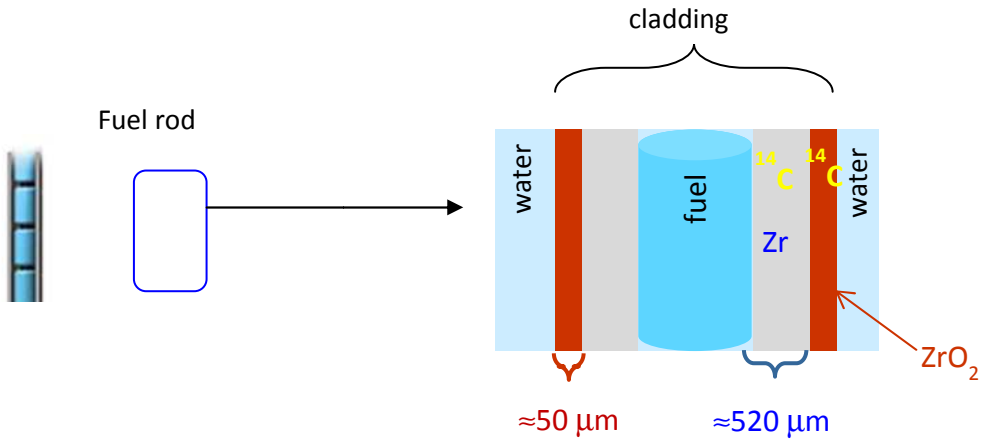

Figure 2: The zirconium layer and oxide layer (ZrO_2) of thefuel cladding

Both parts of the claddings contain numerous activation products such as ^{14}C. It comes from the neutron activation of the isotopic fraction of ^{17}O (1.83×10^{-2} curies/g) and ^{14}N (8.7×10^{-3} curies/g maximum) present in the claddings [D. Wallace, 1977].

$$^{14}_{7}N + ^{1}_{0}n \rightarrow ^{14}_{6}C + ^{1}_{1}p \quad (2)$$

$$^{17}_{8}O + ^{1}_{0}n \rightarrow ^{14}_{6}C + ^{4}_{2}He \quad (3)$$

This neutron irradiation during the reaction at high temperature causes the phase transition from tetragonal to monoclinic zirconia [M. C. Wittels 1956, M. C. Wittels 1959]. Moreover, it induces some defects in the zirconia which has been proved by simulation studies [D. Simeone 2000, D. Simeone 2002, C. G. Mougel 2000, and X. Iltis 1995]. In the oxide layer, the O vacancy concentration is controlled to be as low as possible by decrease the tin level [A. M. Garde 1994].

The process of nuclear waste treatment

In France, the spent nuclear assemblies are sent to AREVA La Hague to perform the nuclear waste treatment. After a cooling period, the claddings are sheared, and dipped in a dissolving bath which is mainly concentrated hot nitric acid to dissolve and extract the remaining fuel and fission products. Then the claddings are cut (Figure 3 panel a), put in case, dried and finally compacted by a 2500 ton force to obtain a pancake cylinder form (Figure 3 panel b), and introduced in containers (Figure 3 panel c) called such as the CSD-C (compacted standard waste containers).

(a) (b) (c)

Figure 3: The process of nuclear waste treatment (a) cut; (b) compacted; (c) introduced in container CSD-C

The CSD-C are intended to be stored in the cells of Intermediary Level Waste Long Lived (ILW-LL) deep storage. For this, four CSD-C are arranged in a concrete disposal packages with enhanced holding capacity (Figure 4).

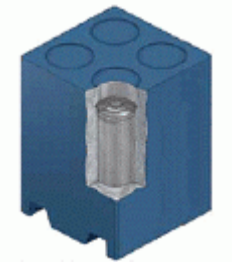

Figure 4: View of a concrete package to enhanced retention capacity storage of CSD-C containers

The containers are intended to be put in cement package and then in deep geological disposal chosen by the French national radioactive waste management agency (ANDRA).

The importance to study the carbon diffusion in the claddings

In order to demonstrate the safety and the CSD-C behavior in deep geological disposal, the behavior of all the radionuclides must be quantified.

The behavior of radionuclides (RN) contained in zirconia and zirconium is currently poorly characterized. Of penalizing manner, ANDRA takes no retention performance of these materials in its safety analysis. In the release model of ANDRA, 100% of the ^{14}C content in waste is considered to be released upon arrival in the storage cell (term major source during the reversibility period for releases - 100 years). Furthermore, it could end ^{14}C in organic form (CO_2 or CH_4) with the arrival of the water in the storage thereby promoting migration. In the absence of data, ANDRA considers the entirety of ^{14}C content in waste is released in organic form.

Some studies are required to improve the waste package storage behavior model from the main family ILW-LL generated by the activities of EDF and AREVA NC (CSD-C) and thus limit its impact on the long-term safe storage.

Regarding ^{14}C, experimental analysis of used cladding is complicated because of its activity. However, it is difficult to represent the used cladding conditions in laboratory. The introduction/implantation of carbon without generating non representative defects is difficult. Moreover, the measure of carbon diffusion as well as zirconia dissolution are not easy because of the slow kinetic of these processes. Consequently, simulations could provide some insights and allow to better quantify the carbon behavior in zirconium and zirconia.

The aim of this thesis is to characterize, by the mean of a multi-scale approach based on *ab initio* calculations and kinetic Monte Carlo method, the carbon diffusion behavior in bulk zirconium and zirconia to help the estimation of the waste safety of the fuel rods' claddings in the storage condition.

Manuscript organization

To study the carbon diffusion behavior in the used fuel claddings, supercells of Zr and ZrO_2 were first optimized to then perform the carbon diffusion in the two structures.

The first chapter presents the simulation methods used in this work: *ab initio* calculations in the framework of the Density Functional Theory (DFT) to determine formation energies of different defects and migration energies during atomic jumps, and the Kinetic Monte Carlo (KMC) method at the macroscopic scale to simulate diffusion coefficient as a function of temperatures in order to predict diffusion coefficients at storage temperature.

In the second chapter, the zirconium metal is considered, the properties of carbon in interstitial positions are investigated, and the carbon diffusion by interstitial mechanism is calculated with the multi-scale approach. The vacancy effect on the diffusion is predicted by using the binding energies.

The monoclinic zirconia of the oxide layer is studied in the third chapter. All the possible interstitial sites of carbon atoms are identified with their formation energies. The atomic jumps by interstitial mechanism are performed and the carbon diffusion coefficient is calculated with the KMC approach. Then, the vacancy effect on the diffusion is also considered. The carbon diffusion by vacancy mechanism and its competition with self-diffusion of oxygen atoms are studied. The density of states (DOS) calculations are performed to help a better understanding of the different defects and their effect on the carbon diffusion.

Finally, a general conclusion will give an overview of the carbon diffusion behavior in bulk of the two structures with and without vacancies by different mechanisms.

References

[P. Bossis 2005] P. Bossis, D. Pêcheur, K. Hanifi, et al., 14th International Symposium on Zirconium in the Nuclear Industry, ASTM STP 1467, 3, 494–525 (2005)

[P. Bouvier 2000] P. Bouvier, PHD thesis of INPG, France (2000)

[H. Boysen 1991] H. Boysen, F. Frey and T. Vogt, Acta Crystallography B, 47, 881 (1991)

[E. A. Garcia 1999] E. A. Garcia and G. Béranger, Journal of Nuclear Materials, 273, 221 (1999)

[A. M. Garde 1994] A. M. Garde, and E. R. Bradley, 10th International Symposium on Zirconium in the Nuclear Industry, ASTM STP, 1245, 760-778 (1994)

[F. Garzarolli 1991] F. Garzarolli, H. Seidel, R. Tricot, 9th International Symposium, Philadelphia, ASTMSPT, 1132, 395 (1991)

[L. Gosmain 2001] L. Gosmain, C. Valot, D. Ciosmak and O. Sicardy, Solid State Ionics, 141-142,633 (2001)

[X. Iltis 1995] X. Iltis, F. Lefebvre and C. Lemaignan, Journal of Nuclear Materials, 224, 109 (1995)

[X. Y. Meng 1985] X. Y. Meng and D. O. Northwood, Journal of Nuclear Materials, 132, 80 (1985)

[C. G. Mougel 2000] C. Gibert-Mougel, F. Couvreur, J. M. Costantini, S. Bouffard, F. Levesque, S. Hémon, E. Paumier and C. Dufour, Journal of Nuclear Materials, 295, 121 (2000)

[J. S. Moyal 2000] J. S. Moya1, M. Diaz, J. F. Bartolomm, E. Roman, J. L. Sacedon and J. Izquierdo, Acta Materialia, 48, 4749 (2000)

[C. Roy 1970] C. Roy, B. Burgess, Oxidation of Metals, 2, 235 (1970)

[D. Simeone 2000] D. Simeone, J. L. Bechade, D. Gosset, A. Chevarier, P. Daniel, H. Pilliaire and G. Baldinozzi, Journal of Nuclear Materials, 281, 171 (2000)

[D. Simeone 2002] D. Simeone, D. Gosset, J. L. Bechade and A. Chevarier, Journal of Nuclear Materials, 300, 27 (2002)

[E. C. Subarao 1974] E. C. Subarao, H. S. Maiti and K. K. Srivastava, Physica Status Solidi., 9, (1974)

[D. Wallace 1977] D. Wallace, "Carbon-14 Production in nuclear reactors", Oak Ridge National Laboratory report (1977)

[M. C. Wittels 1956] M. C. Wittels and F. A. Sherrill, Journal Applied Physics, 27, 643 (1956)

[M. C. Wittels 1959] M. C. Wittels and F. A. Sherrill, Physical Review Letter, 3, 1976 (1959)

Chapter 1

Methodologies

Introduction of quantum mechanics

Ab initio means "from the beginning" or "from first principles". *Ab initio* quantum chemistry distinguishes itself from other computational methods in that it is based solely on established laws of nature: quantum mechanics.

The theoretical foundation for computational chemistry is the time-independent Schrodinger wave equation.

I The Schrödinger equation and Born-Oppenheimer approximation

In quantum mechanics, Schrödinger equation formulated by Erwin Schrodinger (1887-1964) in 1926 [E. Nelson 1966, W. Kohn 1954, A. D. Mclachlan 1964] is used to calculate the system state. The ultimate goal of most approaches in solid state physics and quantum chemistry is the solution of the time-independent, non-relativistic Schrödinger equation although some progress has been made in dealing with fully relativistic Dirac equation. The energy can be expressed by this formula:

$$H\Psi = E\Psi \tag{1}$$

where:

- H is its Hamiltonian which is associated with the observable energy.
- Ψ is the wave function. It is a function of the positions of nuclides and electrons.
- E is the total energy of the system. It is a scalar.

The wave equation is a postulate of quantum mechanics. H contains all the terms that contribute to the energy of a system:

$$\hat{H} = \hat{T} + \hat{V} \tag{2}$$

For a solid made of nucleons with positive charges and electrons with negative charges, the energy of the system is given by:

$$H = \sum_{i=1}^{n} -\frac{\hbar^2 \nabla_i^2}{2m_i} - \sum_{A=1}^{N} \frac{\hbar^2 \nabla_A^2}{2m_A} + \sum_{\substack{A=1 \\ A<B}}^{N} \frac{Z_A Z_B e^2}{R_{AB}} + \sum_{\substack{i=1 \\ i<j}}^{n} \frac{e^2}{r_{ij}} - \sum_{i=1}^{n} \sum_{A=1}^{N} \frac{Z_A e^2}{R_{A_i}} \tag{3}$$

where:

- $\sum_{i=1}^{n} -\frac{\hbar^2 \nabla_i^2}{2m_e}$ is kinetic energy of electrons noted as $T_{e;}$
- $-\sum_{A=1}^{N} \frac{\hbar^2 \nabla_A^2}{2m_A}$ is kinetic energy of nucleons noted as $T_{N;}$
- $\sum_{\substack{A=1 \\ A<B}}^{N} \frac{Z_A Z_B e^2}{R_{AB}}$ is potential energy nucleon / nucleon noted as V_{NN};
- $\sum_{\substack{i=1 \\ i<j}}^{n} \frac{e^2}{r_{ij}}$ is potential energy nucleon / nucleon noted as V_{ee};
- $\sum_{i=1}^{n} \sum_{A=1}^{N} \frac{Z_A e^2}{R_{A_i}}$is potential energy nucleon / electron noted as V_{Ne}.

The *ab initio* calculation can solve the equation when it is time independent without knowing the values of specific parameters.

It is usual to invoke the so-called adiabatic or Born-Oppenheimer approximation [N. C. Handy 1986, O. L. Polyansky 1997, E. F. Valeev 2003]. Since the nucleon mass is much larger than the electron mass ($m_A >> m_i$, the ratio of the electron mass to the nuclei mass m_i/m_A is less than 10^{-5}), the electrons move much faster than the nuclei. Hence, the electrons can be thought as particles responding instantaneously to the motion of the nuclei without requiring a finite relaxation time. Alternatively, during the time of a cycle of electrons motion, the change in nuclear configuration is negligible. So, it can be assumed that the electrons are in the adiabatic equilibrium of their ground state with respect to the positions of nuclei at all the times. The approximation makes it possible to separate the wave function by nucleon wave function and electron wave function. Electrons adapt themselves thus almost immediately to the position of cores. After Born-Oppenheimer approximation, the total wave function is described as (4) and (5):

$$\Psi(r_i, R_A) = \Psi(r_i) * \Psi(R_A) \tag{4}$$

$$H_e \Psi(r_i) = E_e \Psi(r_i) \tag{5}$$

So it can be solved when the nuclear cores were thought to be fixed and the electrons moved around them. However, Eq 5 is still complicated to solve, even for simple atoms or molecules. So further simplifications are introduced to make the total energy calculations performed accurately and efficiently. These include the Hartree-Fock (HF) approximation or the density

functional theory (DFT) method to perform the electron-electron interactions and the pseudopotential theory to deal with the electron-ion interactions.

II The density functional theory (DFT)

Density functional theory (DFT) [BOOK E. K. U. Gross 1995, R. G. Parr 1983, M. Orio 2009, R. Car 1985] is a computational quantum mechanical modeling method used in physics, chemistry and materials science to investigate the electronic structure (the ground state) of many-body systems, in particular atoms, molecules, and the condensed phases. With this theory, the properties of a many-electron system can be determined by using functional spatially dependent electron density. The DFT simulation is presently one of the most successful approaches to compute the electronic structure of matter.

Its applicability ranges from atoms, molecules and solids. In its original formulation, the density functional theory provides the ground state properties of a system, and the electron density plays a key role.

III Kohn-Sham method

To simplify the Hamiltonian, there are different methods. One of them is proposed by Kohn and Sham in 1964 [W. Kohn 1965]. The electronic density ρ(r) can describe all the characters of the total energy. When the density is in its fundamental state $\rho(r) = \rho_0(r)$, the energy of the system is the smallest and corresponds to the fundamental state. The system receives the external potential energy from the nucleons, and the total energy of the electron clouds is calculated by Eq.6:

$$E[\rho] = T[\rho] + V_{ee}[\rho] + E_{xc}[\rho] + \int V_{ext}(r)\rho(r)d^3r \quad (6)$$

where:

- $T[\rho]$ is the kinetic energy of the electron gas without interaction;
- $V_{ee}[\rho]$ is the classical interaction coulomb electron-electron term;
- $E_{xc}[\rho]$ is the exchange and correlation term;
- $\int V_{ext}(r)\rho(r)d^3r$is the interaction of electrons with the external potential created by the nucleons.

IV Generalized Gradient Approximation (GGA)

As discussed above, the Kohn-Sham equation allows an exact treatment of most contributions to the electronic energy including the major fraction of the kinetic energy. So far, the DFT theory is exact. All the calculations were performed within the framework of the generalized gradient approximation (GGA) [J. P. Perdew 1992, J. P. Perdew 1996, Z. Wu 2006]. All remaining uncertainty about the universal functional are folded into the exchange-correlation functional $E_{xc}[\rho]$. By comparison with the Hartree-Fock effective Hamiltonians, this term must contain the exchange energy, correlation energy and the difference between the kinetic energies of non-interacting and interacting systems. To generate the exchange-correlation functional, approximations are necessary to be proposed. There are several methods to calculate the exchange and correlation term, such as LDA (Local Density Approximation) and GGA (Generalized Gradient Approximation). In our calculation, the GGA approximation was used.The first logical step to go beyond LDA is the use of not only the information about the density at a particular point ρ(r), but to supplement the density with information about the gradient of the charge density, $\nabla\rho(r)$, in order to account for the non-homogeneity of the true electron density. So the exchange correlation term becomes a function of ρ and $\Delta\rho$.

$$E_{xc}[\rho] = \int \varepsilon_{xc}(r)[(\rho(r) + \nabla\rho(r)]d^3r \qquad (7)$$

It provides a larger variation than LDA. In the later calculation, we use the functional PW-91 (exchange and correlation of Perdew and Wang) [J. P. Perdew 1992, J. P. Perdew 1996, K. Burke 1998]. GGA's approximations have reduced the LDA errors of atomization energies of standard set of small molecules by a factor 3-5. This improved accuracy has made DFT a significant component of quantum chemistry.

V Plane wave notions

According to Kohn-Sham method, the electronic density ρ(r) can describe all the characters of the total energy. To describe the electronic density, the Plane wave basis sets can be used. In the periodic simulation, a unit cell of atoms is used to model the system by replicating the cell in all dimensions, using periodic approach. When the system has the force convergence, its total energy is locally minimized.

Because the system is periodic, according to Bloch's theorem, the mono electronic wavefunction in a regular repeating lattice (periodic boundary conditions) can be given by:

$$\Psi_k(\vec{r}) = e^{i\vec{k}.\vec{T}} * u_{\vec{k}}(\vec{r}) \quad (8)$$

where:

- $\Psi_{\vec{k}}(\vec{r})$ is the electronic wave function at a point **R** by a direct vector;
- $\vec{k}$is a wave vector set of three quantum number (n_x, n_y, n_z);
- $e^{i\vec{k}.\vec{R}}$is the phase factor.
- $\vec{r}$ is the position.

For any lattice vector $\vec{R}$ of the simulation cell, there is

$$\Psi_k(\vec{r} + \vec{R}) = e^{i\vec{k}.\vec{R}} * \Psi_{\vec{k}}(\vec{r}) \quad (9)$$

where:

- $u_{\vec{k}}(\vec{r} + \vec{R})$=$u_{\vec{k}}(\vec{r})$

If$\vec{R}$ is a replication vector, the electronic wave function must have the same magnitude in the two places, but possibly offset by a plane wave phase factor $e^{i\vec{k}.\vec{R}}$. The quantum numbers are essentially continues in an infinite solid. But in practice, we use a cut-off energy to restrict the set to a sphere in reciprocal space. When $E_{cut\text{-}off}$ is too small, the wave function couldn't correctly describe the electronic density. But if $E_{cut\text{-}off}$ is too large, there would increase a lot of calculation time.

It should make an infinitive plane wave to produce the wave function exactly. In practice, it is not possible. The $E_{cut\text{-}off}$ limits the number of plane wave:

$$\frac{\hbar^2 | \vec{k}^2 + \vec{G}^2 |}{2m} < E_{cut-off} \quad (10)$$

where:

- m: mass of an electron;
- $\vec{k}$is a wave vector set of three quantum number (n_x, n_y, n_z);
- $\vec{G}$are the reciprocal lattice vectors defined by the condition $e^{i\vec{G}.\vec{R}}$ =1.

VI Pseudopotentials

A pseudopotential or effective potential is used as an approximation for the simplified description of real systems.

The projected augmented wave (PAW) method [P. E. Blochl 1994, G. Kresse 1999], as implanted in the Vienna *Ab initio* Simulation Package (VASP) is used here.

In this approximation, core electrons are replaced by a pseudopotential V_{pseudo} which is expressed by the wave function $\Psi_{pseudo.}$ The cut-off energy which corresponds to the different cut-off radius r is used to separate the valence electrons from the core electrons. The VASP calculation will be only applied on the valence electrons. First-principles pseudopotentials are derived from an atomic reference state, requiring that the pseudo and all-electron valence eigenstates have the same energies and amplitude (and thus density) outside a chosen core cut-off radius r_c. When r is increased to r_c, the plan wave is simplified by Ψ_{pseudo} to calculate the total energy of the atom.

The exact all electron wave function is $\Psi(r)$. Inside the radius r_c, the exact wavefunction is replaced by a suitable "soft" pseudo wave function $\Psi_{pseudo}(r)$ (Figure 1).

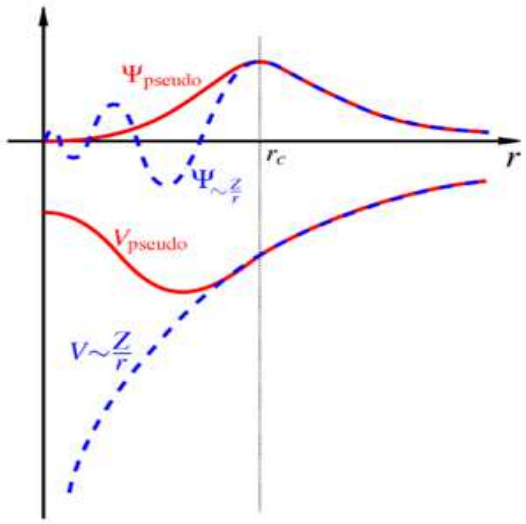

Figure 1: Pseudopotential of atoms

Many different basis sets have been proposed in the literature historically, and the two most prominent ones are:

– Polynomials (Troullier and Martins (Ref N. Troullier 1993))

– Spherical Bessel-functions (Rappe-Rabe-Kaxiras-Joannopoulos (RRKJ) method (Ref A. M. Rappe1990)

The last one is the standard scheme for VASP pseudopotentials, which is also called "optimized". It is standard norm-conserving pseudopotential method.

All the PAW pseudopotentials used in the calculations are chosen in the library developed with the code (Table 1).An extension _h implies that the potential is harder than the standard potential and hence requires a greater energy cutoff. The extension _s means that the potential is softer than the standard version. For each chosen pseudopotential, all the possible combination sets will be calculated and compared. The results and conclusions will be presented in the next chapter 2 and 3. The principle characterization of the pseudopotentials and all the possible sets were listed in the Table 1 and we used the good set for the GGA-PW91 calculations.

atoms	Valence electrons in VASP	Notations in the work
Zr	Zr_4 $d^2 5s^2$ Zr_ $4s^2 4p^6 4d^2 5s^2$	Zr_4 Zr_12
O	O_ $2s^2 2p^4$ O_ $2s^2 2p^4$	O_h O_s
C	C_ $2s^2 2p^2$ C_ $2s^2 2p^2$ C_ $2s^2 2p^2$	C_h C_s C

Table 1: The different pseudopotentials for atom Zr, O, and C from VASP library

VII Periodic DFT code (VASP)

The Vienna *Ab initio* SimulationPackage, VASP, is a code for performing static and dynamics DFT simulations by using a periodic approach. By this approach, the system is defined by a supercell replicated infinitely in the three directions. It is well adapted to the solids and surfaces since it can simulate infinite systems and resolve the board problem. The process to do the calculations is as follow:

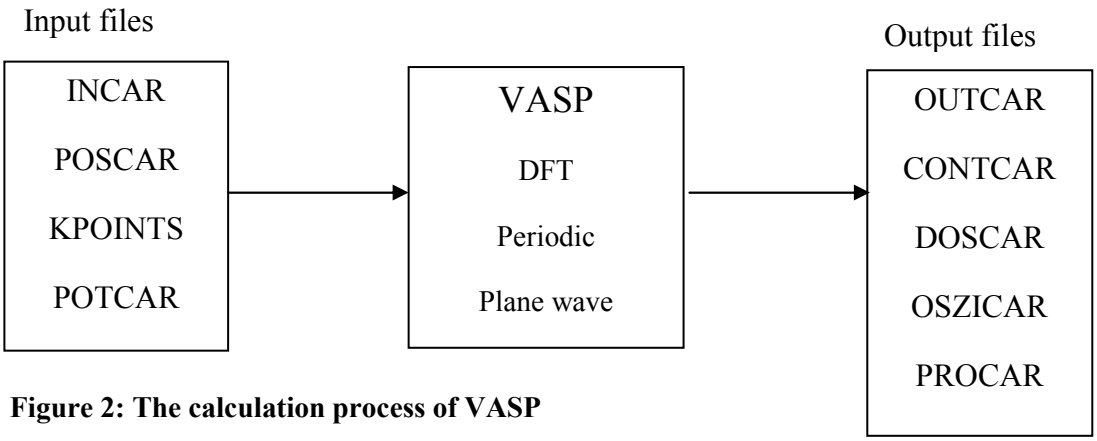

Figure 2: The calculation process of VASP

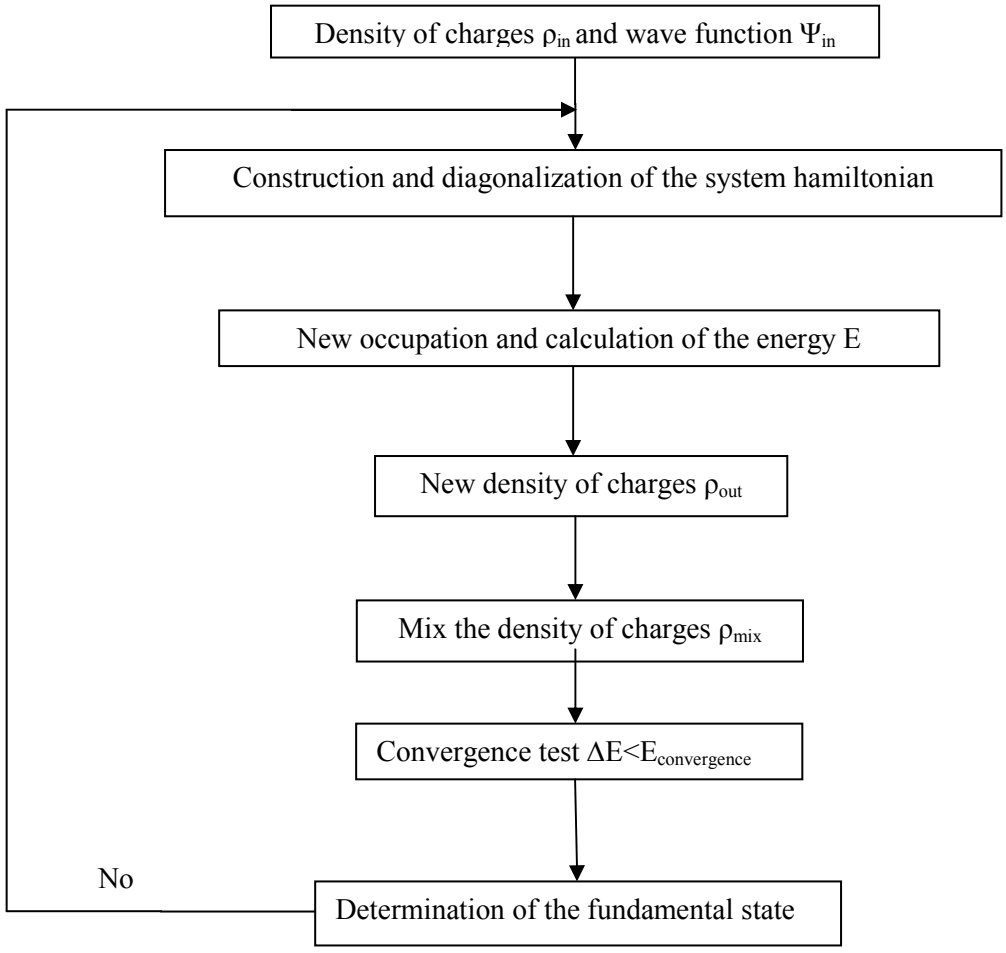

Figure 3: Principle of the VASP auto coherent cycle

Input files:

- INCAR: It includes various keywords for the VASP calculations, the cut-of energy, the convergence parameters, spin-polarization parameters, the smearing parameters, density of states parameters…
- POSCAR: This file contains the starting lattice geometry and ionic positions.
- POTCAR: List of pseudopotentials for each atom. The different parts for each element are in the same order as in the POSCAR file.
- KPOINTS: Number of k-points in the Brillouin zone.

Main analyzed output files:

- CONTCAR: It contains the lattice geometry and the ionic positions after optimization.
- OUTCAR: It records the information during the optimization…
- OSZICAR: It includes the total energy of the supercell, and the total magnetic moments (if ISPIN=2).
- DOSCAR: List of density of states for the atoms of the supercell.
- PROCAR: It contains the spd and site projected wave function character of each band.

VIII Brillouin zone integration

In the VASP calculation, it is important to optimize the number of k-point in the Brillouin zone. So here in this part, the integration in the Brillouin zone will be presented. In solid state physics, the first Brillouin zone is a uniquely defined primitive cell in reciprocal space (Figure 4). The boundaries of this cell are given by planes related to points on the reciprocal lattice. It is found by the same method as for the Wigner–Seitz cell in the Bravais lattice. The importance of the Brillouin zone stems from the Bloch wave description of waves in a periodic medium, in which it is found that the solutions can be completely characterized by their behavior in a single Brillouin zone. The first Brillouin zone is the local points in reciprocal space that are closer to the origin of the reciprocal lattice than they are to any other reciprocal lattice points (see the derivation of the Wigner-Seitz cell). Another definition is as the set of points in k-space that can be reached from the origin without crossing any Bragg plane.

There are also second, third, etc., Brillouin zones, corresponding to a sequence of disjoint regions (all with the same volume) at increasing distances from the origin, but these are used less frequently. As a result, the first Brillouin zone is often called simply the Brillouin zone. (In general, the n-th Brillouin zone consists of the set of points that can be reached from the origin by crossing exactly n − 1 distinct Bragg planes.)

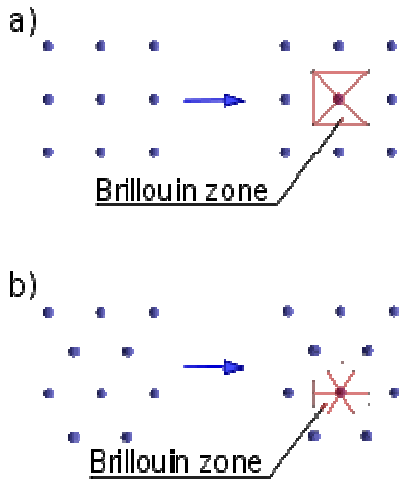

Figure 4: The reciprocal lattices (dots) and corresponding first Brillouin zones of (a) square lattice and (b) hexagonal lattice.

In order to define the Brillouin zone we need to define first the reciprocal lattice. The set of all wave vectors **k** that yield plane waves with the periodicity of a given Bravais lattice is known as its reciprocal lattice. Analytically, **k** belongs to the reciprocal lattice of a Bravais lattice of points **R**, provided that the relation Eq. 11 holds for any **r**, and all **R** in Bravais lattice.

$$e^{i\boldsymbol{k}(\boldsymbol{r}+\boldsymbol{R})} = e^{i\boldsymbol{k}\boldsymbol{r}} \tag{11}$$

Factoring out, we can characterize the reciprocal lattice as the set of wave vectors **k** satisfying Eq. 12for all **R** in the Bravais lattice.

$$e^{i\boldsymbol{k}\boldsymbol{R}} = 1 \tag{12}$$

The reciprocal lattice is itself a Bravais lattice and its primitive vectors can be generated from the vectors of the direct lattice. Let $\boldsymbol{a_1}, \boldsymbol{a_2}, \boldsymbol{a_3}$ be a set of primitive vectors, then the reciprocal lattice can be generated by the three primitive vectors:

$$\boldsymbol{b_1} = \boldsymbol{2\pi}\frac{\boldsymbol{a_2} \times \boldsymbol{a_3}}{\boldsymbol{a_1} \cdot (\boldsymbol{a_2} \times \boldsymbol{a_3})}$$

$$\boldsymbol{b_2} = \boldsymbol{2\pi}\frac{\boldsymbol{a_1} \times \boldsymbol{a_3}}{\boldsymbol{a_1} \cdot (\boldsymbol{a_2} \times \boldsymbol{a_3})}$$

$$\boldsymbol{b_3} = \boldsymbol{2\pi}\frac{\boldsymbol{a_1} \times \boldsymbol{a_2}}{\boldsymbol{a_1} \cdot (\boldsymbol{a_2} \times \boldsymbol{a_3})} \quad (13)$$

Using the relations between direct and reciprocal lattice, it can be shown that the reciprocal lattice of *sc* is *sc* (at **k** space), the reciprocal of *bcc* is *fcc*, and reciprocal of *fcc* is *bcc*.

The first Brillouin zone is defined to be the Wigner-Seitz primitive cell of the reciprocal lattice, or it could be defined as the set of points in **k** space that can be reached from the origin without crossing any Bragg plane. The second Brillouin zone is the set of points that can be reached from the first zone by crossing only one Bragg plane. The (n + 1) th Brillouin zone is the set of points not in the (n - 1) th zone that can be reached from the n th zone by crossing (n – 1) Bragg planes. Alternatively, the n th Brillouin zone can be defined as the set of points that can be reached from the origin by crossing (n – 1) Bragg planes, but no fewer.

IX Density of States (DOS)

The total concentration of available states in certain energy range is provided by an interval of energy, which is

$$dN = \rho_{energy}(E)dE \quad (14)$$

where:

- dN is the interval of electron density presents in the energy range dE;
- $\rho_{energy}(E)$is the density of states.

So the total concentration of available states in the system between energy E1and E2 can be represented as

$$N_{E2-E1} = \int_{E1}^{E2} \rho_{energy}(E)dE \quad (15)$$

Obtaining $\rho_{energy}(E)$ is accomplished through a density of states calculation. The resulting DOS is important since it can provide a better handle on the state distribution of the system.

Using N_{tot} as the total number of electrons, the Fermi level is defined by:

$$N_{tot} = \int_{-\infty}^{Ef} \rho_{energy}(E)dE \quad (16)$$

where:

- E_f is the Fermi energy.

For the VASP calculation, the DOS is integrated numerically in discrete intervals. Thus if localized states are presented (e.g. for vacancy in ZrO_2 or C in ZrO_2, cf Chapter III), they may be not presented in the direct DOS plot.

Nevertheless, the number of electron $N_e(E)$ as function of E (Eq.15) is integrated other all the Brillouin zones and all the states are included. So the integral DOS can be numerically derived from $N_e(E)$:

$$\rho_{derived} = \frac{dN_e(E)}{dE} \quad (17)$$

Different from the direct DOS plot, the derived integral DOS plot can present the localized states.

X Formation and binding energies of defects.

In the used fuel claddings, there are different point defects in the zirconium layer and oxide layer. So it is necessary to consider the effect of the point defects on the carbon diffusion. Here in this part, two point defects are presented with their formation energies and the interaction by binding energies.

A point defect is formed when an atom is missing from a position, creating a vacancy, or when an atom occupies an interstitial site where no atom would ordinarily appear, causing an interstitial site. The point defects are showed in Figure 5.

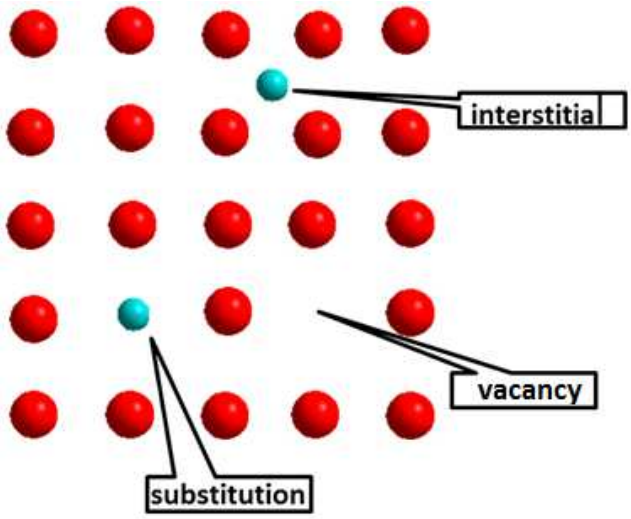

Figure 5: The different point defects in crystal

To understand the stabilities of the simple atom point defects, the formation energy of acarbon interstitial atom or a vacancy is calculated by Eq. 18 and Eq. 19:

$$E_I = E_{C-cell} - (E_C + E_{cell}) \tag{18}$$

where:

- E_{cell} is the total energy of a supercell;
- E_C is an atomic energy in a reference crystal (diamond structure);
- E_{C-cell} is the total energy of a supercell with a carbon atom in an interstitial position.

If the formation energy of an interstitial C atom, E_I is positive, it means E_{C-cell}>$E_C + E_{cell}$, the C atom is less stable in the interstitial position than in the reference crystal (diamond structure).

$$E_{vacancy} = E_{cell(with\ vacancy\ x)} + E_x - E_{cell} \tag{19}$$

where:

- $E_{cell(with\ vacancy\ x)}$ is the total energy of a supercell with a vacancy x in it;
- E_x is an atomic energy in a reference crystal;
- $E_{cell}$is the total energy of a supercell.

If the formation energy $E_{vacancy}$ of a vacancy x is positive, it means $E_{cell(with\ vacancy\ x)} + E_x > E_{cell}$, the atom x is more stable in the vacancy position than in the reference crystal.

When the inserted carbon is in a vacancy position, it is noted as substitution impurity. The formation energy is calculated as

$$E_{sub} = E_{C-cell(with\ substitution)} - [E_C + E_{cell(with\ vacancy)}] \quad (20)$$

where:

- $E_{C-cell(with\ substitution)}$ is the total energy of a supercell with C substitution ;
- E_C is an atomic energy in a reference crystal (diamond structure);
- $E_{cell(with\ vacancy\ x)}$ is the total energy of a supercell with a vacancy x in it.

If the formation energy E_{sub} of a vacancy x is positive, it means $E_{C-cell(with\ substitution)} > E_C + E_{cell(with\ vacancy)}$, the C atom is more stable in the reference crystal than in the vacancy position.

However, the formation energy E_{sub} is compared to E_I , if it is smaller than E_I , it can be said that for the C atom it is favorable to stay in the vacancy position than to be interstitial.

Sometimes there will be interstitial-vacancy interaction and substitution-vacancy interaction, at this time it better to use the binding energy to understand the interaction between the two point defects. The binding energy is calculated as below:

$$E_{binding} = (E_{C(int/sub)-cell} + E_{cell(with\ vacancy\ x)}) - (E_{C(int/sub)-cell(with\ vacancy\ x)} + E_{cell}) \quad (21)$$

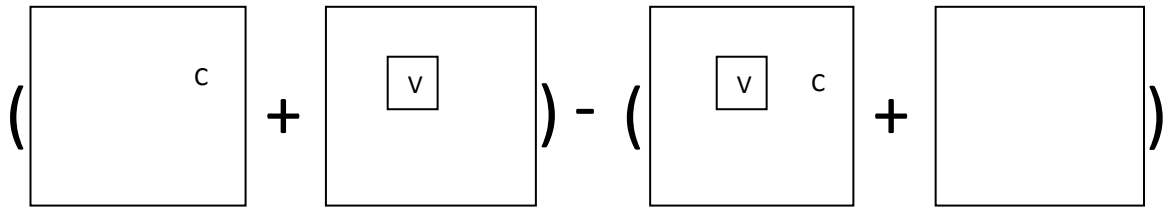

$E_{C(int/sub)-cell} E_{cell(with\ vacancy\ x)} E_{C(int/sub)-cell(with\ vacancy\ x)} E_{cell}$

Figure 6: Binding energy calculation

where:

- $E_{C(int/sub)-cell(with\ vacancy)}$ is the total energy of a supercell with a C atom (interstitial or substitution) and a vacancy x;
- $E_{C(int/sub)-cell}$ is the total energy of a supercell with a carbon atom in an interstitial position or vacancy position;
- $E_{cell(with\ vacancy\ x)}$ is the total energy of a supercell with a vacancy x;
- E_{cell} is the total energy of a pure supercell.

If $E_{binding}$ is positive, which means that $E_{C(int/sub)-cell} + E_{cell(with\ vacancy\ x)} > E_{cell} + E_{C(int/sub)-cell(with\ vacancy\ x)}$, the interaction between C atom and vacancy x is attractive, the C atom is more stable to be near vacancy than to be in the int/sub position far away from the vacancy. Other else, if the binding energy is negative, it means the interaction is repulsive, the C atom is more stable in the int/sub position.

XI Method to calculate the migration energy (NEB) and attempt frequency.

To study the carbon diffusion at atomic scale, it is necessary to characterize all the atomic jumps. For one carbon position, all the possible neighbor sites should be identified with reasonable distance and by using the Transition State Theory (TST) [E. P. Wigner 1937, H. Eyring 1935]. Once the potential landscape has been obtained for each path between neighbor sites, we can compute the transition rate between the initial and final sites (Γ_{if}) along this path. It is a statistical method based on Boltzmann's distribution in phase space which leads to the migration rates through the energy barriers and attempt frequencies.

Diffusion by vacancy or interstitial mechanisms: the jump probability for diffusion is given by:

$$\Gamma = \nu_{if} exp\ (-\frac{E_{mig}}{k_B T}) \tag{22}$$

where:

- ν_{if} is the attempt frequency from the initial site to final site;
- E_{mig} is the migration energy;
- k_B is the constant Boltzmann;

- $T$is the simulation temperature.

ν_{if}andE_{mig} depend on the local environment of the migrating atom. Thus these 2 quantities have to be determined for all the distinct atomic jumps.

E_{mig} is calculated thanks to the NEB method and ν_{if} is calculated by the vibration frequencies of carbon atom at stable site and transition state.

XI.1 Migration energy calculation (NEB)

Using the precedent methodologies, the studied model can be constructed and optimized to find its stable state. To study the behavior of an element (C in our project), first, the possible interstitial sites will be investigated to study its atomic migrations. Then, by using Nudged Elastic Band (NEB) method (Ref H. Jonsson 1998), the Minimum Energy Path (MEP) between these sites will be determined (Figure 7).

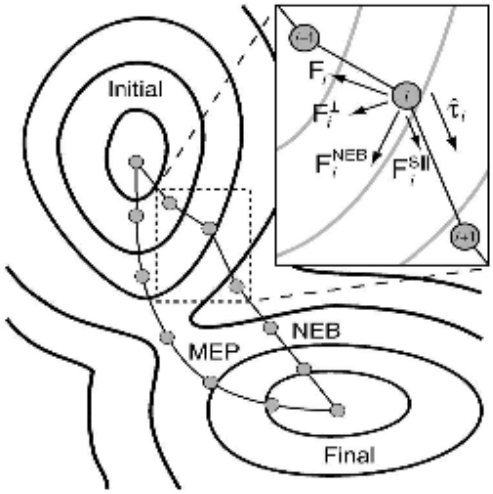

Figure 7: Principle of NEB method [D. Sheppard 2008]

To use the NEB method, the initial state and final state should be stable. So firstly, the initial site and final site are optimized by VASP, and their equilibrium stable positions are used as the limit states. Then, several "images" are built between these two states. These images are specific C positions, "guessed" by locating the diffusing atom in a "thought to be reasonable" diffusion way. After that, each image finds its ionic position which has the lowest energy (or force, depends on the command used), while the images maintain equal spacing with each other. This equal-spacing-maintaining ability is realized by the NEB, who adds

spring forces along the band, and projects out the component of the force due to the potential perpendicular to the band.

There are a few improvements to the NEB method which are not yet included in the current version of VASP. A climbing image method and a better tangent definition combine to allow for the more accurate finding of saddle points using the NEB with fewer images than the original method. The setup and operation of this implementation can be identical to what is described in the VASP manual under the elastic band section. The climbing image method can be turned by setting LCLIMB = .TRUE. in the INCAR file [G. Henkelman, 2000].

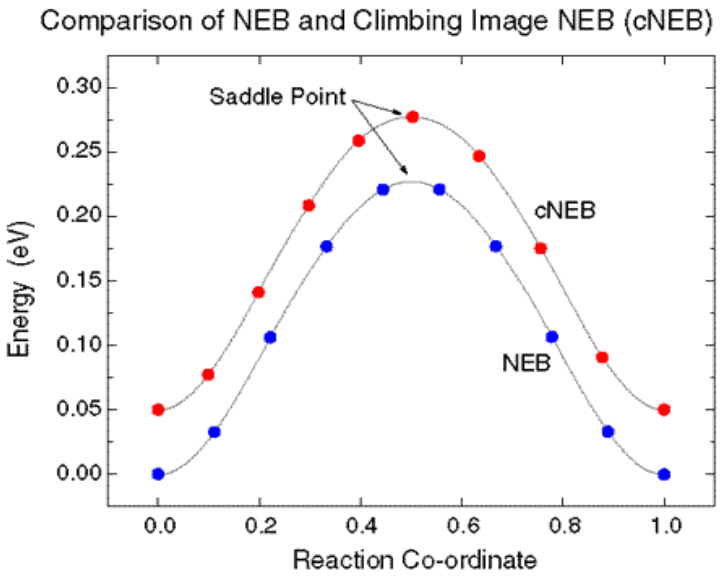

Figure 8: The comparison of NEB and Climbing Image NEB (CINEB) [G. Henkelman, 2000]

With Climbing Image NEB method, it is possible to calculate not only the MEP for the reaction but also the transition state configuration at the saddle point. The climbing image NEB method has one modification which makes the image with the highest energy up to the saddle point (Figure 8). This image does not see the spring forces along the band. Instead, the true force at this image along the tangent is inverted. In this way, the image tries to maximize its energy along the band, and minimize in all other directions. When this image converges, it will be at the exact saddle point.

Because the highest image is moved to the saddle point and it does not feel the spring forces, the spacing of images on either side of this image will be different. It can be important to do some minimization with the regular NEB method before this flag is turned on, both to have a good estimate of the reaction coordinate around the saddle point, and so that the highest

image is close to the saddle point. If the image is initially very far from the saddle point, and the climbing image was used from the outset, the path could develop very different spacing on either side of the saddle point. The energy barrier for diffusion atom to cross during the migration can be calculated to be the energy difference of the initial site and transition site, using

$$E_{mig} = E_{transition} - E_{initial} \tag{23}$$

where:

- E_{mig} is the migration energy for atomic jump from the initial site to final site;
- $E_{transition}$ is the total energy of the system when the diffusion atom is at its transition site;
- $E_{initial}$is the total energy of the system when the diffusion atom is at its initial site.

In our calculation 7 or 8 images are considered for all migration barrier calculations. The simulations of CINEB are performed with k-points grid 2×2×2 on the supercell of 96 atoms.

XI.2 Attempt frequency calculation

When the atom is at the transition state, it is in the equilibrium position. And its potential is harmonic. For one atom, it has three proper modes. So for the N atoms in the bulk, there are 3N frequencies.

For the atom at the transition state, since it is not stable, it has an imaginary frequency, and all the other two frequencies are real. For the model used in the thesis, it contains an atom which does the diffusion in the supercell. Except the diffusion atom, all the other atoms are almost stayed at the same positions, so the change of their vibration frequencies at initial site and transition site can be neglected and only the attempt frequency of carbon atom will be considered. By the Vineyard theory [G. H. Vineyard 1957], the attempt frequency can be calculated using

$$\nu_{if} = \frac{\sum_{3N} \nu_i^{initial}}{\sum_{3N-1} \nu_i^{transition}} = \frac{\nu_1 \nu_2 \nu_3}{\nu_1' \nu_2'} \tag{24}$$

where:

- ν_{if} is the attempt frequency;
- ν_i are the C vibration frequencies at the initial state;
- ν_i' are the C real vibration frequencies at the transition state.

Now, the attempt frequencies for the possible atomic jumps are investigated, so the jump probabilities of carbon atom can be calculated with Eq. 20. The characterizations of carbon migrations at atomic scale have been performed. In the next step, the Kinetic Monte Carlo method can be used in the macroscopic scale simulation to calculate the diffusion coefficient of carbon in bulk.

XII Kinetic Monte Carlo method (KMC)

Once calculating the atomic jumps with NEB method, the carbon diffusion simulation at the macroscopic scale can be performed with the kinetic Monte Carlo (KMC) method. It is a Monte Carlo method intended to simulate the time evolution of some processes occurring in nature. Typically, these are processes that occur with a given known rate. It is important to understand that these rates are inputs to the KMC algorithm, the method itself cannot predict them.

The main idea behind KMC is to use transition rates that depend on the energy barrier between the states, with time increments formulated so that they relate to the microscopic kinetics of the system.

For example,diffusion in the bulk with the activation energy in macroscopic scale is represented at atomic scale with the migration energy of the carbon atom which is energy barrier from one site to another neighbor one (Figure 9) and the rate constant for diffusion can be calculated using VTST theory, which is presented as jump probability in Part XI.

Before starting KMC simulation we have to make a list of all possible events that can be realized during the simulation and calculate rates for each event.

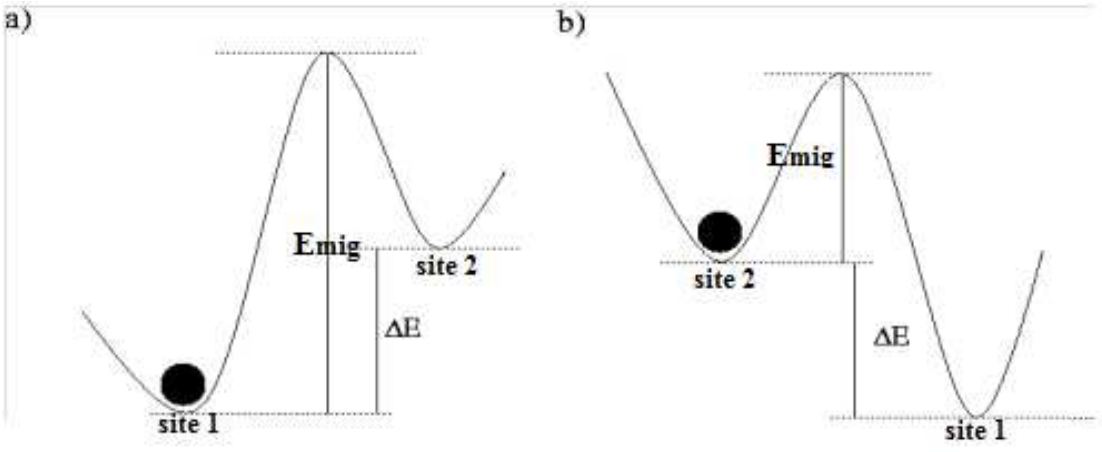

Figure 9: The migration energy barrier a) E_{mig} of migration from site 1 to site 2; b) E_{mig} of migration from site 2 to site 1

When the rate constants of all processes are known, we can perform KMC simulation in the time domain. In the case of a single process, the reciprocal of the rate of the process determines the time required for the reaction occurs. This quantity can be set equal to the KMC time. In the case of a many-particle multi-process system, however, introduction of time is less straightforward and several modifications of KMC exist.

First, the rates of all atomic jumps from the initial site to final states have to be evaluated (Figure 10).

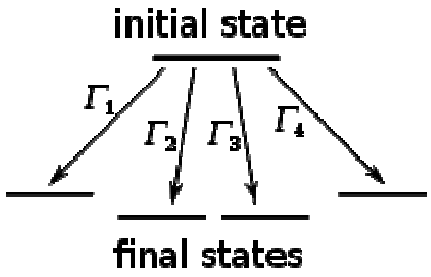

Figure 10: The atomic possible jumps from the initial state to the final states

Figure 11: The corresponding probability of atomic jumps

For a single constant time step, the probability of the considered processes is between 0 and 1 (Figure 11).When the rate constants of all processes are known, we can perform KMC simulation in the time domain. Time increments are defined by the rates of all processes and are formulated so that they relate to the microscopic kinetics of the system. By time residence algorithm [Young 1966], the average residence time dt equals to the inverse of the sum of the probabilities.

$$dt = \frac{1}{\sum_i^n \Gamma_i} \tag{25}$$

This method should be used when kinetics rather than equilibrium thermodynamics dominates the structural and/or compositional changes in the system.

XIII Diffusion coefficient calculation

In the previous part, it is known that the carbon does random jumps in the bulk, the displacement of the atom is noted as r. For the diffusion in three dimensions, there is relation between the mean-square of displacement (MSD) and the diffusion coefficient as below:

$$< r >^2 = 6Dt \tag{26}$$

In Figure 12, the slope of the curve equals to the 6D. So the diffusion coefficient at temperature T could be calculated.

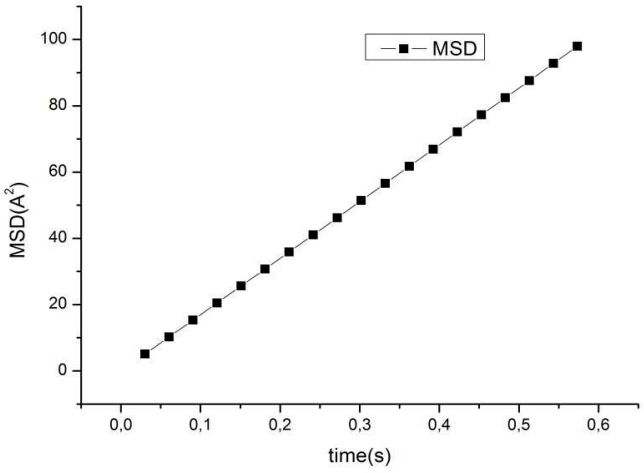

Figure 12: The mean square displacement of carbon atom at temperature T

By repeating the simulation at different temperatures, different diffusion coefficients can be calculated.

The diffusion coefficient in solids at different temperatures is generally found to be well predicted by the Arrhenius equation:

$$D = D_0 \exp\left(-\frac{E_{act}}{k_B T}\right) \quad (27)$$

where:

- D is the diffusion coefficient;
- D_0 is the pre-factor for calculation of D;
- T is the absolute temperature;
- E_{act} is the activation energy in the diffusion;
- k_B is the boltzman constant.

This equation can be transformed to:

$$lnD = lnD_0 - \frac{E_{act}}{k_B T} \quad (28)$$

The equation presents time dependence of diffusion coefficient. The linear relation between lnD and temperature T is presented in Figure 13.

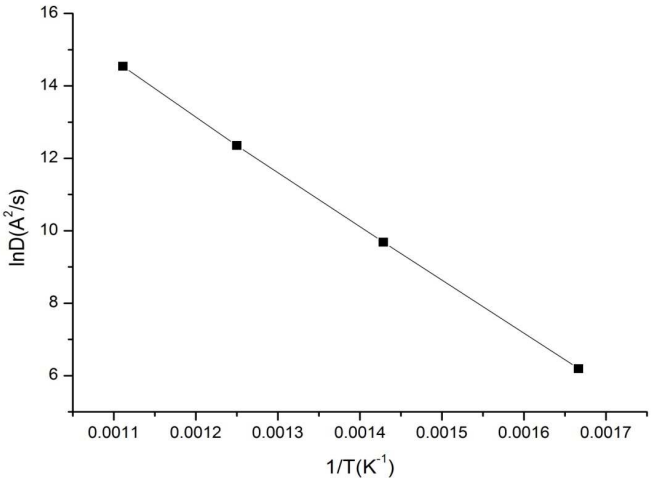

Figure 13: The linear relation of lnD and temperature T

So by simulating the carbon's trajectories at different temperatures, the related diffusion coefficients at the temperatures can be calculated. By doing the Arrhenius plot for T and D, the prefactor D_0 and the activation energy E_{act} can be calculated.

Conclusion

The carbon atom diffusion behavior is performed with multi-scale method simulations in this thesis. At atomic scale, the calculation model is built from the unit cell. The geometrical parameters and calculation parameters such as cut-off energy and pseudopotential set will be optimized by DFT calculations using VASP code. All the calculations are performed with the GGA functional PW91 [Perdew 1992]. Then to study the carbon atomic jumps, all the possible sites will be investigated in a large supercell (to avoid the volume variation caused by carbon insertion). For each two neighbor interstitial sites, the migration energy and attempt frequency will be calculated using VTST theory and the jump probabilities for all possible atomic jumps will be investigated. At macroscopic scale, using the atomic jump results of carbon from the atomic scale simulations, the carbon's trajectory at certain temperature will be performed with KMC approach. By repeating the simulation of carbon at different temperatures, the relation between diffusion coefficient and temperature can be calculated. Finally diffusion coefficient of carbon at storage condition can be calculated.

All the multi-scale simulations will be performed in hcp zirconium and monoclinic zirconia. The diffusion mechanism in this work contains two types of mechanism: diffusion by interstitial sites, and diffusion by vacancy sites.

References:

[P. E. Blochl 1994] P.E. Blochl, Phys. Rev. B 50, 17953-17979 (1994)

[K. Burke 1998] K. Burke, J. P. Perdew, and Y. Wang, Electronic Density Functional Theory, 81-111, Springer US, New York (1998)

[R. Car 1985] R. Car, and M. Parrinello, Physical review letters 55, 2471 (1985)

[H. Eyring 1935] H. Eyring, J. Chem. Phys., **3**, 107 (1935)

[N. C. Handy 1986] N. C. Handy, Y. Yamaguchi, and H. F. Schaefer, J. Chem. Phys. B, 84, 4481 (1986)

[G. Henkelman 2000] G. Henkelman, B. P. Uberuaga, and H. Jonsson, J. Chem. Phys., **113**, 9901 (2000)

[P. Honenberg 1964] P. Honenberg, W. Kohn, Phys. Rev. B 136, 864-871 (1964)

[H. Jonsson 1998] H. Jonsson, G. Mills and K.W. Jacobsen, Classical and quantum dynamics in condensed phase simulations, World Scientific Inc, 385-404 (1998)

[G. Kresse 1999] G. Kresse, D. Joubert, Phys. Rev. B 59, 1758-1775 (1999)

[W. Kohn 1954] W. Kohn, and N. Rostoker, Phys. Rev. 94, 111 (1954)

[W. Khon 1965] W. Kohn, and L. J. Sham, Physical Review, 140, A1133 (1965)

[E. K. U. Kross 1995] Proceedings of a NATO Advanced Study Institute on Density Functional Theory, Plenum Press, New York (1995)

[A. D. Mclachlan 1964] A. D. Mclachlan, Molecular Physics, 8, 409 (1964)

[E. Nelson 1966] E. Nelson, Phys. Rev. **150**, 1079 (1966)

[B. Olinger 1973] B. Olinger and J.C. Jamieson, High Temp. High Pressures 5, 123-131 (1973)

[M. Orio 2009] M. Orio, D. A. Pantazis, and F. Neese, Photosynth Res, 102, 443-453 (2009)

[R. G. Parr 1983] R. G. Parr, Annual Review of Physical Chemistry, 34, 631-656 (1983)

[R. G. Parr 1989] R.G. Parr, W. Yang, Density Functional Theory of Atoms and Molecules, Oxford University Press (1989).

[J. P. Perdew 1992] J.P. Perdew, J.A. Chevary, S.H. Vosko, et al., Phys. Rev. B 46, 66-71 (1992)

[J. P. Perdew 1993] J. P. Perdew, J. A. Chevary, S. H. Vosko, et al., Physical Review B 48, 4978 (1993)

[J. P. Perdew 1996] J. P. Perdew, K. Burke, et al., Physical review letters 77, 3865 (1996)

[O. L. Polyansky1997] O. L. Polyansky, N. F. Zobov, S. Viti, J. Tennyson, P. F. Bernath, and L. Wallace, Science 277, 346 (1997)

[A. M. Rappe 1991] A. M. Rappe, K. M. Rabe, E. Kaxiras, and J. D. Joannopoulos, Phys. Rev. B. **41**, 1227-1230 (1990)

[D. Sheppard 2008] D. Sheppard, R. Terrell, and G. Henkelman, J. Chem. Phys., **128**, 134106 (2008)

[N. Troullier 1993] N. Troullier, and José Martins, Phys. Rev. B 43, 8861 (1993)

[E. F. Valeev 2003] E. F. Valeev and C. D. Sherrill, J. Chem. Phys. 118, 3921 (2003)

[G. H. Vineyard 1957] G. H. Vineyard, J. Phys. Chem. Solids, 3, 121-127 (1957)

[A. F. Voter 1986] A. F. Voter, Phys. Rev. B **34**, 6819 (1986)

[E. P. Wigner 1937] E. P. Wigner, J. Chem. Phys., **5**, 720 (1937)

[Z. Wu 2006] Z. Wu, and R. E. Cohen, Physical Review B, 73, 235116 (2006)

[W. M. Young 1966] W. M. Young and E. W. Elcock, Proc. Phys. Soc. 89, 735 (1966)

Chapter 2

Carbon diffusion in bulk zirconium

Introduction

In the PWR reactor, the cladding is made of zircaloy-4, which is principally zirconium (98.4%) and contains oxygen atoms, which may become C14 under irradiation. So to study the carbon behavior and diffusion in the claddings, it is necessary to perform the carbon simulation in the zirconium. The hexagonal close packed (hcp) structure is the crystallographic structure of zirconium alloys. So in this study, the hcp phase was chosen for the simulation in zirconium bulk. The simulations are performed to characterize, by the mean of a multi-scale approach, the carbon diffusion behavior in the Zr hexagonal close packed bulk to estimate the waste safety of the fuel rods' claddings in the storage condition.

Very few experimental studies of C in Zr have been published. In the G. Murch's experiments, the measurements at constant hydrostatic pressure rather than constant volume were made as implied in the lattice gas treatment. It was found that the compositional dependence of the tracer carbon diffusion coefficient was reasonably well represented using the partial molar energy of carbon as input to the equation for the diffusion coefficient [G. E. Murch 1979]. So it means that in theoretical study, an isolated carbon atom with its molar energy could be chosen to perform the carbon behavior which can describe the carbon diffusion coefficient very well.

For the C behavior in the zirconium bulk, there was only one old experimental study to measure the diffusion coefficients of C. The diffusion of carbon in zirconium was studied in the temperature range 873-1523 K, using the residual activity technique. [R. P. Agarwala 1975]. It showed that the diffusion coefficient at 923 K was 5.1×10^{-15} cm^2/s.

However, regarding theoretical calculations, to our knowledge, no calculation of C behavior in bulk hcp zirconium have been performed.

Few simulation studies by first principle calculations have been performed with Zr. For example, the self-diffusion was performed by the first principal calculation in the reference in which the average value of the migration energy was found to be in a very good agreement with available experimental data. The activation energies obtained, assuming vacancy mechanism, are in good agreement with experiments [G. Verite 2007]. For the interstitial mechanism diffusion, several element diffusions (such as H, Al, Fe, etc) in hcp zirconium were studied by simulations methods [C. Domain 2006, R. A. Perez 2008, R. C. Pasianot

2009] and experiments [M. Iwasawa 2008]. For the diffusion in the grain boundaries, it was proved by calculations that both the formation energies and the migration free energies were significantly lower than in the bulk which demonstrates the role of the grain boundary as a vacancy sink and a fast diffusion channel [J. R. Fernandez 2000].

In this chapter, the carbon diffusion coefficient in the zirconium has been investigated using a multi-scale approach: atomic scale using the periodic density functional theory (DFT) and macroscopic scale with Kinetic Monte Carlo (KMC) simulations.

In the first part, a Zr bulk model was optimized and the possible interstitial carbon sites were investigated. Then, for each interstitial carbon site, all the neighbor interstitial sites were identified so that all the migration possibilities between each two neighbor sites were characterized. For the possible jumps, the migration energies, the attempt frequencies and the migration rates were calculated.

In the second part, all the results of the previous calculations were used to simulate the carbon diffusion by using the Kinetic Monte Carlo (KMC) method. Once knowing the carbon diffusion behavior in the perfect hcp Zr, the vacancy effect was considered to calculate the carbon diffusion in a more realistic environment.

I: Carbon behavior inzirconium

In this work, the carbon diffusion simulation will be performed using multi-scale simulations. That means the simulation has two scales: atomic scale to study the atomic jump between two neighbor sites and macroscopic scale to study the macroscopic diffusion in bulk.

I.1 Atomic scale simulations

As the first step, in atomic scale simulations, calculation parameters were optimized by comparing calculated properties to experimental ones for zirconium bulk.

I.1.A Optimization of the calculation parameters

A-1 Zr model

The zirconium metal under ambient environment is a hexagonal close-packed (hcp) structure, atomic number 40, and atomic mass of 91.224. Its space group is P63/mmc,

numbered 194[B. Olinger 1973], with parameters: a=3.232 Å, b=3.232 Å, c=5.147 Å, α=90°, β=90°, γ=120°.

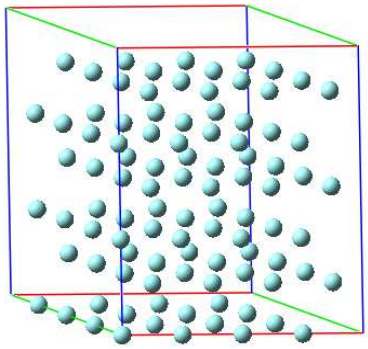

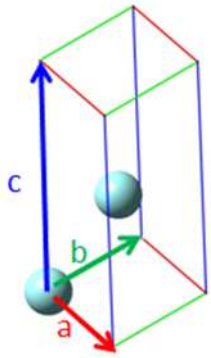

Figure 1: Zirconium HCP structure **Figure 2: Unit-cell of Zirconium HCP structure**

The crystal structure of Zr can be constructed by 2 atoms in one unit cell (Figure 2), a motif with coordinates (0, 0, 0) and $(\frac{2}{3}, \frac{1}{3}, \frac{1}{2})$. Once the initial structure was built, the corresponding pseudopotential has to be chosen to do the simulation.

The zirconium electron configuration is: $1s^2 2s^2 2p^6 3s^2 3p^6 3d^{10} 4s^2 4p^6 4d^2 5s^2$. In this case, two pseudopotentials are considered for Zr: Zr_4 and Zr_12. For the Zr_4 pseudopotential, the last four electrons ($4d^2 5s^2$) are considered as valence electrons. For the Zr_12 pseudopotential, the last twelve electrons ($4s^2 4p^6 4d^2 5s^2$) are considered as valence electrons. The pseudopotential was evaluated by comparing the total energy convergence and geometrical parameters with the experimental values when the cut-off energies and k-points change.

The geometrical optimization was performed with different k-points and different cut-off energies. For Zr_12, the total energy converges from 400 eV cut-off energy with a 11×11×11 k-points grid. But, for Zr_4, the total energy had already converged at 200 eV with a 11×11×11 k-points grid. With (Zr_4) and (Zr_12), the calculated bulk parameters of hexagonal zirconium are the same: a= 3.23 Å, c= 5.17 Å which have a good agreement with the experiment ones 3.23Å and 5.15 Å [C. Kittel 2005]. Since Zr_12 contains more valence electrons and has a higher convergence energy which needs more calculation time, (Zr_4) is thought to be more suitable to be used in the later calculations.

In order to compare the optimization result of bulk Zr with previous theoretical and experimental results, the cohesive energy for a Zr unit cell was also calculated, using the following formula:

$$E_{cohesive} = (E_{total} - E_{atom} * N_{atom})/N_{atom} \quad (1)$$

where:

- E_{total}: total energy of the Zr unit cell;
- E_{atom}: energy of an isolated Zr atom;
- N_{atom}: number of atoms in the Zr unit cell.

Since in the Eq (1), it is necessary to know the energy of a single Zr atom, a cell of 10 Å×10 Å×10 Å with a single Zr atom in its center was built to calculate it. Then the cohesive energy for a Zr unit-cell can be calculated. The results were listed in Table 1.

	$E_{cohesive}$ (eV):	Parameter a, b (Å):	Parameter c (Å):
VASP This work	6.73	3.23	5.14
VASP [R. Li 2013]	6.74	3.23	5.17
VASP [N. Poletz 2006]	6.36	3.25	5.15
Experimental [C. Kittel 2005]	6.49	3.23	5.15

Table 1: Cohesive energies and lattice parameters for a hcp Zr unit –cell, using Zr_4

The Zr_4 pseudopotential gives accurate results comparing with the experimental and theoretical values. So Zr_4 can be used for this system.

Now, in order to study the carbon diffusion, the carbon's pseudopotential has to be tested. First, a pure diamond structure is considered to perform the pseudopotential evaluations.

A-2 Diamond C structure

The pure diamond under ambient environment is a diamond-cubic structure, atomic number 6, and atomic mass 12.011 a.m.u. Its space group is Fd3m, numbered 227 [K. Kobashi 2005] with parameters: a=3.567 Å, b=3.567 Å, c=3.567 Å, α= 90°, β= 90°, γ= 90°.

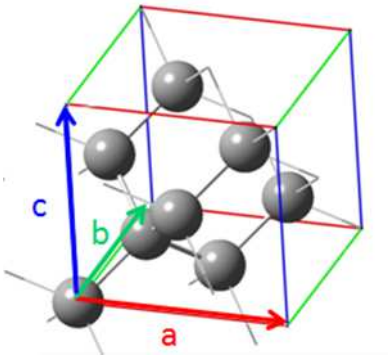

Figure 3: Unit-cell of C diamond structure

In our simulation, the crystal structure of diamond was built with 8 atoms in one unit cell, a motif with coordinates (0, 0, 0) $(\frac{1}{4},\frac{1}{4},\frac{1}{4})$, $(0,\frac{1}{2},\frac{1}{2})$, $(\frac{3}{4},\frac{1}{4},\frac{3}{4})$, $(\frac{1}{2},0,\frac{1}{2})$, $(\frac{1}{4},\frac{3}{4},\frac{3}{4})$, $(\frac{1}{2},\frac{1}{2},0)$, and $(\frac{3}{4},\frac{3}{4},\frac{1}{4})$.

The electron configuration of carbon is: $\boldsymbol{1s^2 2s^2 2p^2}$. Three types of pseudopotentials of carbon noted "C", "C_s" and "C_h" are tested in this part. They all have 4 valence electrons ($\boldsymbol{2s^2 2p^2}$). As indicated in their name, "C_s" is a "soft" pseudopotential, "C_h" is a "hard" pseudopotential, and "C" is a "normal" one. A "hard" pseudopotential means it has strongly oscillating pseudo-wave functions, and requires many pseudo-wave functions in calculations.

By comparing the convergence of associated total energy and geometrical parameters depending on the cut-off energies and k-points mesh, the more suitable pseudopotential is found.

For "C", the total energy converges from k-point 5×5×5, but slowly with cut-off energy (550 eV). The geometrical parameters converge from 3×3×3 k-point and a cut-off energy of 450 eV.

For C_s, the total energy converges from k-point 5×5×5 with a cut-off energy of 550 eV. Geometrical parameters converge from 3×3×3 k-point and a cut-off energy of 350 eV.

For C_h, the total energy and geometrical parameters converge from 3×3×3 K-point, but very slowly with the cut-off energy.

So C_h pseudopotential is not suitable for the future calculations because of its slow convergence of total energy and geometrical parameters. C and C_s are both good candidatures for future calculations.

Also, to compare our optimization result with the previous calculation results and experiment ones, the cohesion energy will be calculated. A cell of 10Å×10Å×10Å with a single C atom in its center was built to get the energy of one carbon atom E_{atom}.

So the cohesive energy could be calculated using Eq (1). The results were listed in Table 2.

	$E_{cohesive}$ (eV):	Parameter a, b, c(Å):
VASP This work for C	7.68	3.57
VASP This work for C_s	7.66	3.58
Experimental[H. J. Mcskinmin 1972]	7.37	3.57

Table 2: Diamond carbon cohesive energy and lattice parameter

So it is provided that both C and C_s give accurate results comparing with experimental values. In this case, both can be used for this system.

A-3 ZrC structure

In the previous parts, it is found that the Zr_4, C and C_s pseudopotential are good candidates for pure Zr and C structure. In this part, to verify if the pseudopotentialscan accurately describe the Zr-C bonds, the ZrC structure was calculated.

The zirconium carbide under ambient environment is a cubic close packed structure. Its space group is Fm3m, numbered 225, with parameters: a=4.698 Å, b=4.698 Å, c=4.698 Å, α= 90°, β= 90°, γ= 90° [D. R. Lide 1998].

In our simulation, we construct the crystal structure of ZrC using 4 Zr atoms and 4 C atoms in one unit cell, a motif with coordinates (0, 0, 0) $(0,\frac{1}{2},\frac{1}{2})$, $(\frac{1}{2},0,\frac{1}{2})$, $(\frac{1}{2},\frac{1}{2},0)$ for Zr and $(\frac{1}{2},0,0)$, $(0,0,\frac{1}{2})$, $(\frac{1}{2},\frac{1}{2},\frac{1}{2})$, $(0,\frac{1}{2},0)$ for C was used.

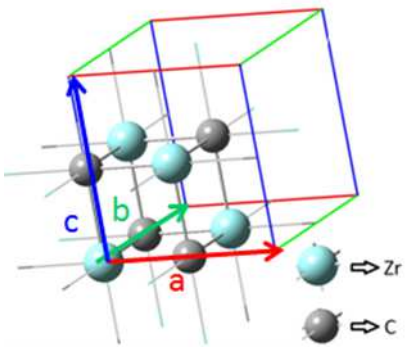

Figure 4: Unit-cell of ZrC structure

Two combinations of pseudopotentials are tested in this part. We study one ZrC structure using the first set of pseudopotentials (Zr_4/C), and the other one using the second set of pseudopotentials (Zr_4/C_s). By comparing their total energy convergence and geometrical parameters as a function of the cut-off energies and k-points, we can determine which set of pseudopotentials is more suitable for this system.

For the set (Zr_4/C), the total energy converges from 9×9×9 K-points with a cut-off energy of 500 eV, and the geometrical parameters converge with a cut-off energy of 450 eV and k-point 5×5×5.

For the set (Zr_4/C_s), the total energy converges from 9×9×9 K-points with a cut-off energy of 450 eV, and the geometrical parameters converge with a cut-off energy of 350 eV and k-point 5×5×5.

By comparing the convergences of total energy and geometrical parameters as a function of the cut-off energies and k-points grids, similar results are found. Therefore, (Zr_4/C_s) can be chosen with an energy cut-off of 350 eV and a 9×9×9 k-points grid in the later calculations since its lower calculation time cost and good description of the structure. The parameters a, b, and c are 4.725 Å, which have a good agreement with experimental results 4.68 Å [A. C. Lawson 2007] and theoretical values 4.72 Å [F. Vines 2005].

Total energies and geometrical parameters for the (Zr 4/C) set:	Total energies and geometrical parameters for the (Zr 4/C s) set:

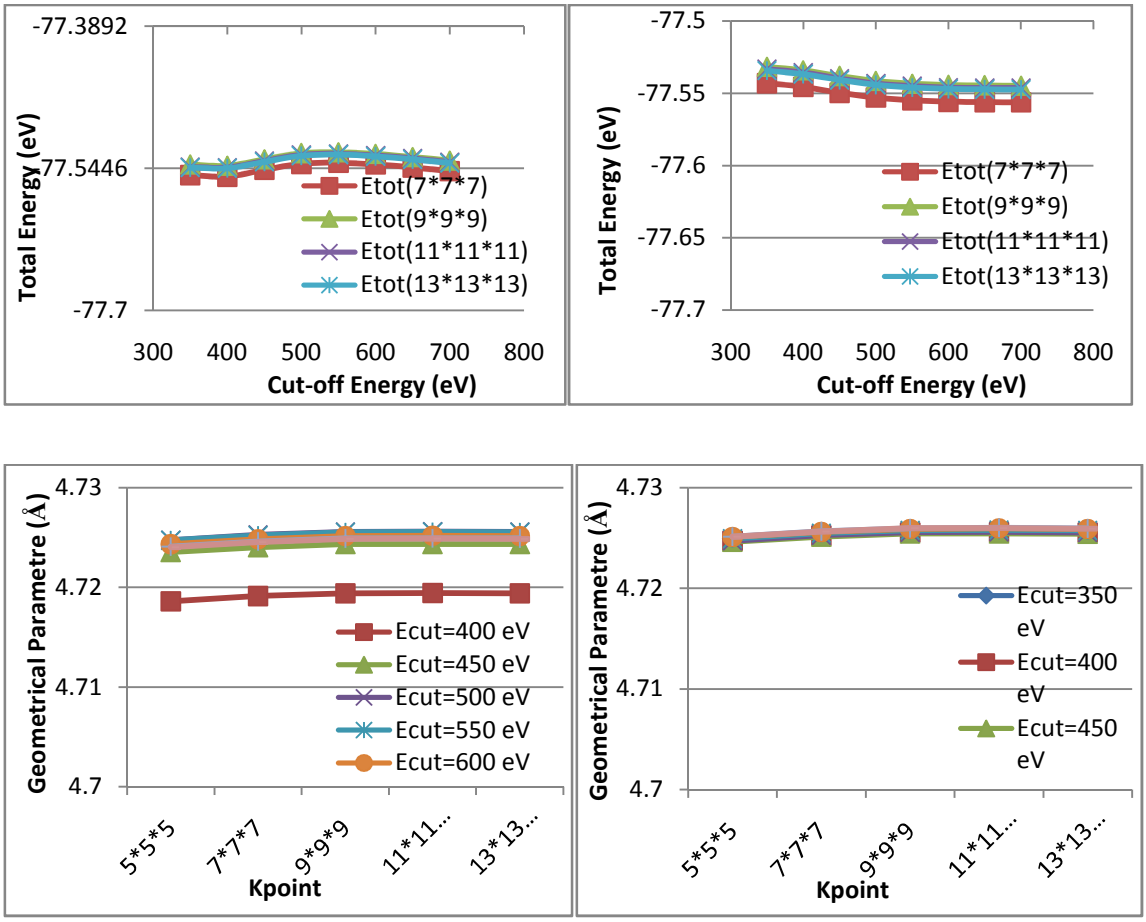

Figure 5: ZrC total energies and geometrical parameters with different values of k-points and cut-off energies, for the (Zr_4/C) and (Zr_4/C_s) pseudopotentials

The cohesive energy is also compared with experimental and theoretical values. Results were listed in Table 3, which prove a good agreement with experiment data.

	$E_{cohesive}$ (eV):	Parameter a, b, c (Å):
VASP This work	16.22	4.725
VASP PW91[F. Vines 2005]	16.08	4.72
Experiment [V. P. Zhukov 1985]	15.86±0.19	4.68

Table 3: ZrC cohesive energy and lattice parameter

A-4 Summary

Based on the previous results, the pseudopotential set (Zr_4/C_s) will be used in the later simulations.

I.1.B. Optimization of the Zr bulk super-cell size

In the previous parts of this study, pseudopotentials, cut-off energies and k-points grids were optimized to simulate pure Zr and C structures as well as ZrC one. However, to simulate the behavior of one carbon atom in the Zr hexagonal compact structure, it is necessary to optimize the size of a Zr model which should be big enough to correctly describe the real system when a carbon is inserted (which means a weak geometrical relaxation of the cell volume in order to perform later, calculation at constant volumes, and to simulate low carbon concentration).

In this part, the geometrical parameters are calculated for different supercell sizes of Zr before and after the insertion of one carbon atom. By comparing the cell volume differences (before and after insertion), an accurate supercell model can be optimized to study C behavior in the Zr hexagonal close-packed structure.

By reproducing the unit cell of zirconium (Figure 6) in three dimensions, different sizes of supercells were obtained. For example, if the unit cell is reproduced 2 times along each axe (a, b and c), it will be a 2×2×2 supercell.

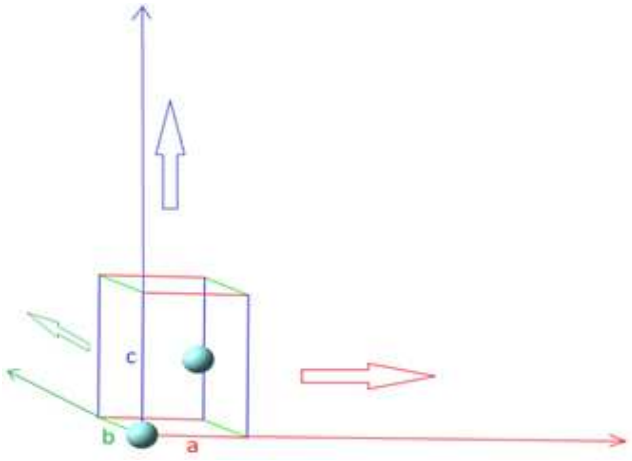

Figure 6: Zr hexagonal close-packed unit cell

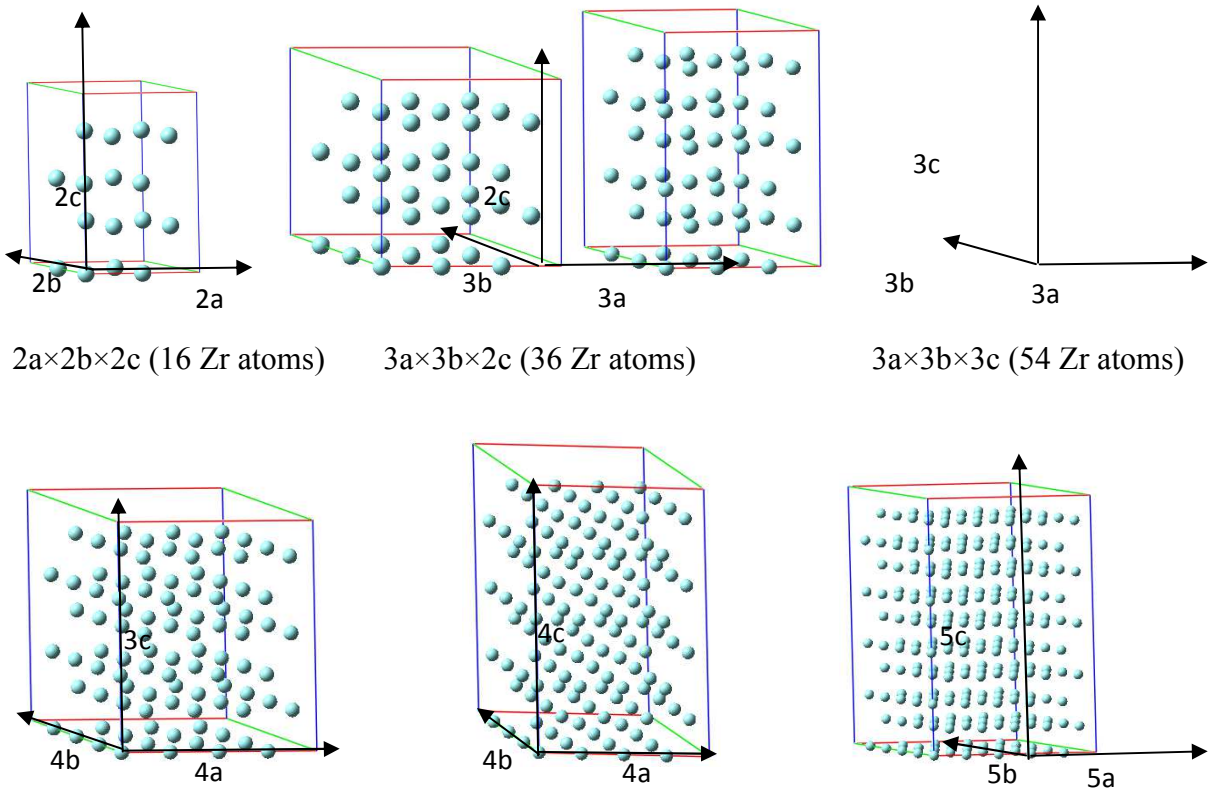

2a×2b×2c (16 Zr atoms) 3a×3b×2c (36 Zr atoms) 3a×3b×3c (54 Zr atoms)

4a×4b×3c (96 Zr atoms) 4a×4b×4c (128 Zr atoms) 5a×5b×5c (125 Zr atoms)

Figure 7: Supercells with different sizes (without carbon)

At the first step, the variation sizes of supercells are calculated, when one carbon atom is added in the structure in site 8 (Table 4). The following supercells were tested (Figure 7).

E_{cut}=450 eV								
n(atom)	Size	**Δ(a) (Å)**	Δ(a) (%)	**Δ(c) (Å)**	Δ(c) (%)	**Δ(V) (Å^3)**	Δ(V) (%)	k points grid
16	2a×2b×2c	**0.029**	0.888	**0.028**	0.534	**8.730**	2.310	6×6×6
36	3a×3b×2c	**0.012**	0.385	**0.011**	0.220	**8.369**	0.990	4×4×6
54	3a×3b×3c	**0.007**	0.203	**0.018**	0.355	**9.644**	0.762	4×4×4
96	4a×4b×3c	**0.004**	0.125	**0.006**	0.117	**8.266**	0.368	3×3×4
128	4a×4b×4c	**0.003**	0.099	**0.002**	0.043	**7.236**	0.241	3×3×3
250	5a×5b×5c	**0.002**	0.047	**0.002**	0.036	**7.570**	0.129	3×3×3

Table 4: Volume variations before and after the insertion of one carbon in site 8 for different supercell sizes

Taking into account: acceptable calculation time; small variation of geometric parameters; convenience for future calculation of vacancy defect, the 4×4×3 supercell has been chosen for next calculations (Figure 8).

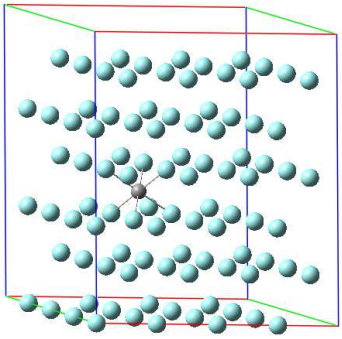

Figure 8: Supercell 4×4×3 of Zr with one interstitial carbon atom in (O) site (grey atom)

At the second step, calculation will be performed at constant volume, the cut-off energies are optimized, using the K-points large enough. We find that the cut-off energy of 300 eV can be used in the future calculation.

At the third step, we optimize the k-points grid, and find the k-points 3×3×3 can be used in the future calculation. Now in the next part, the investigation of possible carbon interstitial sites can be calculated.

I.1.C Investigation of the carbon interstitial sites

The supercell model used in this part was built from the 2 atomic unit cell extended by 4×4×3 in the three directions as presented in the last part. By the optimization results, k-points mesh was optimized to 3×3×3 with a cut-off energy of 300 eV and constant volume calculations will be performed with this model.For the frequency calculation the convergence criteria of the force on atoms is set to be 10^{-5} eV/Å in order to get an accurate relaxed configuration which is required to obtain an imaginary frequency at the saddle point.

To calculate the carbon diffusion in the Zr bulk, at first, the possible C interstitial sites were identified as well as their relative stabilities. It showed that there are two possible interstitial sites in the Zr hexagonal compact structure: an octahedral site named as O site (Figure 9 panel b), and a distorted basal tetragonal one named as BT_d site (Figure 9 panel c). For the BT_d

site, the neighbor Zr atoms were displaced to get a stable state of the structure. The distances between Zr and C were changed relative to an ideal BT site (Fig. 9 panel a).

In fact, from an initial BT position (Fig. 9 panel a) after the relaxation process, it was found that there are three stable symmetrical BT_d sites as a triangle (Figure 9 panel c). The distances between a starting BT position and BT_d sites are very small at about 0.4 Å.

The formation energy of a carbon in interstitial position (E_I) was calculated using Eq (2):

$$E_I = E_{C-Zr} - (E_C + E_{Zr}) \quad (2)$$

where:

- E_{Zr} is the total energy of a 96 atomic zirconium supercell;
- E_C is a carbon atomic energy in a diamond structure;
- E_{C-Zr} is the total energy of a 96 atomic zirconium supercell with a carbon atom in an interstitial position.

Calculations showed that the carbon in the O site has a formation energy of -1.70 eV for Zr_4 or -1.68 eV for Zr_12 and in the BT_d site the formation energy is -0.25 eV for Zr_4 and -0.14 eV for Zr_12. It means that the O site is the more favorable one ($\Delta E = E_I(BT\_d) - E_I(O)$=1.45 eV for Zr_4 and 1.54 eV for Zr_12). Thus, most of the carbon would stay in the O site (cf Table 5).

Configuration (eV)	Zr_4	Zr_12
O	-1.70	-1.68
BT_d	-0.25	-0.14

Table 5: Formation energy (in eV) for the different C interstitial positions

By comparing the formation energy, it was found that for the two pseudopotentials (Zr_4 and Zr_12), the formation energies are very similar for O site, but there is a small difference for the distorted BT site. Since a carbon can jump between different interstitial sites, the migration energies for all possible jumps of Zr_4 and Zr_12 will be calculated in the migration part. However, the calculations of diffusion coefficient were only performed with Zr_4, the results of Zr_12 are given for comparison.

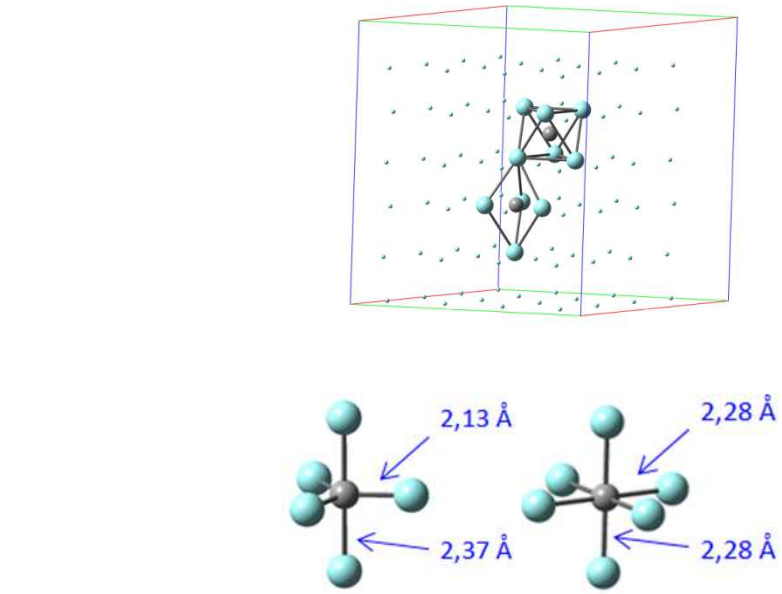

(a)

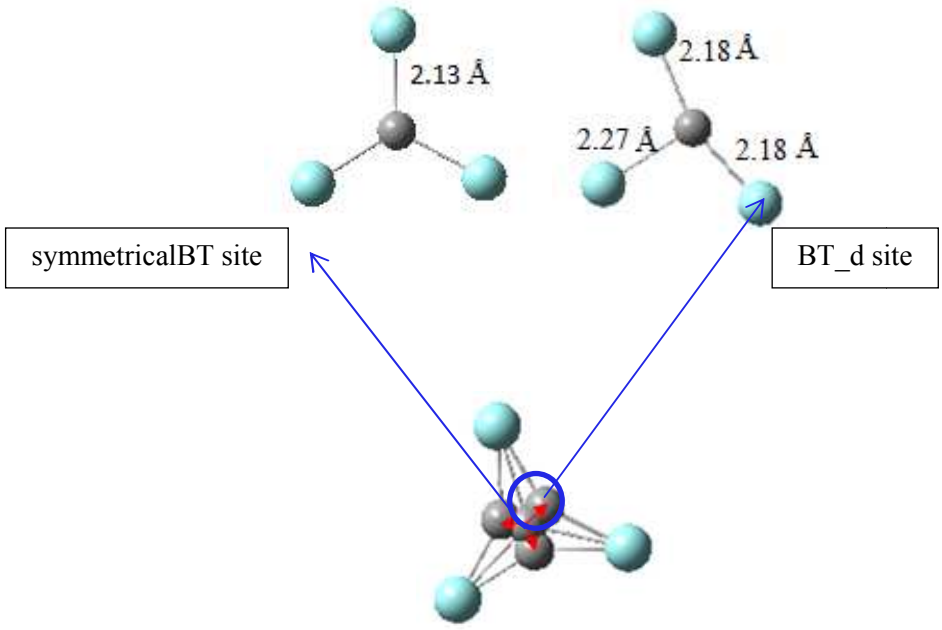

Figure 9: The interstitial sites for C in the Zr model composed of 96 Zr atoms. a: basal tetragonal site (BT); b: octahedral site (O); c: BT_d sites (three BT_d sites around one BT site)

I.1.D Migration between neighbor sites

To study the carbon's diffusion in zirconium bulk, it is first necessary to calculate the needed migration energy, E_{mig}, to jump from one interstitial site to a neighbor one.

D-1 Migration energies (NEB)

The Nudged Elastic Band method (NEB) [H. Jonsson 1998] was used to calculate the minimum energy pathway between the possible jumps in order to identify transition states and migration energies (Chapter I.X).

Following each migration pathway between two neighbor sites, several (7 or 8) carbon positions (images) were considered. After optimization, the energetic profile was plotted according to the total energy of these different points (Figure 10).

First, we test the jump between two neighbor BT_d sites in the zirconium bulk and it was found that the migration path would always pass through the BT position with an energy barrier 0.40 eV which corresponds to the energy difference of the two types of site (Figure 10 panel a).

Then, the migration between BT_d site and O site was calculated. As it can be seen in Figure 10 panel b, if C migrates from BT_d site to O site, it needs 0.70 eV to cross the migration barrier. However, it is much harder to migrate from O site to BT_d site, which needs 2.13 eV to pass the barrier. The migration path between neighbor BT_d site and O site is always following the path: BT_d site BT_d site (n times)→ O site→ BT_d site …

When the carbon migrates between two neighbor O sites, it needs 3.51 eV to overcome the barrier (Figure 10 panel c).

As a summary, for C migration in Zr bulk, there are four possible jumps (O site → O site, O site → BT_d site, BT_d site → O site, and BT_d site → BT_d site). All the migration energies of the possible migrations are listed in Table 6.

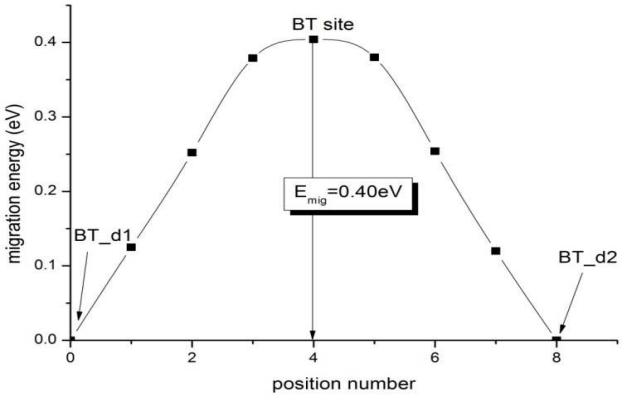

(a)

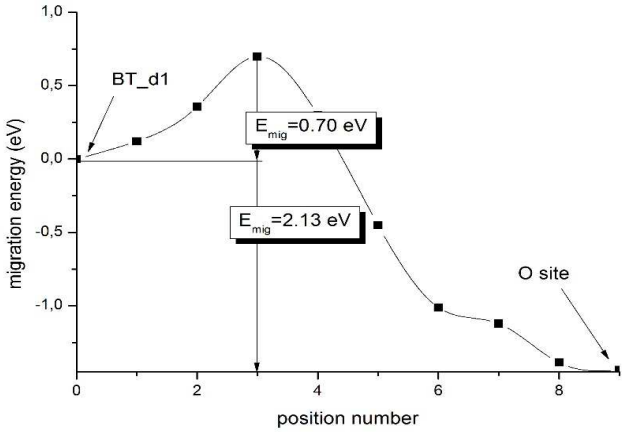

(b)

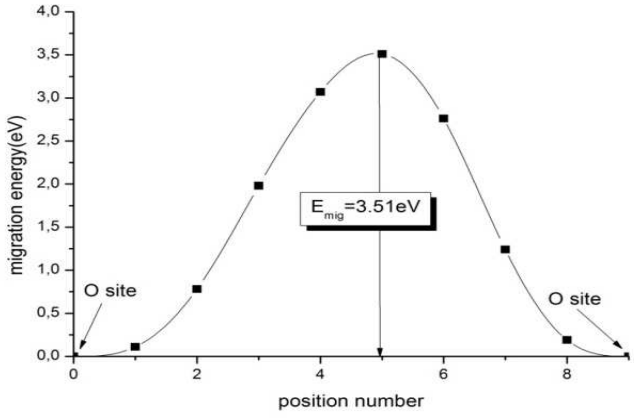

(c)

Figure 10: Migration between two neighbor sites for C in Zr bulk (Zr_4). a: migration path from BT_d1 site to BT_d2 site; b: migration path between BT_d site and O site; c: migration path between two neighbor O sites

initial site \ final site	O site	BT_d site
O site	3.51 / (3.40)	2.13 / (2.21)
BT_d site	0.70 / (0.66)	0.40 / (0.26)

Table 6: Migration energies (in eV) of the possible migration pathway in zirconium bulk for Zr_4 and (Zr_12) in parenthesis

D-2 Attempt frequencies and jump rates

To study the possible jumps of carbon through interstitial sites, the possible neighbor sites were identified. A carbon in BT_d site has 2 O sites and 2 BT_d sites as neighbor sites and for a carbon in O site, it has 6 neighbor BT_d sites and 2 neighbor O sites. So for a carbon in the O site, it can do 8 possible jumps, and for a carbon in the BT_d site, it can do 4 possible jumps. As summarize, there are four kinds of atomic jumps: O site → BT_d site; BT_d site → O site; O site → O site; BT_d site → BT_d site…

In order to calculate the transition rate associated to each possible jump, the TST theory presented in Chapter 1 is used

$$\Gamma = \nu_{if} exp\ (-\frac{E_{mig}}{k_B T}) \quad (3)$$

Since all the migration energies for the possible atomic jumps have been calculated, for certain temperature T, the corresponding attempt frequency ν_{if} should be calculated to get the jump probability.

The results of the calculated attempt frequencies corresponding to the possible migration were listed in the Table 7. The chosen displacement of the C atom at the stable sites and transition states in the 3 directions is 0.005 Å.

final site / initial site	O site	BT_d site
O site	$1.3\times10^{13}s^{-1}$	$1.7\times10^{13}s^{-1}$
BT_d site	$1.6\times10^{13}s^{-1}$	$1.3\times10^{13}s^{-1}$

Table 7: The attempt frequencies ν_{if} of the possible migration pathway in zirconium bulk for Zr_4

As the first conclusion, at low temperature, the interstitial carbon should preferentially diffuse through the path BT_d site and O site, which are connected. For all possible migration paths, the migration energies, the attempt frequencies and their jump probabilities were calculated in this part. The results were summarized in Table 8.

Possible jump	E_{mig}	ν_{if}	Γ_{if}
O site → O site	3.51 eV	$1.3\times10^{13}\ s^{-1}$	$1.3\times10^{13}s^{-1}exp\ (-\frac{3.51\ eV}{k_BT})$
O site → BT_d site	2.13 eV	$1.7\times10^{13}\ s^{-1}$	$1.7\times10^{13}s^{-1}exp\ (-\frac{2.13\ eV}{k_BT})$
BT_d site → O site	0.70 eV	$1.6\times10^{13}\ s^{-1}$	$1.6\times10^{13}s^{-1}exp\ (-\frac{0.70\ eV}{k_BT})$
BT_d site → BT_d site	0.40 eV	$1.3\times10^{13}\ s^{-1}$	$1.3\times10^{13}s^{-1}exp\ (-\frac{0.40\ eV}{k_BT})$

Table 8: The results of all possible atomic jumps between each two neighbor sites

I.2 Macroscopic scale simulations

After doing the elementary mechanism calculations at the atomic scale, the macroscopic scale simulations were performed by using Kinetic Monte-Carlo simulations (KMC) [C. Kittel 2005, H. Jonsson 1998] to study the carbon diffusion in the zirconium bulk. The main idea behind KMC is to use migration rates that depend on the energy barrier between the states and the time step is given by the residence time algorithm [C. S. Becquart 2010]

I.2.A KMC simulations

The isolated carbon used in the KMC simulation does a random walk. From the carbon's trajectory of three dimensions at a given temperature (Figure 11), the mean square displacement of the carbon could be calculated.

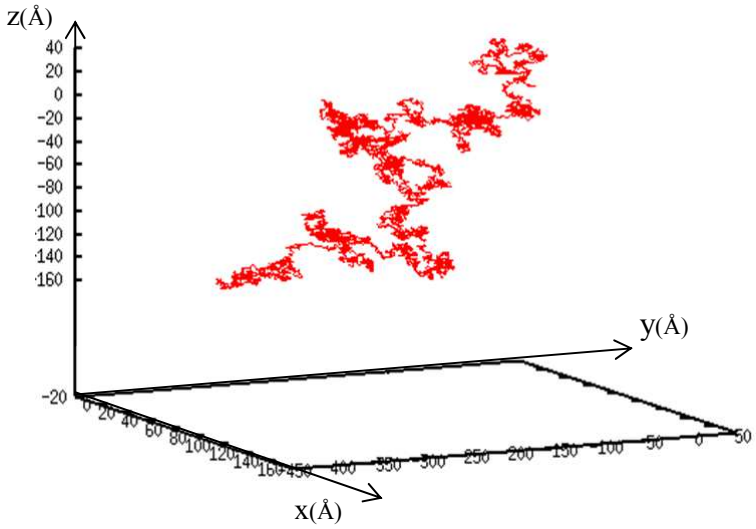

Figure 11: Example of C's atomic trajectory at T=900K for 100000steps

Its linear relation with the residence time could be proved by drawing the graphic of $< r^2 >$ as a function of time t.

The theoretical relation between r^2 and t could be described with the formula:

$$< r^2 >= 6Dt \tag{4}$$

where:

- r is the displacement of carbon;
- D is the C diffusion coefficient;
- $t$is the diffusion time.

The diffusion coefficient, at a fix temperature, can thus be obtained from the slope of Eq. (4).

Take an example at 900 K here in Figure 12, MSD is mean square displacement$< r^2 >$, the slope of the curve is 6D. So by the figure, the diffusion coefficient at 900 K is calculated to be 2.93×10^{-14} cm^2/s.

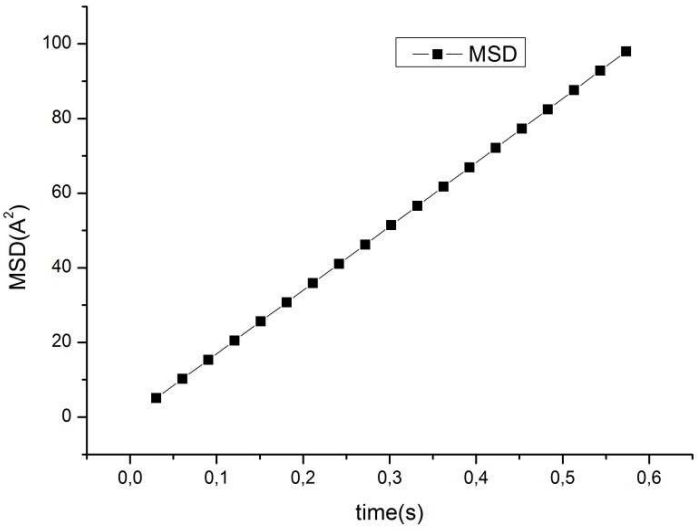

Figure 12: The mean square displacement of carbon atom at 900 K.

After doing the same simulations for different temperatures from 700 K to 1100 K, the diffusion at different temperatures were calculated and summarized in Table 8.

Temperature (K)	Diffusion coefficient (cm^2/s)
700	1.72×10^{-17}
800	1.13×10^{-15}
900	2.93×10^{-14}
1000	3.97×10^{-13}
1100	3.34×10^{-12}

Table 8: Different diffusion temperatures of carbon atom at different temperatures in the monoclinic zirconia

The relation between diffusion coefficient and the effective activation energy can be obtained using Eq. 5:

$$D = D_0 \exp\left(-\frac{E_{act}}{k_B T}\right) \tag{5}$$

where:

- D is the diffusion coefficient;
- D_0 is the prefactor of D;
- T is the temperature;
- E_{act} is the effective activation energy.

Indeed, Eq. 5 can be changed as Eq. 6 to find the linear relation between lnD and $1/T$.

$$lnD = lnD_0 - \frac{E_{act}}{k_B T} \tag{6}$$

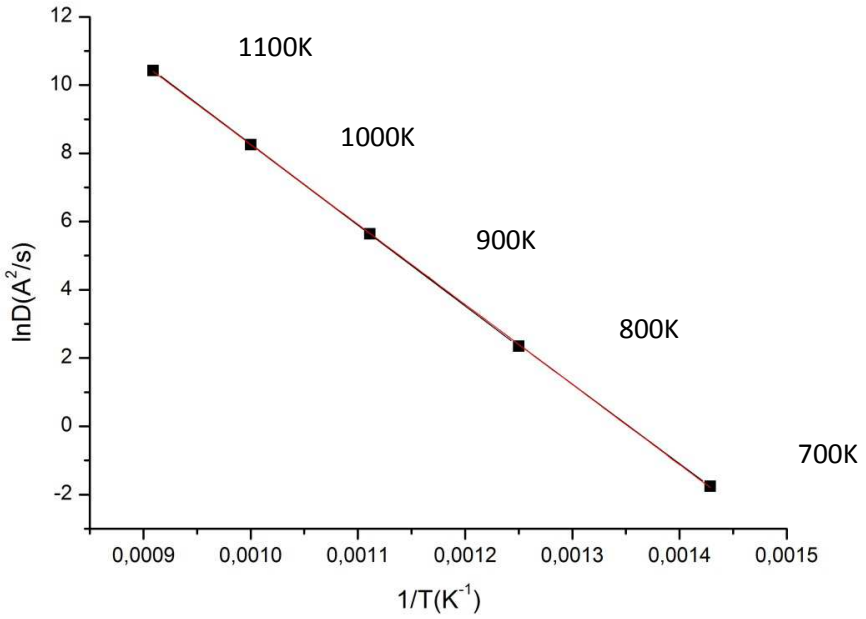

Figure 13: linear relation between lnD and 1/T from KMC simulations

I.2.B Determination of the Diffusion coefficient

By applying the formula on the calculation results in different temperatures (Figure 13), the prefactor of diffusion coefficient D_0 was calculated as 6.02×10^{-3} cm^2/s and the effective activation energy of carbon's diffusion turned out to be 2.02 eV, leading to:

$$D = 6.02 \times 10^{-3} (cm^2/\mathrm{s}) \exp\left(-\frac{2.02\ eV}{k_B T}\right) \qquad (7)$$

By looking at the carbon trajectory, the carbon diffusion pathway is through: O site → BT_d site → BT_d site → BT_d site (n times) → O site….

The storage temperature condition for the used fuel claddings is at around 50°C, so the diffusion coefficient of a carbon by interstitial mechanism in perfect Zr crystal at this temperature is calculated to be ~10^{-34} cm^2/s.

I.3 Conclusion

The calculated diffusion coefficient is so small that we could conclude the carbon in perfect Zr bulk would be blocked in it since it is very hard for carbon to diffuse and so to exit from an ideal zirconium bulk structure.

Comparing our result with the experimental value, for C diffusion in Zr, the experimental diffusion coefficient at 923 K is about 5.1×10^{-15} cm^2/s [R. P. Agarwala 1975] and in our calculation at 923 K the carbon diffusion coefficient is 5.6×10^{-14} cm^2/s which has a good agreement.

II: Carbon behavior in zirconium bulk with point defects

So far, the carbon behavior in the zirconium bulk had been studied. In the fuel claddings, there is not perfect zirconium but point defects are present especially under and after irradiation. So it is important to study the effect of vacancy on C behavior in the bulk. All the calculations of defects were performed on the 96 atomic zirconium supercell.

II.1. Zr vacancy in pure Zr bulk

The formation energy to form an atomic vacancy was calculated using the Eq. 8:

$$E_{vacancy} = E_{cell(with\ vacancy)} + E_{Zr} - E_{cell} \quad (8)$$

where:

- $E_{cell(with\ vacancy)}$ is the total energy of the 95 atomic zirconium supercell with a Zr vacancy in it;
- E_{Zr} is a zirconium atom's energy in the 96 atomic zirconium supercell;
- $E_{cell}$is the total energy of the 96 atomic zirconium supercell.

The formation energy to form a zirconium vacancy is 1.87 eV. The value has a good agreement with previous theoretical ones 1.90 eV and 1.86 eV which were obtained by using DFT simulations [P. Gasca 2010, C. Domain 2005].

II.2. Substitution of Zr by carbon

In the case of substitution in zirconium, a carbon was placed in the position of a Zr vacancy. The total energy after geometrical optimization was noted as $E_{C\text{-}Zr(with\ substitution)}$.The formation energies of C in a Zr vacancy were calculated using the Eq. 9:

$$E_{sub} = E_{C-Zr(with\ substitution)} - [E_C + E_{cell(with\ vacancy)}] \quad (9)$$

where:

- $E_{C-Zr(with\ substitution)}$is the total energy of 96 atomic supercell with a Zr substitution by one carbon;
- $E_C$is the reference carbon atom's energy in a diamond crystal;
- $E_{cell(with\ vacancy)}$is the total energy of the 95 atomic zirconium supercell with a Zr vacancy.

The formation energy is 1.82 eV for a C substitution in a Zr vacancy position. So, the carbon atom is less stable in the position of a zirconium vacancy than in an interstitial position (by 3.52 eV relative to O site). A carbon atom always preferred to be in an interstitial position than to be in a substitution one.

II.3 Interstitial carbon with a nearest Zr vacancy

In this last part, the Zr vacancy effect on the formation energy of an interstitial C has been investigated using Eq. 10:

$$E_{int-vacancy} = E_{C-Zr(with\ vacancy)} - [E_C + E_{cell(with\ vacancy)}] \quad (10)$$

where:

- $E_{C-Zr(with\ vacancy)}$is the total energy of 96 atomic supercell with a nearest Zr vacancy from an interstitial carbon;
- $E_C$is a carbon atomic energy in a diamond crystal;
- $E_{cell(with\ vacancy)}$is the total energy of the 95 atomic zirconium supercell with a Zr vacancy.

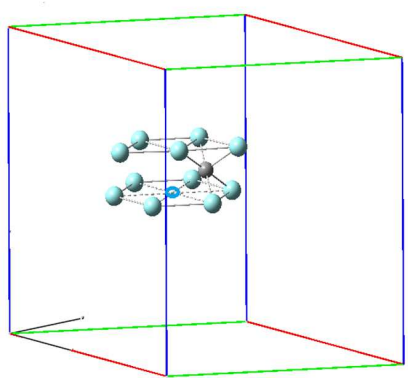

(a)

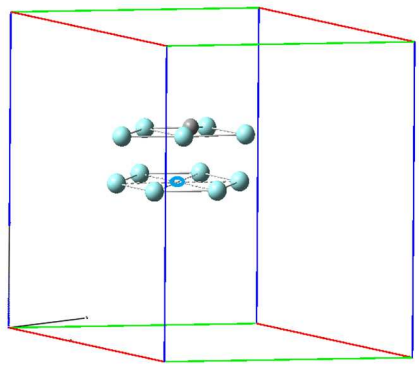

(b)

Figure 14: A C in interstitial site (gray color) with a neighbor Zr vacancy (blue cycle) in the 95 atomic zirconium supercell. a: C in O site with a neighbor Zr vacancy; b: C in BT_d site with a neighbor Zr vacancy

Different interstitial positions within the vacancy have been investigated, close to O, and BT_d.

The result of formation energies turned out to be -0.85 eV for C in O site and 0.46 eV for C in BT_d site when there is a nearby vacancy (Figure 14).

It showed that the carbon is relatively stable at the interstitial O site even when there is a nearby vacancy, comparing with the substitution formation energy 1.82 eV. So it was more stable for C to be in the interstitial position than in the substitution. However, considering the -1.70 eV formation energy for C in O site for an interstitial carbon without a vacancy, it is found that the carbon is getting less stable when it is near the vacancy.

II.4 Vacancy effect on carbon diffusion by calculation of binding energy

This conclusion can also be found by calculating the binding energy. The binding energy is the interaction energy between the vacancy and the interstitial carbon. It can be calculated using Eq. 11:

$$E_{binding} = (E_{c-Zr} + E_{cell(with\ vacancy)}) - (E_{C-Zr(with\ vacancy)} + E_{cell}) \qquad (11)$$

where:

- $E_{C-Zr(with\ vacancy)}$is the total energy of 96 atomic supercell with a nearest Zr vacancy from an interstitial carbon;
- E_{C-Zr} is the total energy of a 96 atomic zirconium supercell with a carbon atom in an interstitial position;
- $E_{cell(with\ vacancy)}$ is the total energy of the 95 atomic zirconium supercell with a Zr vacancy;
- $E_{cell}$is the total energy of the 96 atomic zirconium supercell.

The vacancy-carbon binding energy is -0.86 eV considering C in O as reference (Table 9). The negative value means that it is less stable when the carbon interstitial has a vacancy nearby than the carbon interstitial is far away from the vacancy.

Energy (eV)	Zr_4 E_{for}	Zr_4 E_b	Zr_12 E_{for}	Zr_12 E_b
Subs	1.82	-3.50	1.90	-3.56
BT_d	0.46	-2.16	0.41	-2.09
O	-0.85	-0.86	-0.86	-0.83

Table 9: Vacancy – carbon formation energy (E_{for}) and binding energy (E_b) for substitution and interstitial with a nearby vacancy (in eV)

Therefore, it can be said that the closer an inserted carbon is to a Zr vacancy, the less stable it is. So the carbon always prefers to stay away from zirconium vacancies. In the hand of diffusion, we can say that the zirconium vacancy wouldn't decrease the carbon diffusion.

Conclusion

We have calculated the carbon diffusion coefficient in pure Zr bulk to model the carbon behavior in used fuel claddings by coupling atomic and macroscopic scale simulations. For the DFT atomic scale simulation, a 96 atomic hcp zirconium supercell was considered. Two types of stable interstitial sites for carbon were found: BT_d site which is less stable than the O site by 1.45 eV for Zr_4. The migration energies calculated from the DFT-NEB approach showed that the easiest migration pathway for diffusion should be the successive diffusion between BT_d site and O site. Then, the attempt frequencies for each possible jump were calculated in order to get, from the transition state theory, the migration rates between each two neighbor sites.

In a second step, a macroscopic simulation by the Kinetic Monte-Carlo approach (KMC) was performed using jump probabilities. From the KMC simulations at different temperatures, the effective activation energy as well as the diffusion coefficient as a function on temperature was calculated. It was found that 2.02 eV effective activation energy corresponded to the lowest migration energy path: O site → BT_d site → BT_d site → BT_d site (n times) → O site → BT_d site… (compared to O site → O site path) The C diffusion coefficient in perfect Zr crystal, at the maximum storage temperature (50°C), is calculated to be very small (~10^{-34} cm^2/s). Therefore, in this condition, it will be very difficult for a carbon atom to diffuse in a perfect Zr crystal. However, even though there arevacancies in Zr, it was calculated that the C stability decrease when it gets closer to a Zr vacancy. Therefore, the zirconium with vacancies wouldn't increase the carbon diffusion by the interstitial diffusion mechanism. Carbon would be blocked in the bulk zirconium.

References

[R. P. Agarwala 1975] R. P. Agarwala, A. R. Paul, Journal of Nuclear Materials, 58, 25-30 (1975)

[C. S. Becquart 2010] C. S. Becquart, C. Domain, Phys. Status. Solid. B, 247, 9-22 (2010)

[C. Domain 2005] C. Domain, and A. Legris, Philosophical Magazine, 85, 569-575 (2005)

[C. Domain 2006] C. Domain, Journal of Nuclear Materials, 351, 1-19 (2006)

[J. R. Fernandez 2000] J. R. Fernandez, A.M. Monti, R.C. Pasianot, and V. Vitek, Philosophical magazine A, 80, 1349-1364 (2000)

[P. Gasca 2010] P. Gasca, PhD, University Lille 1 (2010)

[M. Iwasawa 2008] M. Iwasawa, T. Ohnuma, and N. Soneda, Materials Transactions, 49, 2765-2769 (2008)

[H. Jonsson 1998] H. Jonsson, G. Mills and K.W. Jacobsen, Classical and quantum dynamics in condensed phase simulations, World Scientific Inc, 385-404 (1998)

[C. Kittel 2005] C. Kittel.Introduction to Solid State Physics, 8th edition. Hoboken, NJ: John Wiley & Sons Inc, Berkemey 50 (2005)

[K. Kobashi 2005] K. Kobashi , Structure of diamond, Diamond films: chemical vapor deposition for oriented and heteroepitaxial growth, Elsevier, 9, (2005)

[A. C. Lawson 2007] A. C. Lawson, D.P. Butt, J.W. Richardson, et al., Philosophical Magazine, 87, 2507-2519 (2007)

[LI 2013] R. Li, internship report of master, Orsay, 2013

[D. R. Lide 1998] D. R. Lide, Handbook of Chemistry and Physics (87 ed.), Boca Raton, CRC Press, 4–96, (1998)

[H. J. Mcskimin 1972] H. J. Mcskimin and P. Andreatch, Jr., J. Appl. Phys. 43, 985 (1972)

[G. E. Murch 1979] G.E. Murch, Acta Metallurgica, 27, 1701-1704 (1979)

[B. Olinger 1973] B.Olinger and J.C.Jamieson, High Temp. High Pressures, 5, 123-131, (1973)

[R. C. Pasianot 2009] R. C. Pasianot, R.A.Perez, V.P. Ramunni, et al., Journal of Nuclear Materials, 392, 100-104 (2009)

[R. A. Perez 2008] R. A. Perez, M. Weissmann, Journal of Nuclear Materials, 374, 95-100 (2008)

[N. Poletz 2006] N. Poletz, A. Legris, C. Domain, MATERIAUX (2006)

[F. Vines 2005] F. Viñes, C. Sousa, P. Liu, et al., The journal of chemical physics, 122, 174709 (2005)

[F. Vines 2005] F. Viñes, C. Sousa, P. Liu, J. A. Rodriguez, and F. Illas, The Journal of chemical physics, 122, 174709 (2005)

[V. P. Zhukov 1985] V. P. Zhukov and V. A. Gubanov, J. Phys. Chem. Solids 46, 1111, (1985)

Chapter 3

Carbon Diffusion in the bulk monoclinic zirconia

Introduction

In the previous chapter, the carbon diffusion coefficient in hcp zirconium has been calculated. Since the external part of zirconium cladding contacts with water, it will form an oxide layer composed of monoclinic zirconia and tetragonal zirconia. At the storage temperature, monoclinic zirconia is the most stable phase in the oxide layer, so this phase is chosen to perform the carbon diffusion behavior. As the same as zirconium, the simulations are performed in bulk in this chapter.

On the one hand, some experiments have proved that the monoclinic structure is the most stable one for zirconia [A.S.Foster 2001].

On the other hand, some DFT calculations have been performed for zirconia, either monoclinic structure or tetragonal structure[G. Stapper 1999, G. M. Hood 1993, H. Jiang 2010]. The static simulations were used to confirm the good geometrical parametersand structures of zirconia. The theoretical results are in a good agreement with some experiments, such as the parameters of zirconia. However, theyarenotin agreement with other experimental results, such as the activation energy. In this work, the theoretical results will be compared to the experimental results and other theoretical ones.

In this chapter, the carbon diffusion calculations were performed with multi-scale approach in bulk zirconia. For the pure bulk, the diffusion by interstitial mechanism will be studied. Different interstitial sites for carbon will be investigated and the atomic jumps between interstitial sites will be calculated through the migration energies and transition rates. The macroscopic scale simulations using KMC method will be performed to evaluate the diffusion coefficient at storage temperature. However, there are vacancies in the oxide layer after irradiation. So, the diffusion by vacancy mechanism will also beinvestigated. First, the self-diffusion of O will be calculated. Calculations will also be performed to investigate the possibilities of carbon diffusion by vacancy mechanism.

I Carbon behavior in perfect zirconia

I.1 Atomic scale simulations

The study of carbon behavior in monoclinic zirconia is performed as the one in bulk zirconium, by using the multi-scale simulations: the atomic jumps with DFT simulations at

the atomic scale, and the diffusion with KMC approach at the macroscopic scale. So at first, a unit cell of monoclinic zirconia will bebuilt to study carbon diffusion.

I.1.A Optimization of zirconia calculation parameters

To do the simulation of carbon behaviour in zirconia, a 12 atomic cell will be built which is the smallest cell to model the monoclinic zirconia. To decide which pseudopotential set can better describe the structure of monoclinic zirconia, different pseudopotentials were used for Zr, O and finally ZrO_2.

The optimization of bulk zirconium (which is also hexagonal close packed phase here) was done in Chapter II, Part I.1. Both Zr_4 and Zr_12 can well describe the hcp structure of zirconium except Zr_12 which demands higher cut-off energy to convergebothforce and energy. So the next step is to choose the pseudopotential set of Zr/O to better describe the monoclinic zirconia.

For pseudopotential of O, two kinds of pseudopotentials were tested: O_s and O_h which both contains 6 valence electrons. Since O_h demands an higher cut-off energy to arrive the convergence of geometrical parameters, O_s is better to describe the O_2 molecule.

For ZrO_2, different pseudopotentials were compared separately for Zr and O. So now it is important to estimate the different pseudopotential set to verify which one can better describe the Zr-O bond.

Monoclinic zirconia has a structure with space group P21/c (Figure 1)[G. M Rignanese 2005, C. J. Howard 1988].The model of 12 atoms was built with atomic coordinates in Wyckoff notation (x, y, z), (-x, y+1/2, 1/2-z),-(x, y, z),-(-x, y+1/2, 1/2-z).In the bulk structure, there are two types of O, the first has three bonds with zirconium, noted as O1, and the other one has four bonds with zirconium noted as O2. The zirconium is six coordinated by the oxygen atoms (Figure 2).

The convergence of the total energy were tested with different k-points and different cut-off energies for the 4 sets of pseudopotentials, (Zr_4/O_s), (Zr_12/O_s), (Zr_4/O_h), and (Zr_12/O_h).Different total energies with different geometrical parameters a, b, c were calculated, to evaluate the proper values of $E_{cut\text{-}off}$ and cell parameters which can well describe the monoclinic zirconia.

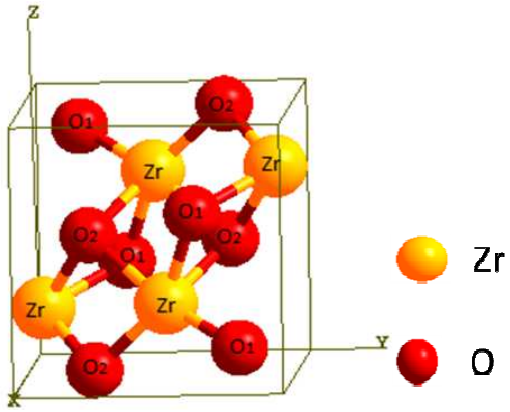

Figure 1: The 12 atomic supercell of monoclinic zirconia

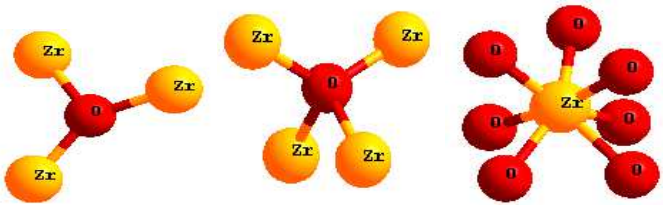

(a) **(b)** **(c)**

Figure 2: The structure of O1 (a), O2 (b), and Zr (c) with the neighbor atoms

* For (Zr_4/O_h/) and (Zr_12/O_h/), the situations are similar. The cell parameters still do not converge while the cut-off energy is already as high as 700eV.

* For (Zr_4/O_s) and (Zr_12/O_s), the total energy and the geometrical parameters of the unit-cell begin to converge at $E_{cut\text{-}off}$= 350 eV. There is no significant difference of the total energy with different k-points grids. The 5×5×5 k-points grid is chosen. Here are the figures of total energy and geometrical parameter for the pseudopotential set Zr_4/O_s (Figure 3 and Figure 4).

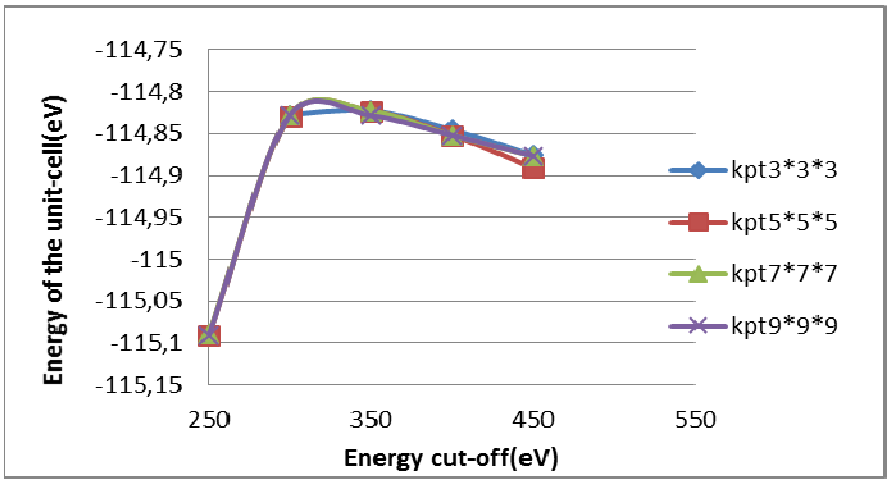

Figure 3: The total energy of the zirconia unit-cell with different k-points and $E_{cut-off}$ for (Zr_4/O_s)

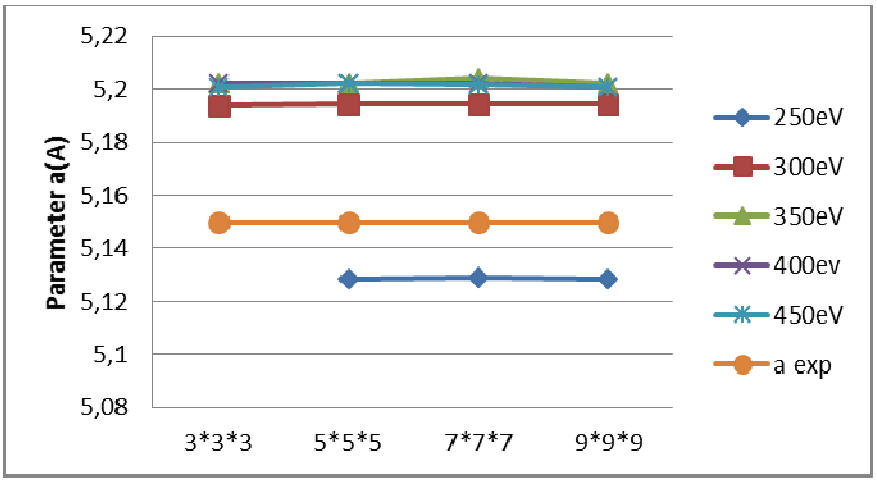

Figure 4: Lattice parameter of the monoclinic structure with different k-points and $E_{cut-off\ for}$ (Zr_4/O_s)

Geometrical parameters	Zr_4 O_s	Zr_12 O_s	Exp [Ref G. M. Rignanese 2005, C. J. Howard 1988]
b/a	1.01	1.01	1.01
c/a	1.03	1.03	1.03
a (Å)	5.20	5.21	5.15

Table 1: Geometrical parameters of the monoclinic zirconia for different pseudopotential sets

At 350 eV, the Zr with 4 e^- orthe Zr with 12 $e^-$with O_s have similar results, comparing to the experimental data (Table 1). But Zr_12 which contains more valence electrons need more calculation time.

Since the set of pseudopotentials Zr_4 and O_s seems to be a goodchoice in this part, it was chosen to optimize the ZrO_2cubic and tetragonal structure.

I.1.B Study of relative stability of the three phases of ZrO_2(tetragonal, and cubic)

ZrO_2 has 3 types of structures: monoclinic, tetragonal, cubic. Now, the optimizations of parameters for structure cubic and tetragonal are also performed to study their stabilities.

- Cubic ZrO_2

For cubic ZrO_2, the 12 atomic supercell is composed with 4 motifs of 3 atoms with space group fm3m (Figure 5)[C. J. Howard 1988].

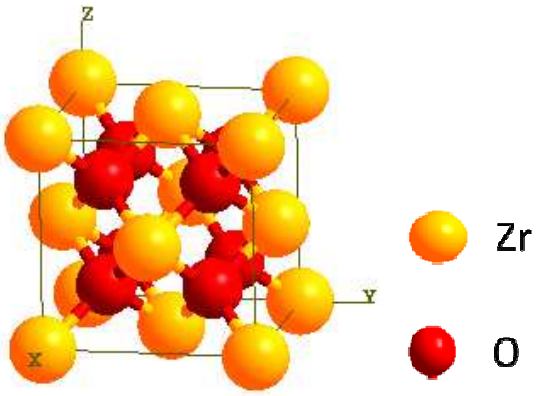

Figure 5: Cubic Zirconia structure

The influence of the different k-points grids in the Brillouin zones and different cut-off energies to the total energy of the 12 atomic supercell from 3×3×3 to 9×9×9 are showed in Figure 6 and Figure 7.

After relaxation, the value chosen for parameter calculations of cubic zirconia is k point grid 5×5×5 with $E_{cut\text{-}off}$=350eV. The optimized parameters are listed in Table 2. Comparing with the other DFT calculation results and experiment data, they have good correlation.

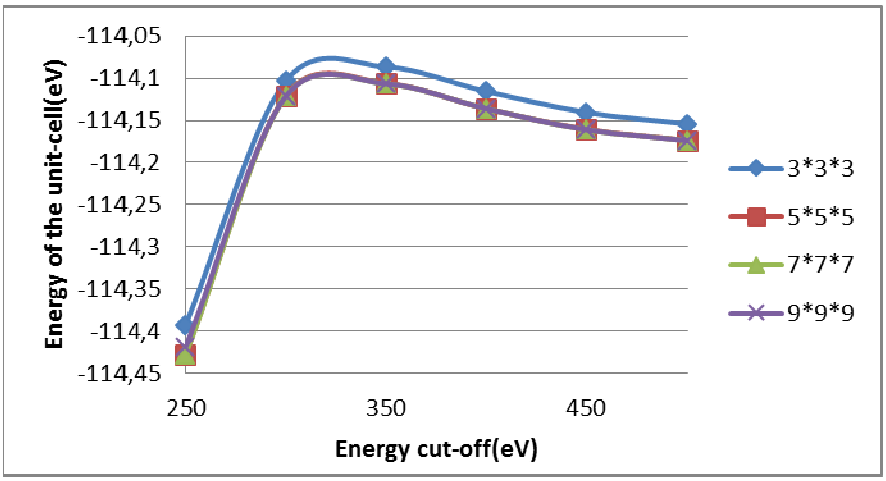

Figure 6: The energy of a cubic structure unit-cell ZrO_2 with different k-points and Ecut-off

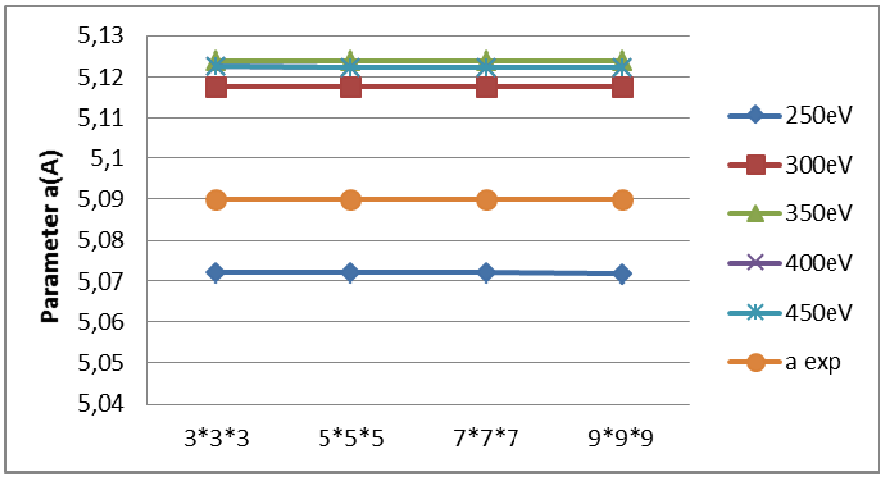

Figure 7: Cell geometrical parameter of cubic structure $ZrO_2$with different k-points and $E_{cut-off}$

Geometrical property	calculated	DFT [A. S. Foster 2001, G. Jomard 1998]	Experimental [Ref C. J. Howard 1988]	Δd % (calculated-exp)
a(Å)	5.12	5.09 / 5.15	5.09	0.59
Motif volume($Å^3$)	33.60	32.97 / 34.06	32.97	1.91

Table 2: Geometrical parameters of the cubic zirconia

- Tetragonal ZrO_2

For ZrO_2 tetragonal, the 6 atomic cell which is the smallest structure to reproduce the tetragonal bulk is composed of 2 motifs of 3 atoms with space group P42/nmc, parameters a=b≠c (Figure 8). The oxygen atoms were displaced by pair along the z direction which the

distance is noted as dz. The report of c/a is set to be 1.414 before optimization [C. J. Howard 1988].

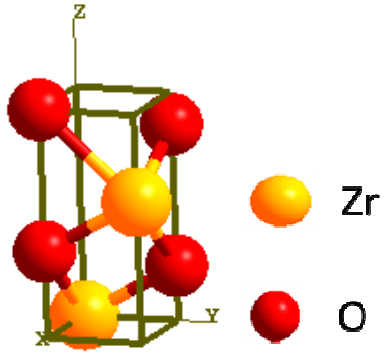

Figure 8: Tetragonal Zirconia structure

As the same as in the case of bulk cubic ZrO_2, the convergence of the total energy was tested with the different k-points meshes and different cut-off energies. It was found that the total energy of the unit-cell begins to converge at 5×5×5, and the geometrical parameters begin to converge at $E_{cut\text{-}off}$ = 400 eV. The optimized structural parameters were compared with other work in Table 3. The calculated values are in agreement with the DFT results from the literature.

Cell parameters	calculated	DFT [Ref G. Jomard 1998]	Exp [Ref C. J. Howard 1988]	d % (calculated-exp)
a (Å)	3.63	3.63	3.57	1.68
c/a	1.44	1.45	1.45	-0.69
Dz	0.05	0.05	0.06	-16.66
Motif volume($Å^3$)	33.00	34.55	34.07	-3.14

Table 3: structural parameters of the tetragonal zirconia

To study the relative stability of the three ZrO_2 structures, the cohesive energy of the three phases were also calculated and compared by using the formula:

$$E_{cohesive} = E_{supercell} - [N_{Zr}E_{Zr-bulk} + N_O(E_O)] \quad (1)$$

where:

- $E_{cohesive}$ is the cohesive energy of supercell;
- N_{Zr} is the atom numbers of Zr in the supercell;

- $E_{Zr-bulk}$ is the atomic energy of Zr in hcpzirconium;
- N_O is the atom number of O in the supercell;
- $E_O$is the atomic energy of O in molecular O_2.

The cohesive energiesfor the cubic, tetragonal, monoclinic structures are respectively-11.51 eV, -11.57 eV and -11.69 eV for a 12 atomic supercell respectively, which are ina good agreement with the available experimental values: -11.26 eV for cubic structure and -11.68 eV for the monoclinic structure, turning out that the monoclinic is the most stable structure, which corresponds to the experimental results [C. Arhammar 2009].

Structure	Cubic	tetragonal	monoclinic
Calculated (eV)	-11.51	-11.57	-11.69
DFT [A. S. Foster 2001]	-10.96	-11.04	-11.15
Exp[C. Arhammar 2009]	-11.26	/	-11.68

Table 4: Cohesive energy (in eV) for the three phases of zirconia

So as showed in Table 4, the relative stability of the three phases are in the flowing order:

monoclinic> tetragonal > cubic

The resultsarein good agreement with the experimental and theoretical ones, showing that our calculations can correctly describe the ZrO_2structures.

As discussed above, ZrO_2 could adopt various phases in different ranges of temperature and pressure. In particular, the three low pressure phases: cubic, tetragonal, and monoclinic structures have been extensively studied for both their scientific and technological importance [F. F. Lange 1992, G. Teufer 1962]. At ambient pressure, ZrO_2 has a monoclinic structure up to a temperature of 1450K [J. D. Mccullough 1959]. At temperature higher than 1450K, the monoclinic to tetragonal transition occurs with a decrease in unit cell volume since the 7-fold coordination in monoclinic phase of Zr changes to 8-fold in tetragonal phase[M. Wilson 1996]. For the cubic structure, it is only thermodynamically stable at temperatures higher than 2650 K [O. Ruff 1929]. All the transition results are ina good agreement with the stability evaluation by using Eq.1. Therefore, the phase transition mechanisms have been well understood through modeling studies and experimental observations.

I.1.CMonoclinic zirconia supercell construction

Since there is low concentration of carbon in monoclinic zirconia, to simulate a carbon atom behavior, it is necessary to construct a larger size of zirconia supercell. Moreover, to perform calculation in constant volume, the relaxation of the supercell has to be refigured when one carbon atom is inserted.

To compare the results with other literature calculation ones [A. S Foster 2001, G. Jomard 1998], the most used supercell in the references contains 96 atoms and only 3.27% volume relaxation was chosen to perform the calculations (Figure 9). It was extendedfrom the 12 atomic supercell by two in each directions.

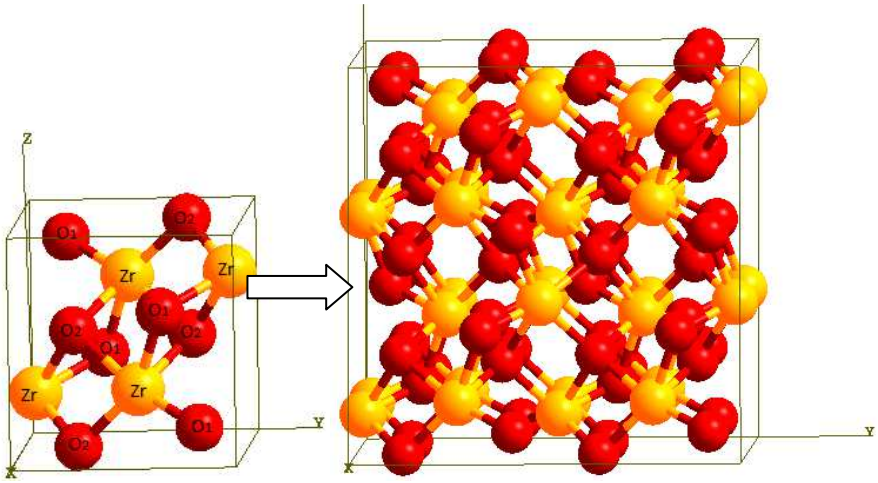

Figure 9: 96 atomic supercell of monoclinic zirconia extended from the 12 atomic cell

Geometrical parameters of the supercell were optimized with different k-point grids and cut-off energies. 2×2×2 and 350 eV were chosen to do the carbon interstitialinvestigation.

I.1.D Investigation of carboninterstitials in the supercell of zirconia

Once building a supercell of monoclinic zirconia, a carbon atom isinserted to investigate its possible interstitial sites to study its diffusion behavior. In the Chapter II, different pseudopotential sets were used for the ZrC structure, and Zr_4/C_s pseudopotential set was found to correctly describe the Zr-C bond. So in the simulation of carbon in bulk monoclinic zirconia, the same pseudopotential of C is used: C_s.

In order to know the stability of a carbon in the model of ZrO_2 monoclinic, the possible positions to insert it should be investigated.

At first, a carbon is inserted in the center of different available volume cages and optimized to find its minimum energy state. But it was found that for one cage, since the anisotropic character of monoclinic structure through the three directions x, y and z, there are different interstitial sites in one volume cage. By this method, the possible interstitial sites could not be completely found. So the investigation of interstitial sites should be performed by the way of a code.

Therefore, a code was developed and performed on the 12 atomic supercell in the 96 atomic supercell to find all the possible interstitial sites. The 96 atomicsupercell was equally separated by 20 times in each direction. Since the supercell is made by a 12 atomic cell extended by 2 in each direction, the 12 atomic cell is separated by 10 (Figure 10), and each grid is a cubic cage with dimension about 0.5 Å×0.5 Å×0.5 Å.

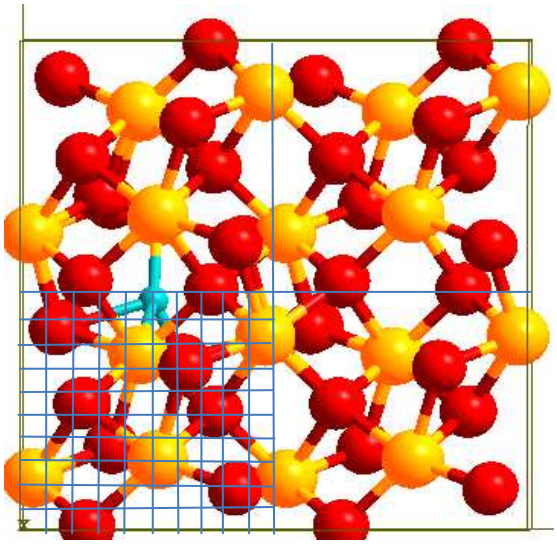

Figure 10: The small grids for the monoclinic supercell (10 times of separation for the 12 atomic supercell)

First, a carbon was put in a random position of each small cubiccell with reasonable distance C-O (>1,3 Å) and C-Zr(>1.9 Å), the cut-off energy is set to be 300 eV and k points mesh is 1×1×1, then it was optimized to get the total energy convergence and geometrical parameters convergence.

Then at the second step, the optimized carbon was displaced by about 0.2 Å separately by the direction x, y, and z. The carbon in the new direction will be optimized again. If it gets back to the optimized position in the first step, it would be kept to verify its stability in the next step. If it goes to another position, then it would be deleted.

The third step is the last but also the most complicated step for carbon to verify if it is a possible interstitial position sites. For all the relaxed carbon positions, the vibration frequencies were calculated. If their values are all real (without imaginary value), it will bean interstitial site position for a carbon atom.

So by all the three steps performed by the code, 78 positions in the 12 atomic supercell are found. All their total energies and structures were analyzed. In Figure 11, the total energies of 96 atomic supercellfor carbon in the 78 positions are presented.

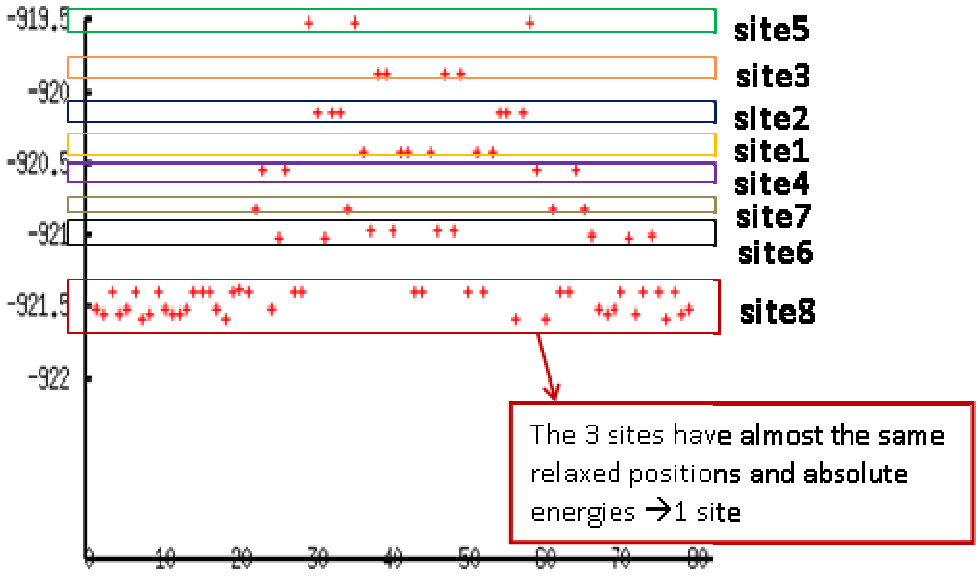

Figure 11: The founded positions with their total energies

There are 10 different system energies in the Figure 12. The three lowest ones have closed energies, similar structures, and they are closed within distance smaller than 0.2 Å. So to make the simulation simpler, only the most stable sites were kept, and the other two interstitial sites were considered to be the same position as the most stable ones (red color in Figure 11). After neglecting the two types of interstitial positions, the types of interstitial sites are still as many as eight. For each type of interstitial position, the structure around the interstitial carbon is analyzed in detail.

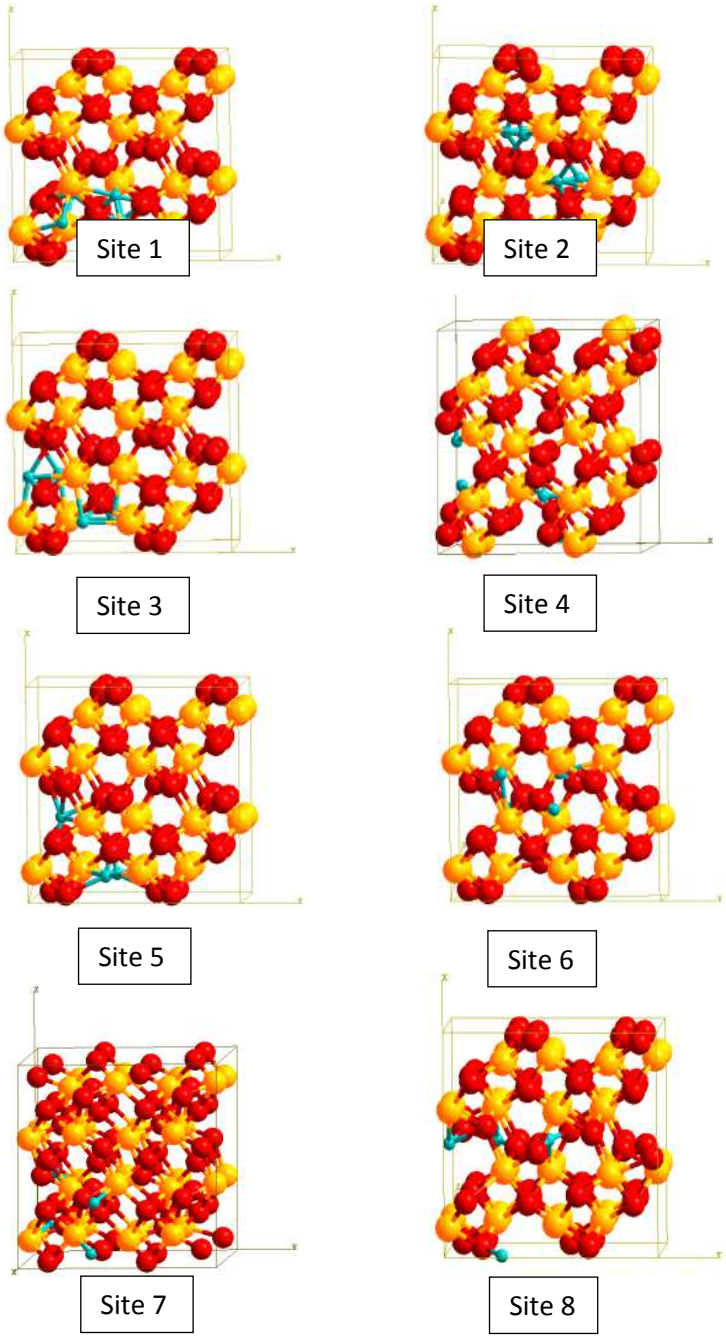

Figure 12: Eight types of interstitial sites in monoclinic zirconia

Eight distinct possible sites have been found in the monoclinic structure (Figure 12) and for each site there are four symmetric positions in the 12 atomicsupercell which have the same structure around carbon but in different orientations. Here as example, the four symmetrical positions of site 2 are presented in Table 5.

Estimation of the formation energy of an interstitial carbon atom was calculated by the formula:

$$E_I = E_{C-ZrO_2} - (E_C + E_{ZrO_2}) \quad (2)$$

The results of interstitial formations energies for the eight types of sites were listed in Table 6. The insertion formation energies are positive, which means $E_{C\text{-}ZrO2} > (E_C+E_{ZrO2})$. So considering diamond carbon as ground state, the insertion of an interstitial carbon is not favorable in the perfect ZrO_2 monoclinic bulk.

Site	structure	Distance (Å)
S2	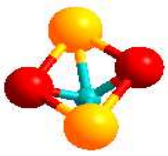	d(C-Zr)=1.98 / 2.00 d(C-O)=1.49 / 1.61
S2’		d(C-Zr)=1.92 / 1.96 d(C-O)=1.46 / 1.55
S2’’	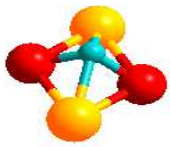	d(C-Zr)=1.95 / 1.98 d(C-O)=1.54 / 1.54
S2’’’	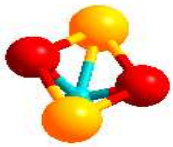	d(C-Zr)=2.17 / 2.16 d(C-O)=1.47 / 1.57

Table 5: Four symmetrical positions of site 2 with their structures around carbon

Site	1	2	3	4	5	6	7	8
N(site)	4	4	4	4	4	4	4	4
E_I(eV)	7.23	7.50	7.76	7.11	8.13	6.67	6.57	6.05

Table 6: E_I is the formation energy for the eight different interstitial sites of carbon in monoclinic zirconia. N is the number of equivalent site in the 12 atom supercell.

I.1.EMigration of C between two neighbor sites in the monoclinic zirconia without defects

Now, all the possible interstitial sites were investigated. In the monoclinic zirconia without defects, to calculate the carbon diffusion coefficient in bulk, the diffusion by interstitial

mechanism will be determined. Since the diffusion at atomic scale is atomic jumps, here in this part, the migration of carbon between different neighbor sites will be calculated. Starting from the interstitial sites investigated in the last part, the first step is to identify all the neighbor sites for each interstitial site. Since there are four symmetrical positions for one type of sites, for each interstitial site position, there are many neighbor sites. In the atomic jump, to make the migration simple to calculate, for one interstitial position, among all its neighbor sites, the atomic jump study will concentrate only the nearest neighbor position of each type, which means there are eight neighbor positions from the eight types of sites. So within the 12 atomic supercell, all the neighbor sites are identified with their corresponding migration vectors (Figure 13).

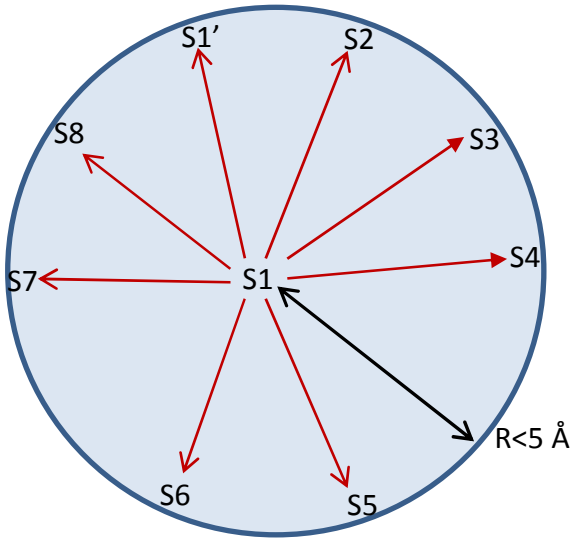

Figure 13: Example of site 1's neighbor sites

Then for each two neighbor sites, the NEB calculations are performed to test the possibility of migrations.

During the NEB calculation, the migration energies (E_{mig}) from one site to its neighbor site are firstly calculated with the migration vectors. For each migration, 8 imagepositions were built from the relaxed initial to thefinal equilibrium position. After the optimization the saddle points have been determined. It is found that for two neighbor sites, sometimes there is no direct migration path (the carbon would prefer to go to another neighbor site first), so it is not possible to do a direct atomic jump. For all atomic jumps, to study their jump probabilities, the attempt frequencies were also calculated, as in Chapter II.

All the migration barriers were calculated for all the possible atomic jumps and the results for energy barriers were listed in Table 7. For each possible atomic jump, the attempt frequencies were listed in Table 8. All the possible inserted sites were characterized and the migration probabilities between every two neighbor sites were calculated in monoclinic zirconia.

E_{mig}(eV) i/f	site 1	site 2	site 3	site 4	site 5	site 6	site 7	site 8
site 1	0.72	0.68	0.94	X	X	1.31	X	X
site 2	0.39	X	0.37	X	0.72	X	X	0.35
site 3	0.41	0.11	X	X	X	0.04	X	X
site 4	X	X	X	X	X	0.54	X	1.00
site 5	X	0.09	X	X	X	0.29	X	0.29
site 6	1.87	X	1.12	0.82	1.75	X	X	0.03
site 7	X	X	X	X	X	X	X	0.02
site 8	X	1.78	X	2.04	2.38	0.63	0.58	0.20

Table 7: The migration energies from site i to site f of the possible migration pathway in zirconia bulk (X means there is no direct migration path between the two neighbor sites）

Frequency (10^{13} s^{-1}) i/f	site 1	site 2	site 3	site 4	site 5	site 6	site 7	site 8
site 1	1.35	3.48	2.22	X	X	1.42	X	X
site 2	3.15	X	0.30	X	0.22	X	X	2.21
site 3	1.00	0.18	X	X	X	1.58	X	X
site 4	X	X	X	X	X	2.72	X	2.35
site 5	X	0.29	X	X	X	0.62	X	1.45
site 6	0.95	X	2.36	1.66	0.42	X	X	0,89
site 7	X	X	X	X	X	X	X	1.53
site 8	X	2.24	X	1.37	1.14	1.03	1.24	0.64

Table 8: The attempt frequencies from site i to site f for the possible migration pathway in zirconia bulk (X means there is no direct migration path between the two neighbor sites）

I.2 Macroscopic scale simulations

At the atomic scale, the migration vectors, migration energies and the attempt frequencies have already calculated to study atomic jumps. Then, at the macroscopic scale, the Kinetic Monte-Carlo method [H. Jonsson 1998] using the residence time algorithm can be used to determine the diffusion path and diffusion coefficient in the monoclinic zirconia.

First, the KMC calculation wasperformed from 300 K, it was found that carbon could not diffuse in three dimensions until 2500 K. So to study the carbon diffusion, the carbon's trajectories from 2500 K to 3500 K were calculated. The diffusion coefficients at each simulation temperature were calculated and listed in Table 9.

T(K)	D (cm^2/s)	lnD ($Å^2/s$)
2500	6.38×10^{-6}	24.88
2700	9.61×10^{-6}	25.29
3000	1.60×10^{-5}	25.80
3500	3.09×10^{-5}	26.46

Table9: Different diffusion coefficient at the simulation temperatures

The results of different diffusion coefficients as function of temperatures for C in pure monoclinic zirconia are in the Figure 14.

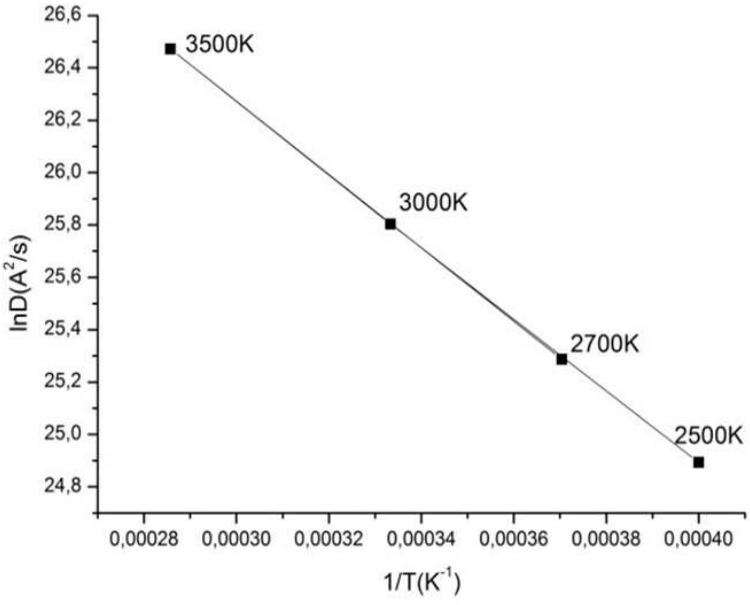

Figure 14: The diffusion coefficient of C in the perfectzirconia

So it corresponds to the formula, the prefactor D_0 equals to 1.6×10^{-3} cm^2/s and the effective activation energy E_{act} is 1.19 eV, leading to:

$$D = 1.6 \times 10^{-3}(cm^2/s)e^{-\frac{1.19\ eV}{k_B T}} \quad (3)$$

At the real storage condition, the higher final temperature is around 50 °C, the carbon diffusion in the perfect zirconia bulk at the storage condition was calculatedas $\sim10^{-22}$ cm^2/s. As example, in the claddings where the zirconia layer is about 50 μmof thickness, if a carbon atom is in the center of the oxide layer, it will take to the carbon 10^{11} years to go out from the zirconia layer. It provides that the carbon does not diffuse in the perfect ZrO_2 bulk at the storage temperature.

II Carbon behavior in zirconia with point defects

The carbon diffusion in perfect zirconia was calculated in the last part. However, in the real claddings, in the oxidation layer, there are point defects. So it is interesting to complete this study to analyze the vacancy effect on the carbon diffusion in zirconia.

II.1Vacancyand carbon substitution in the zirconia supercell

II.1.A Vacancy of O1, O2and Zr in monocliniczirconia

There are two types of oxygen in the ZrO_2 monoclinic: O1 which is three coordinated with zirconium and O2 which is four coordinated with zirconium (Figure 2). So a vacancy of O1, O2, and Zr would be first considered in the supercell of 96 atoms. The formation energies to form a vacancy werecalculated by the formula:

$$E_{vacancyx} = E_{cell(with\ vacancyx)} + E_x - E_{cell} \quad (4)$$

where:

- $E_{vacancyx}$: the formation energy for the supercell to form a vacancy x;
- $E_{cell(with\ vacancyx)}$:the total energy of supercell with a vacancy x;
- E_x: the atom energy of x, where x is the atom of vacancy;
- E_{cell}: the total energy of the pure supercell.

E_x was considered to be the atomic energy in the pure bulk for Zr (or C) and in themolecular O_2 for O. The formation energies for O1, O2, and Zr are calculated to 6.63 eV, 6.58 eV and 15.99 eV respectively (Table 10).

Comparing these formation values with the other theoretical values for a vacancy O1, O2, Zr which are 6.26 eV (5.88 eV), 6.15 eV (6.63 eV) and 16.44 eV (16.16 eV)[G. Jomard 1999, K. S. 1982 and J. X. Zheng 2007], it is shown that our calculations are ina good agreement.

Vacancy formation energy		DFT [G. Jomard 1999]	DFT [J. X. Zheng 2007]
v Zr	15.99 eV	16.44	16.16
v O1	6.63 eV	6.26	5.88
v O2	6.58 eV	6.15	6.63

Table 10: The different vacancy formation energies $E_{vacancyx}$in the monoclinic zirconia

For the formation energy results, the value is positive, which means the monoclinic zirconia is less stable when there is a vacancy. For Zr vacancy, the formation energy is larger than the one of an O vacancy, which provided a Zr vacancy less stable than an O vacancy. It is easier to form an O vacancy than a Zr one.

II.1.BSubstitution of O and Zr by carbon

Substitution calculationswere performed to verify whether a carbon prefers to stay in a vacancy or not. A carbon was positioned in the position of a vacancy O1, O2 or Zr. The total energy after geometrical optimization is noted as $E_{C\text{-}ZrO2(with\ substitution)}$.The energies to form the substitution were calculated by the formula:

$$E_{subx} = E_{C-ZrO_2(with\ substitution)} - [E_C + E_{cell(with\ vacancyx)}] \qquad (5)$$

where:

- E_{subx}: the formation energy for the supercell to form a vacancy x, where x is the atom of vacancy;
- $E_{C-ZrO_2(with\ substitution)}$: the total energy of the supercell with a carbon substitution;
- E_C: the atom energy of carbon;
- $E_{cell(with\ vacancyx)}$:the total energy of supercell with a vacancy x.

For the three kinds of carbon substitutions inO1, O2, and Zr positions, the formation energies are 3.06 eV, 3.33 eV, -7.02 eV respectively (Table 11).

Substitution energy	
sub Zr	-7.02 eV
sub O1	3.06 eV
sub O2	3.33 eV

Table 11: The different C substitution energies E_{subx}in the bulk monoclinic zirconia

So the carbon atom insertion in the position of a zirconium vacancy is very favorable. After comparing these formation energies with the interstitial energies (6.05 eV to 7.76 eV), it turned out that a carbon atom always preferred to be in a vacancy position than in an interstitial one. When there is an O vacancy, the carbon atom might diffuse by vacancy mechanism. The structure surrounding the carbon in the case of the substitution of type O1, O2 were almost like the structure before the insertion of carbon substitution.The substitution by C was three-coordinated or four-coordinated (Figure 15 panel a and Figure 15 panel b) and the relaxed distances are given. The C – Zr distances are around 0.1 Å larger than O – Zr distances. The configuration of Zr substitution is particular. After optimization, the carbon has a strong relaxation, and is not in the same position as the Zr vacancy but in the zone of the vacancy. The structure before and after the substitution are displayed (Figure 15 panel c). It can be seen that when there was no substitution, a Zr has 6 neighbor oxygen atoms. After it was substituted by a carbon atom, the carbon atom has only 2 neighbor oxygen atoms with formation energy -7.02 eV.

Since it is proved that carbon is stable as substitution of zirconium and there is more space in the substitution site, it should be tried to insert more than one carbon atoms in the site of a zirconium atom.The formation energies calculated by the Eq. (5) from one to four substitution carbon atoms were listed in Table 12.

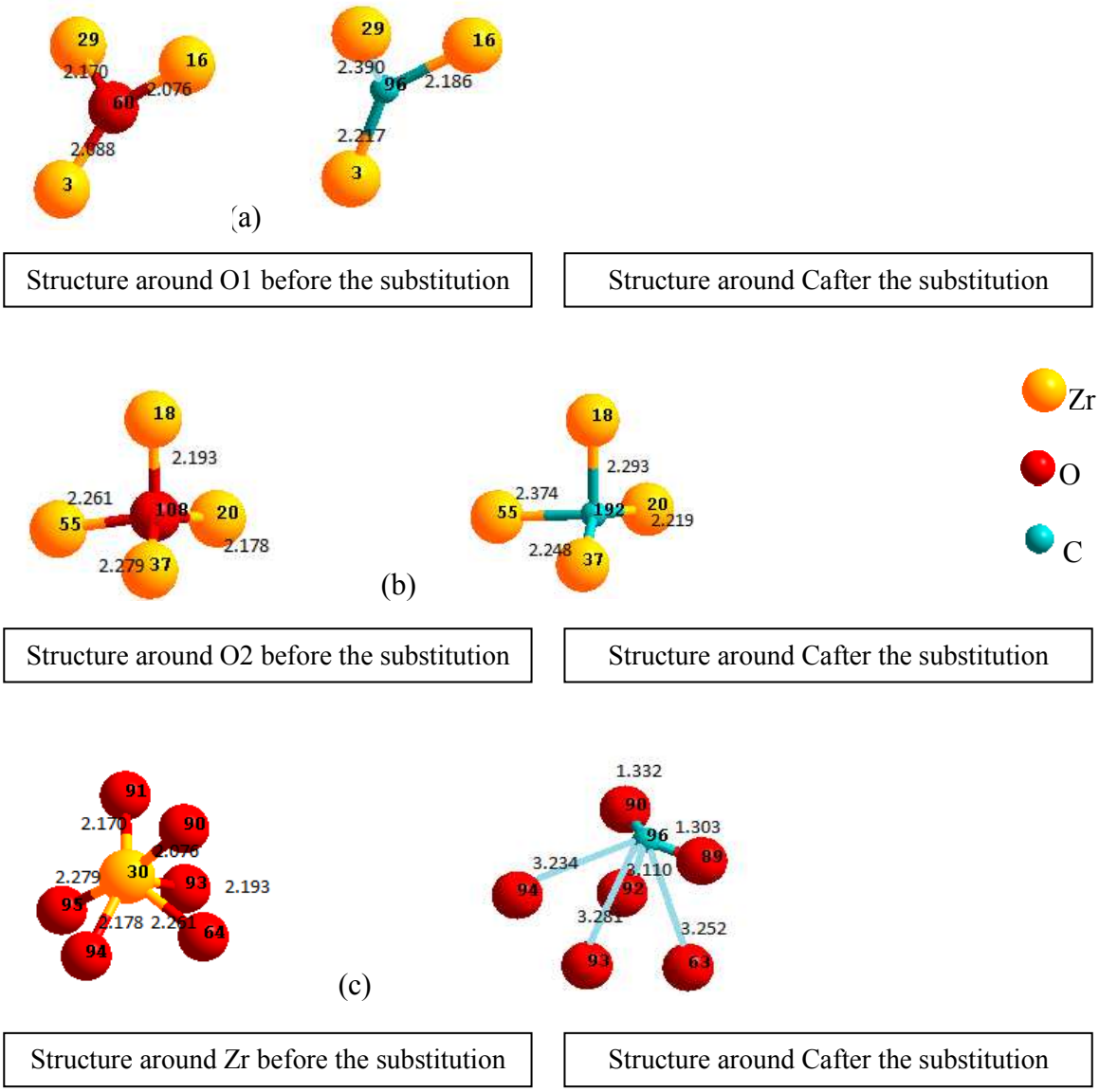

Figure 15: Structures before and after the carbon substitution

Since it is proved that carbon is stable as substitution of zirconium and there is more space in the substitution site, it should be tried to insert more than one carbon atoms in the site of a zirconium atom.The formation energies calculated by the Eq. (5) from one to four substitution carbon atoms were listed in Table 12.

N_{br} C	1	2	3	4
E_{sub}(eV)	-7.02	-5.53	-1.84	0.89

Table 12: The formation energy for different numbers of carbon in the Zr vacancy site

As we can see in Table 12, the formation energy is negative until the fourth carbon atoms was inserted in Zr vacancy site, which means the supercell was more stable when the carbons were in the vacancy site. All the carbon substitutions in the Zr vacancy site formed a framework in the space (Figure 16). Comparing with the formation energy of carbon in interstitial position, the inserted carbon atoms still preferred to be in Zr vacancy site than be in interstitial position. So if there are Zr vacancies in the zirconia, the carbon atoms will be trapped in the vacancy sites and it won't diffuse.

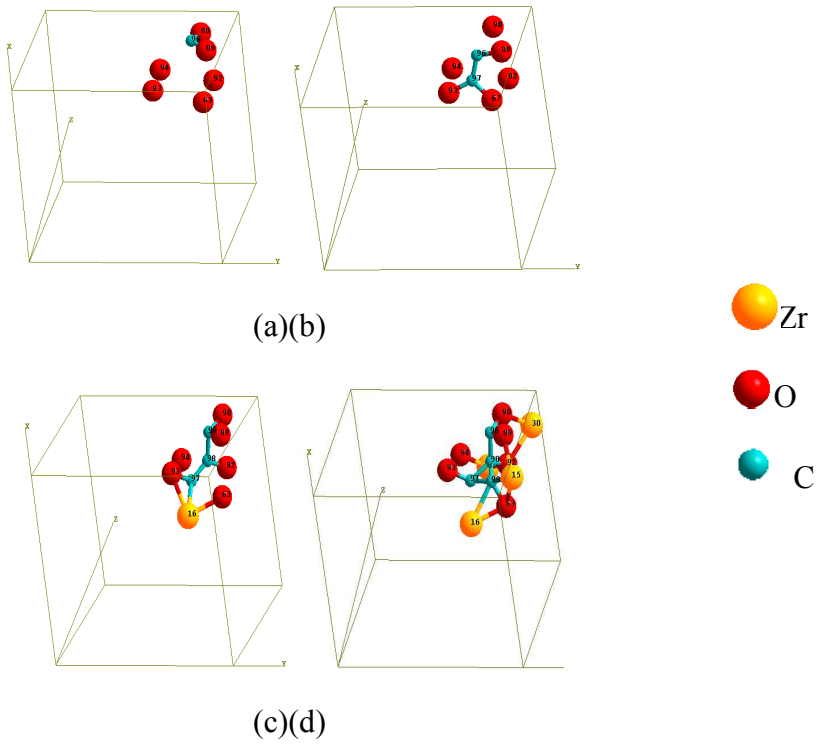

Figure 16: The framework of carbons in the position of a Zr vacancy (a) one C substitution; (b) two C substitutions; (c) three C substitutions; (d) four C substitutions.

II.1.C Migration by vacancy mechanism

In the previous part, the carbon is found to be more stable in the vacancy position than in an interstitial position. When there is a Zr vacancy, the carbon atom will be trapped in the vacancy. When there is an O vacancy, the carbon atom is more stable in the vacancy position than being in the interstitial sites. So it is necessary to test the possibility of carbon diffusion by oxygen vacancy mechanism in bulk zirconia.

To make the vacancy effect more clear, a model of an O vacancywith neighbor atoms were simulated (Because in the real condition, there are mostly O vacancies since the zirconia came from the oxidation reaction of zirconium.).

C-1Self-diffusion of O by vacancy mechanism without carbon

At first, in the 96 atomic supercell, an O vacancy was included to study the O migration by vacancy mechanism. Since there are two kinds of oxygen atoms in bulk monoclinic zirconia: one is three coordinated with neighbor zirconium noted as O1 and the other is four coordinated with neighbor zirconium noted as O2, the oxygen migration to an O vacancy wereperformed and summarized in two parts: O1 vacancy and O2 vacancy. All the migration barriers for the neighbor oxygen atoms were calculated.

1) Migration to a vacancy O1

As example, if atom No.35 was taken away to form an O1 vacancy, there are 10 neighbor O atoms (Figure 17)in the radius of 3.5 Å. There are five O1 atoms includingtwo symmetrical neighbor atoms No.34 and No.66, two symmetrical neighbor atoms No.44 and No.60, and one neighbor atom No.41.

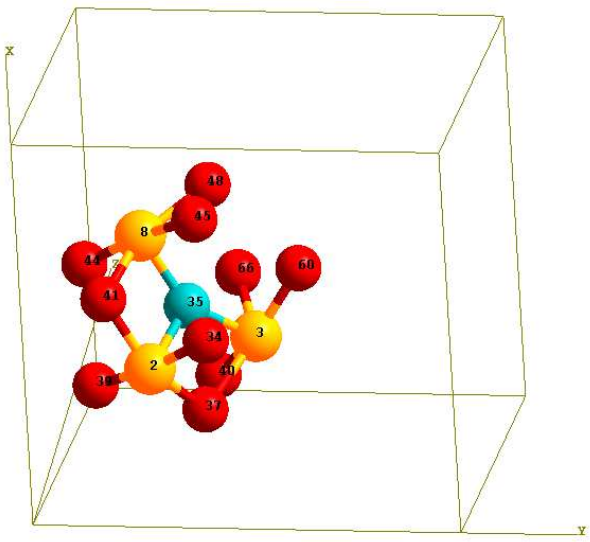

Figure 17: The neighbor O atoms around an O1 vacancy (blue position)

The distances between the O1 vacancy and neighbor O1 atoms were noted in red color in Table 13. There are also five neighbor O2 atoms: No.48, No.45, No.37, No.40 and No.39. The

distances between the O1 vacancy position and neighbor O2 atoms were noted in green color in Table 13.

Possible jumps	34/66 (O1)	44/60 (O1)	41 (O1)	48 (O2)	45 (O2)	37 (O2)	40 (O2)	39 (O2)
E_{mig}(eV) i→O1	1.29	1.80	2.55	2.31	2.26	2.11	2.64	2.35
Distance(Å)	2.78	2.84	2.58	2.97	3.02	2.53	3.25	2.97

Table 13: Migration energies for all the neighbor O atoms migrate to the O1 vacancy

It is found that O2 atom No. 37 and O1 atom No.41 are the nearest O2 atom and the nearest O1 atom. Also for atom No.37, it needs the smallest migration energy of the five neighbor O2 atoms, but for the nearest O1 atom No.41, it needs the largest migration energy of the five neighbor O1 atoms. So there is no correlation for the migrations of the neighbor O atoms. It is concluded that for one O1 vacancy, the energy barrier of a neighbor O2 atom's migration is relevant about the distance between the vacancy and the neighbor atom. For the neighbor O1 atoms, the two pairs of symmetrical atoms are much easier to migrate to the O1 vacancy site.

2)Migration to a vacancy O2

As example, if the atom No.48 was taken away to form an O2 vacancy, there were 9neighbor atomsin the radius of 3.5 Å: five neighbor O1 atoms with distances noted in red color, and four neighbor O2 atoms with distances noted in green colorwhich includes two symmetrical atoms No.45 and No.77 (Figure 18, Table 14).

Possible jumps	35 (O1)	43 (O1)	66 (O1)	74 (O1)	60 (O1)	45/77 (O2)	78 (O2)	94 (O2)
E_{mig}(eV) i→O2	2.38	2.71	2.33	2.18	2.42	2.74	2.34	3.04
Distance(Å)	2.97	3.25	3.02	2.53	2.97	2.66	2.59	2.73

Table 14: Migration energies for all the neighbor O atoms migrate to the O2 vacancy

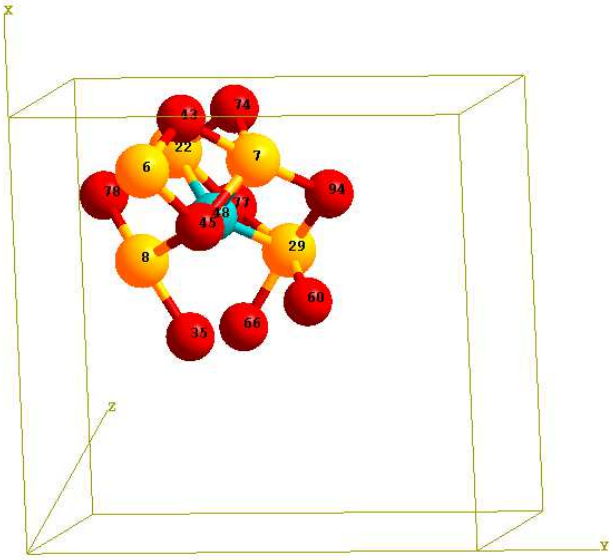

Figure 18: The neighbor O atoms around an O2 vacancy (blue position)

It is found that the migration energies of neighbor O atoms in the same type were relevant with their distances from the O2 vacancy. For the same distance, the migration energy of a neighbor O2 atom to the O2 vacancy is larger than a neighbor O1 atom.For neighbor O2 atoms, the nearest neighbor O2 atom had the smallest migration energy, and the symmetrical neighbor O2 atoms have the same migration energies. The neighbor O1 atom No.74 has the smallest migration energy to the O2 vacancy which is 2.18 eV.However, it is larger than the smallest migration energy to an O1 vacancy (1.29 eV), because the O atom is more stable in O2 position which has four coordinates with neighbor Zr atoms than in O1 positionwhich has three coordinates with neighbor Zr atoms.

So for the diffusion of O by vacancy mechanism, the neighbor O atom around the O vacancy site can do atomic jumps with the migration energies between 1.29 eV and 3.04 eV.

C-2 Migration of C by vacancy mechanism

Now, without considering the self-diffusion of O, the migrations of carbon through neighbor sites by vacancy mechanism were calculated. The calculations were performed and summarizedin two parts:O1 or O2vacancy. At first, the stability of a neighbor C beside an O vacancy was evaluated by calculating the binding energy between the carbon in different neighbor positionsand the oxygen vacancy.

When the value of $E_{binding}$ is positive, it means that carbon substitution is more stable in the neighbor O substitution position of an O vacancy site than to stay far away from the O vacancy.

1) C substitution in a neighbor O position of an O1 vacancy

When C is substituted in a neighbor O position of an O1 vacancy, there are 10 different O positions for C, as seen previously, there are 10 neighbor O atom positions for an O1vacancy. To compare with the migration of O without carbon, still the O1 vacancy No.35 was considered with all its neighbor positions. The binding energies for C in the neighbor positions were calculated and listed in Table 15with their corresponding distances to the O1 vacancy.

All the binding energies have positive values, meaning that the carbon is more stable in neighbor O positions of the O1vacancy site than being in the position far away from the vacancy.

In a second time, the migrations of a neighbor carbon atom from the different neighbor positions were calculated. The energy barrier for carbon in some neighbor positions does not exit since there is no direct migration path (Table 15).

sites	34/66 (O1)	44/60 (O1)	41 (O1)	48 (O2)	45 (O2)	37 (O2)	40 (O2)	39 (O2)
$E_{binding}$	3.15	3.27	3.33	3.73	3.35	4.55	3.68	3.70
E_{mig} (eV) i→O1	0.83	X	2.40	1.88	2.03	1.47	X	1.13
Distance(Å)	2.79	2.84	2.58	2.97	3.02	2.53	3.25	2.97

Table 15: The binding energies (in eV) between C in different neighbor O positions and the O1 vacancy and the migration energy of C with the corresponding distance(X: no direct migration path)

It was found that for an O1 vacancy, the carbon in the pair of symmetrical positions has the smallest migration energy 0.83 eV. Comparing with the O migration in the C-1 part, it was also smaller than the migration energies of O self-diffusion in bulk without carbon. So for O1 vacancy, it should be calculated the migration of O with a carbon atom in a neighbor O

position to verify the carbon effect on the migration energies of O, to understand what is competition between migration of O and migration of C to the same vacancy.

2) C substitution in a neighbor O position of an O2 vacancy

When the C is substitution in a neighbor O position of an O2 vacancy, there are 9 different O positions for C, since as seen previously, there are 9 neighbor O atom positions for an O2 vacancy. To compare with the migration of O without carbon, still the O2 vacancy No.48 was considered with all its neighbor positions. The binding energies between carbon atomin different neighbor O positions and the O2 vacancy site were calculated and listed in Table 16.

The calculated binding energies arealways positive, which means that that the carbon is more stable in a neighbor O position of the O2 vacancy than in a substitution O2 position far away from the vacancy. The carbon atom prefers to go near the O2 vacancy. All the energy barriers of C atom in different positions migrate to the O2 vacancies were listed in Table 16.

sites	35 (O1)	43 (O1)	66 (O1)	74 (O1)	60 (O1)	45/77 (O2)	78 (O2)	94 (O2)
$E_{binding}$	2.34	3.44	2.54	3.34	3.13	3.45	3.62	3.30
E_{mig}(eV) i→O2	0.39	X	0.78	0.17	0.48	1.59	1.09	1.62
Distance(Å)	2.97	3.25	3.02	2.53	2.97	2.66	2.59	2.73

Table 16:The binding energies (in eV) between C in different neighbor O positions and the O2 vacancy and the migration energies of C with corresponding distances(X: no direct migration path)

It is found that,for the carbon in the nearest position of O1 atom No.74,it is much easier to do the migration since the energy barrier (0.17 eV) was smaller than that one of O self-diffusion in bulk without carbon calculated in C-1 part. So for O2 vacancy, as the same as for O1 vacancy, it should be calculated the O migration with a carbon substitution nearby to check what is the competition.

As a conclusion for the migration of C by vacancy mechanism (C-1 and C-2), if a carbon atom diffuses by migration path of vacancy O2-O1-O2, the smallest energy barrier path for C

is No.74 → No.48 → No.37. The migration energy is 1.47 eV, which is already larger than the effective activation energy of C in interstitial mechanism diffusion.

C-3Migration of O with a neighbor carbon to a vacancy: competition effects

The carbon ina neighbor oxygen position of an O vacancy sitemay change the energy barriers of neighbor oxygen atoms. Now suggesting that the neighbor C would stay in its substitution positions, the migrations of neighbor O atoms were performed to the vacancy.

It was much more complicated than the migration of O without carbon since the position of C in different neighbor sites of the vacancycould affect the migration barrier. So first, the carbon is fixed in an O position, and the migrations of O wereperformed. Since the carbon could be in O1 or O2 positions, and there is O1 vacancy or O2 vacancy site, the atomic migration of neighbor O atoms were performed and analyzed by four conditions.

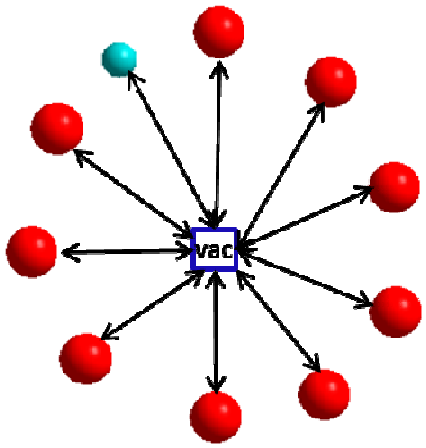

Figure 19: the O1 vacancy with all the neighbor O atoms (red) and the C substitution (blue)

1)Carbon in a neighbor O1 position of the O1 vacancy

The O1vacancy No.35 was still used in this part of calculations. There are five O1 positions for carbon substitution.

When the carbon is in the nearest neighbor O1 position No. 41 of O1 vacancy, the binding energy between carbon and the vacancy is 3.33 eV, which means that the carbon is stable to stay in No.41 than stay far away from the vacancy. Different O migration energies were calculated for all the nineother neighbor O atoms. The results were listed in Table 17.

Possible jumps	34 (O1)	66 (O1)	44 (O1)	60 (O1)	48 (O2)	45 (O2)	37 (O2)	40 (O2)	39 (O2)
E_{mig} (eV)i→j j→i	1.18 /1.38	1.00 /0.32	1.19 /1.75	1.41 /0.77	1.94 /0.98	2.58 /2.31	1.02 /0.27	2.74 /1.44	2.48 /1.61
Distance(Å)	2.79	2.79	2.84	2.84	2.97	3.02	2.53	3.25	2.97

Table 17: Migration energies for neighbor O atoms of O1 vacancy with their correspondingdistances when there is a carbon atom in neighbor O1 position No.41

It was found that the two pairs of symmetrical neighbor O1 atoms did not have the same migration energy, which means that the neighbor carbon changed the migration energy of neighbor O atoms. Here comparing the migration energies for a neighbor O atom which migrates to the O1 vacancy or inverse (two energy barriers for each O atom), it was found that only the neighbor O atoms No.34 and No.44 were more stable after the migration. All the other neighbor O atoms got less stable after migrating to the O1 vacancy site. In the previous part, the migration energy of carbon to the vacancy was calculated to be 2.40 eV. So it is the neighbor O atom which migratesmore easily into the vacancy(Figure 20panel a).

The calculations when carbon atom was in the other O1 positions were also performed. Comparing the migration energies of neighbor O atoms to the vacancy with the migration energies of carbons atomin neighbor O positions in the previous part, it was found that the substituted carbonmigrated more easily when it was in the second nearest O1 position (Figure 20panel b), otherwise it was the neighbor O atoms which can easier migrate to the O1 vacancy site(Figure 20 panel c).

The energy barriers of neighbor O atoms are the same when C is in No.34/66 or No.44/60 since they are two pairs of symmetrical positions.

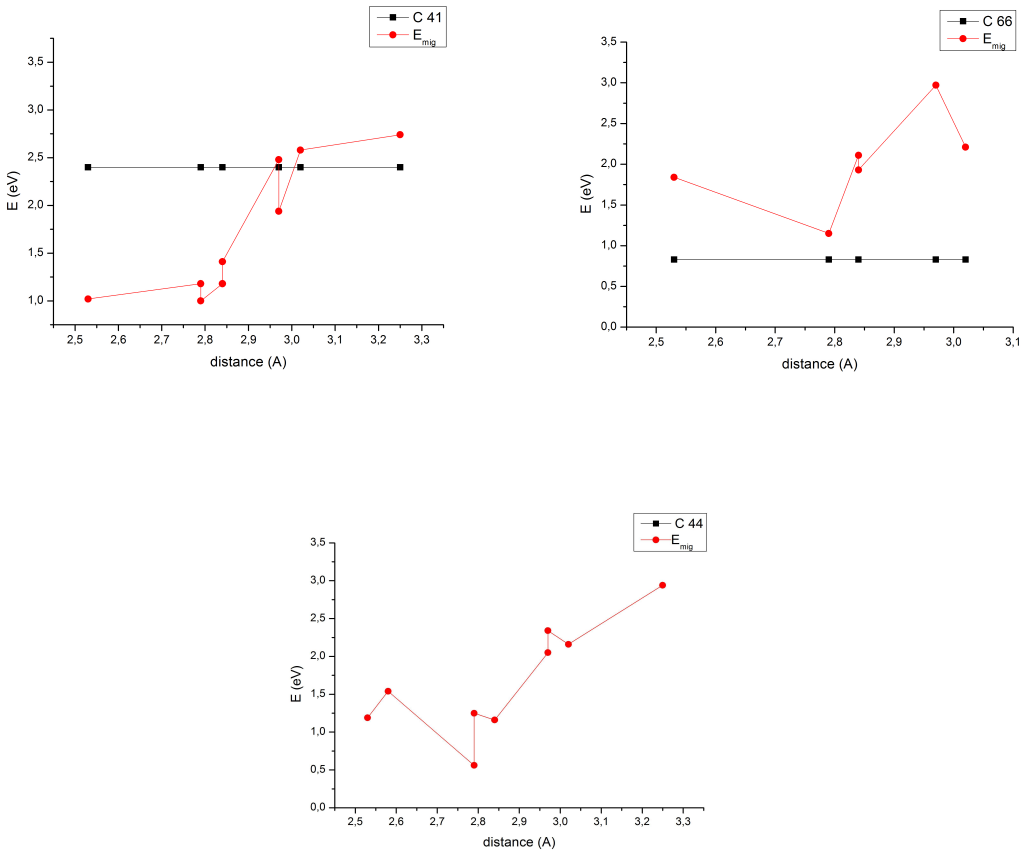

(c)

Figure 20: The migration energies of neighbor O atoms to an O1 vacancy when C is in different neighbor O1 positions (a) C in No.41; (b) C in No.66; (c) C in No.44 (no possible atomic jump for C)

2) Carbon in a neighbor O2 position of the O1 vacancy

For the O1 vacancy No.35, there are four O2 positions for carbon substitution. When the carbon is in the nearest O2 position No.37, the binding energy is 3.27 eV which has been calculated in Part C-1.1. Different O migration energies were calculated for all the nine neighbor O atoms and results were summarized in Table 18.

It was found that the migration energies of neighbor O atoms were changed when there was a neighbor Catom, even the two pairs of symmetrical atoms 34/66, 44/60 had different migration energies now. Since here the migration energy of the C atom is 1.47 eV, there is competition between migration of O and migration of C. It was the nearest O1 atom No.34 which had the smallest migration energy.

Possible jumps	34 (O1)	66 (O1)	44 (O1)	60 (O1)	41 (O1)	48 (O2)	45 (O2)	40 (O2)	39 (O2)
E_{mig}(eV) i→j j→i	1.19 /0.33	X	1.58 /0.66	1.37 /0.76	1.26 /0.83	2.26 /0.43	2.22 /0.47	3.20 /2.00	2.66 /2.32
Distance (Å)	2.79	2.79	2.84	2.84	2.58	2.97	3.02	3.25	2.97

Table 18: Migration energies for neighbor O atoms of O1 vacancy with their corresponding distanceswhen there is a carbon atom in neighbor O2 position No.37 (X: no direct migration path)

The migrations of O when carbon atom is in the other neighbor O2 positions have also been calculated, and it is found that there is always a neighbor O atom can migrate with smaller migration energies (Figure 21).

It is found that when the carbon atom is in No.39, it has the smaller migration energy than all the other neighbor O atoms to the O vacancy No.35. Other else, it is always the nearest O atom can do the jump to the O vacancy with smallest migration energy.

Comparing the migration of carbon atom presented here with the migration of carbon atom by interstitial mechanism, the migration barriers are found to be comparable. Since there exits competition from the migration of neighbor O atoms, it makes the carbon migration more difficult.

3) Carbon in a neighbor O1 or O2 position of an O2 vacancy

The O2 vacancy No.48 was still used in this part of calculations. For carbon atom in one of the nine neighbor positions, the migrations of all the neighbor O atoms were performed. For carbon atom in neighbor O1 position, the different migration energies of neighbor O atoms were calculated and presented in Figure 22.

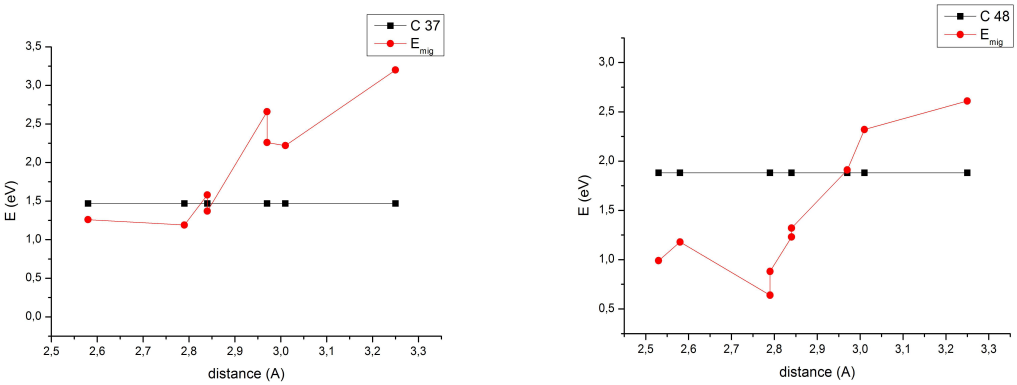

(a)(b)

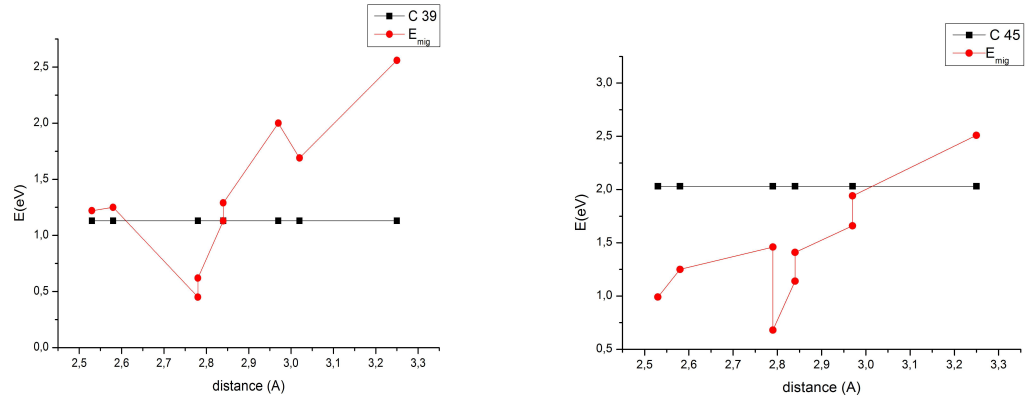

(c)(d)

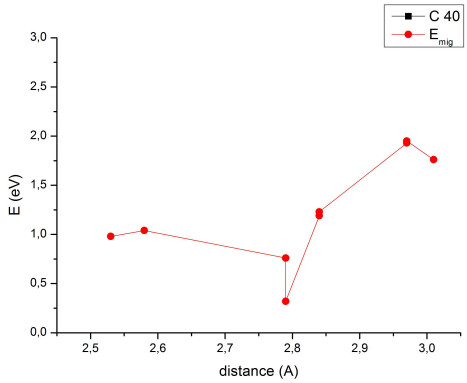

(e)

Figure 21: The migration energies of neighbor O atoms to an O1 vacancy when C is in different neighbor O2 positions (a) C in No.37; (b) C in No.48; (c) C in No.39; (d) C in No.45; (e) C in No.40 (no possible atomic jump for C).

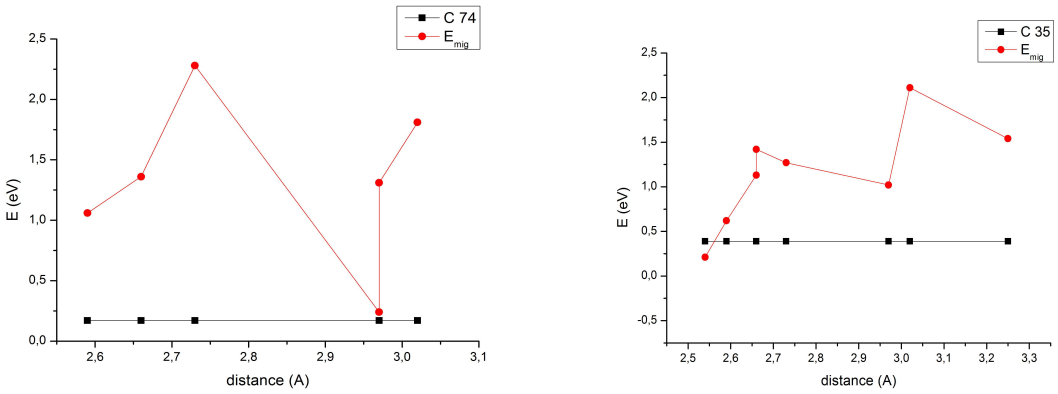

(a)(b)

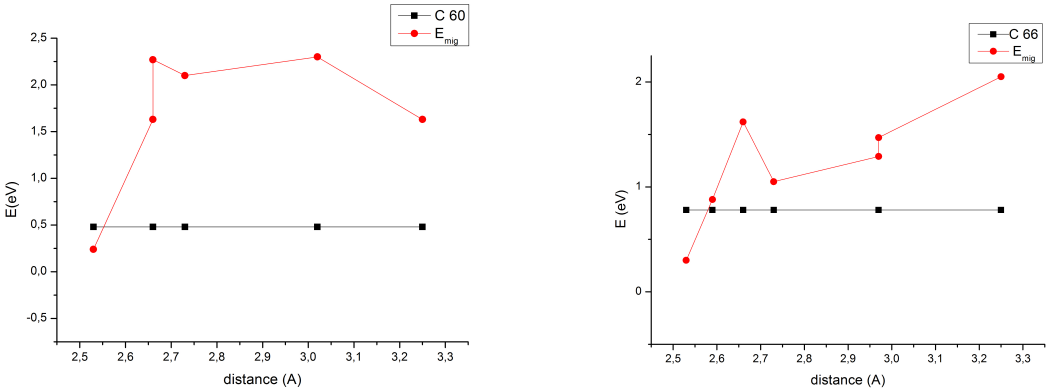

(c)(d)

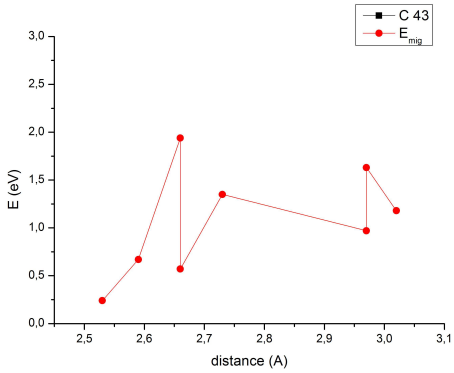

(e)

Figure 22: Migration energies of neighbor O atoms when C is in different neighbor O1 position of vacancy O2 (No.48) (a) C in No.74; (b) C in No.35; (c) C in No.60; (d) C in No.66; (e) C in No.43(no possible atomic jump for C)

It was found that the migration of substituted carbon atom was easier than the neighbor O atoms only when it was in the nearest O1 position (Figure 22 panel a). Other else, it was

always the nearest O atom which could migrate to the O2 vacancy by the smallest energy barrier.

When carbon atom was in aneighbor O2 position, the different migration energies of neighbor O atoms were calculated and presented in Figure 23. The energy barriers of neighbor O atoms are the same when C is in No.77 or in No.45 since these two positions are symmetric.

It was found that when the C atom is in position No.78, and No.77/45, it was always the nearest O atom to the vacancy could migrate with the smallest barrier energy. Except when C is in No.94 which is the furthest O2 position, it was the second nearest O atom which had the smallest migration barrier energy.

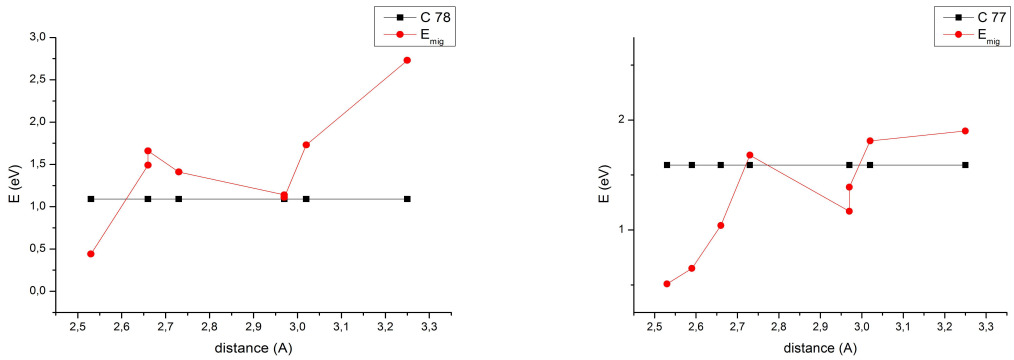

(a)(b)

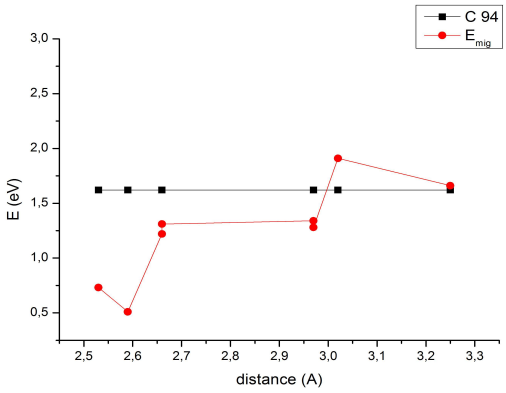

(c)

Figure 23: Migration energies of neighbor O atoms when C is in different neighbor position of O2 (a) C in No.78; (b) C in No.77; (c) C in No.94

So, the migration competition between the neighbor O atoms and the neighbor C atom of the vacancy always exists, which makes the carbon migration more difficult than that one by interstitial mechanism.

C-4 Conclusion

For neighbor O atoms of an O vacancy, the migration energies get smaller when there is a carbon in neighbor O position than without carbon.The energy difference between the condition with C and without C is afforded by the Catom to make the O atommuch easier to go to the vacancy site. By comparing the distance between carbon and neighbour O which does the migration, there is no direct relation between the distance C-O and the migration energy. It would be competition between migration of O atom and migration of C atom according to their competitive migration distances and competitive migration energies.

The binding energy decreaseswhen the distanceincreases. Since the binding energy calculated here is always larger than 2 eV, the DOS calculations were performed to test the electron structure effect on the binding energy.

II.2 Electronic structure: Density of states

In the last part, the different migrations mechanisms of O or C have been determined. Since the competition is complicated and also the position of C have a large effect on the energy barrier of migrations, to better understand the total energy of bulk with different defects, the density of states are performed.

At the first step, the DOS of the 96 atomic supercell will be calculated as reference and also will help to understand the composition of the density of states.

Then, at a second step, three DOS of supercells with different defects were calculated. First a supercell with a carbon atom in interstitial position was considered to study the effect of inserted carbon on the electron density. Then the DOS of a supercell with an O vacancy was calculated to see the vacancy effect on the electron density. Since the carbon atom prefers to go to vacancy position than the interstitial site, the DOS of supercell with a carbon substitution in O vacancy was calculated to evaluate the electronic density.

At last, the DOS of supercell which contains a C substitution and an O vacancy will also be calculated.The binding energy between neighbor C substitution and the O vacancy will be discussed.

II.2.A DOS of the perfect 96 atomic supercell of monoclinic zirconia

The DOS were calculated in the structure of 96 atoms without carbons or defects. After cell optimization, the file POSCAR was replaced by CONTCAR, and a larger k-points mesh (5×5×5) was used to do the DOS calculations. Only the electrons with energies in the range (-20 eV, 20 eV) weretaken into account in the calculations. The Fermi state was shifted at the 0 eV point, the total density of states (Figure 24) and partial density of states for a Zr atom and an O atom were plotted (Figure 25).

The DOS for the monoclinic phase is very similar to the DOS obtained for the cubic and tetragonal phases and has three clear bands. The total DOS is composed of two valence bands, where one is centered around -17 eV with O_2s character and the other lies between 0 eV and -5 eV corresponding to O_2p principally and Zr_4d. They are separated fromtheZr-4d conduction band by a gap of about 3.4 eV which is in good agreement with the theoretical values (3.4 eV/3.42 eV) of the literatures [J. X. Zheng 2007, Jomard1999]. It was smaller than the value 5.83 eV found by Ultraviolet absorption experiments [R. H. French 1994] and 4.2 eV found by electron-energy-loss spectroscopy[D. W. Mccomb 1996]. It should be noted that the energy gap calculated by DFT may display discrepancies with experimental data since this theory is strictly valid for the ground state properties.

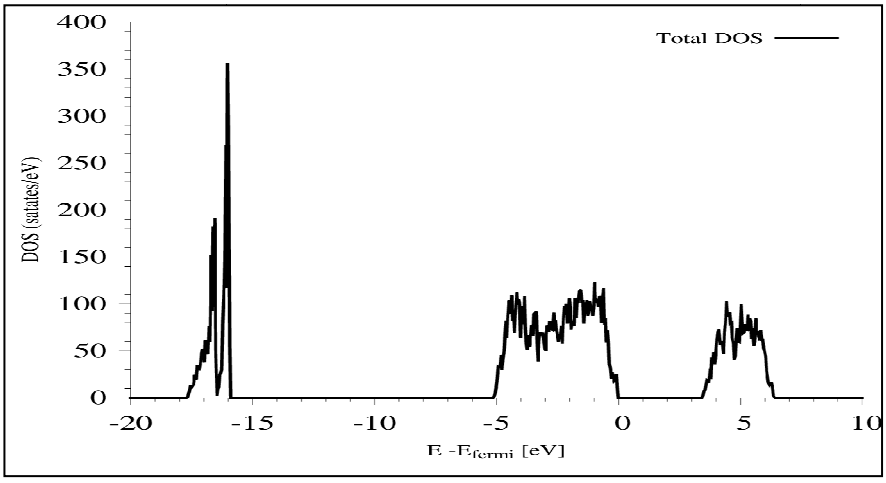

Figure 24: The total DOS of monoclinic ZrO_2 (96 atoms)

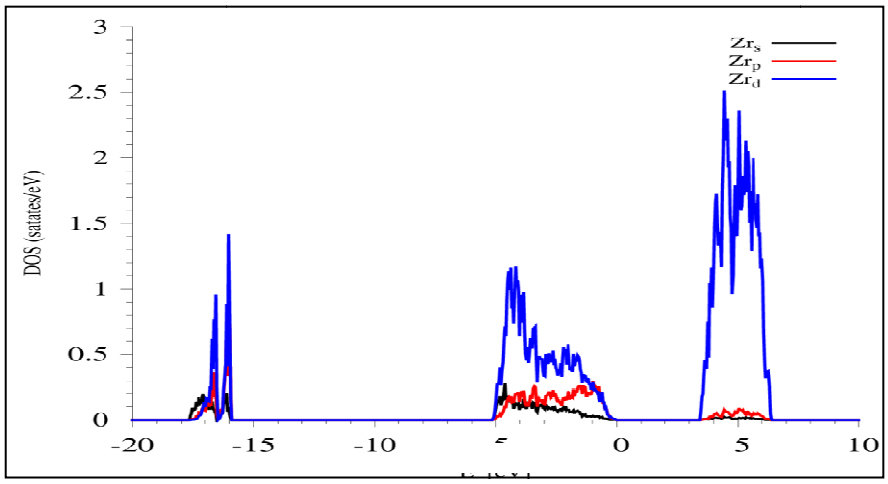

(a)

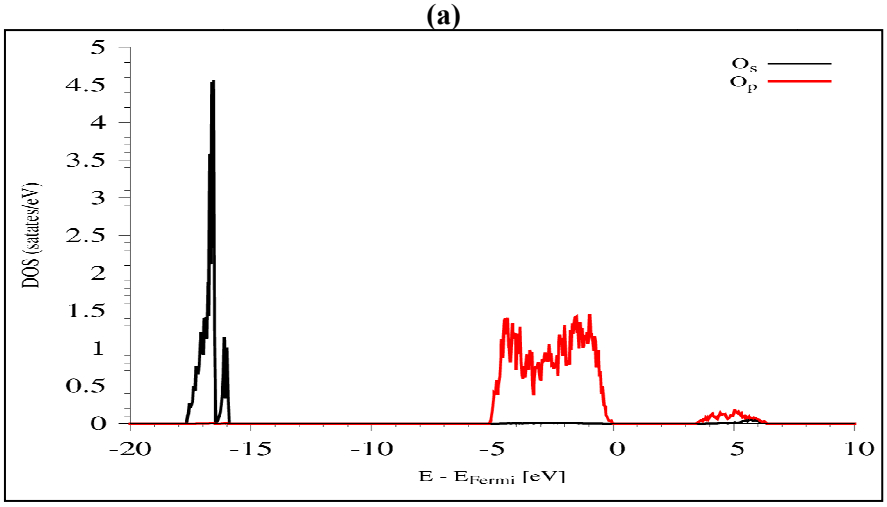

(b)

Figure 25: The partial DOS of one Zr atom (panel a) and one O atom (panel b)

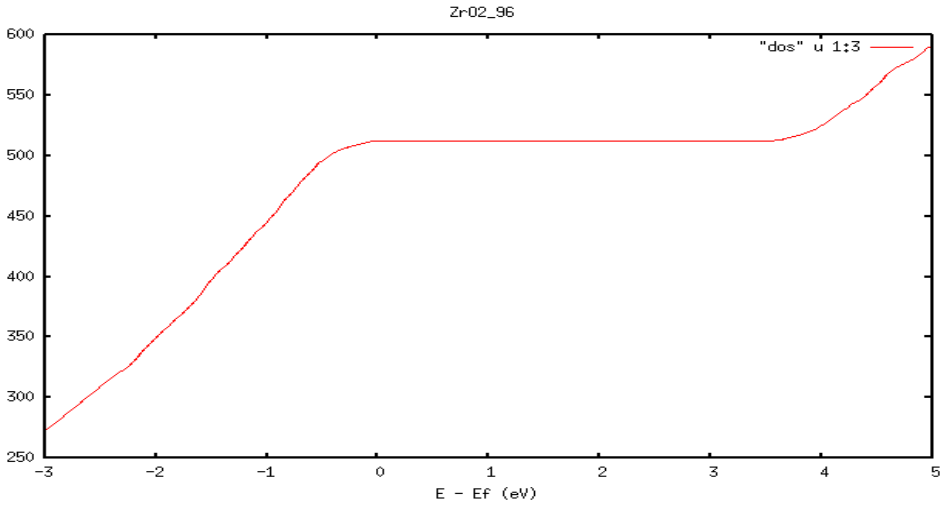

Figure 26: The DOS integral of 96 atomic zirconia supercell

The number of electrons in the material is the integral of the density of states (Figure 26).

As presented in Figure 26, for the supercell which contains 96 atoms (32 Zr and 64 O), the electron number is calculated to be 32x4+64x6=512.

II.2.B DOS of the 96 atomic supercell of monoclinic zirconia with defects

All defect calculations were made using a 96 atomic supercell, which wasgenerated by extending the 12 atomic monoclinicsupercell by two in all three dimensions. For the optimized supercell, the four types of models which are: 1) supercell with an interstitial carbon atom, 2)supercell with an O vacancy, 3) supercell with a carbon substitution,4) supercell with a carbon substitution and an O vacancy will be calculated. During defect calculations the lattice vectors of the supercell were frozen which means the volume wasconstant and all atoms were allowed to relax until atomic forces were converged with a variation smaller than 0.001 eV/Å. The change of electrons numbers caused by the defects is very small comparing to the total electron numbers of the supercell (512 electrons for 96 atomic supercell), so it is sometimes very difficult to get the DOS peaksof defects. At this time, it is necessary to do the derivation of the integral density to get a more accurate DOS.

As explication in Chapter I, the derived of the integral density of states is defined as below:

$$\rho_{derived} = \frac{dN_e(E)}{dE} \tag{6}$$

By derivation of the integral DOS, any change of electron numbers will be shown..

B-1 DOS of 96 atomic supercell with a carbon interstitial atom

DOS for the 96 atomic supercell with a carbon in interstitial position was calculated to see the change of electron density caused by a carbon atom in interstitial position. Here is DOS plotted for the supercell when there is a C atom in site 8 which is the most stable interstitial position (Figure 27). At this time, the total DOS plot did not present the peaks caused by defects while the derived integral DOS plot showed the new peaks.For static calculations, the file PROCAR contains the spd and site projected wave function character of each band.Comparing with the total DOS of perfect supercell, the compositions of the different peaks can be analyzed from the PROCAR (Table 19). In all the analyses by PROCAR, the spd site projected wave function character of the band located at the peak value at Gamma point were listed in the table (with RWIGS value of RWIGS_C = 1.00Å, RWIGS_O = 1.05 Å, RWIGS_Zr = 1.75 Å).

Peak (eV)	-10.2	-7.3	-1.4	0
total	0.856	0.826	0.819	0.838
C	0.314	0.132	0.235	0.289
O	0.207	0.198	0.097	0.056
Zr	0.043	0.043	0.060	0.216

Table 19: The compositions of different peaks in DOS of supercell with a carbon interstitial atom

There are two new electron peaks centered at -1.4 eV and 0 eV. By analyzing the DOSCAR and PROCAR, the two peaks were identified as C_2p from the inserted carbon, and C_2p Zr_4d respectively.

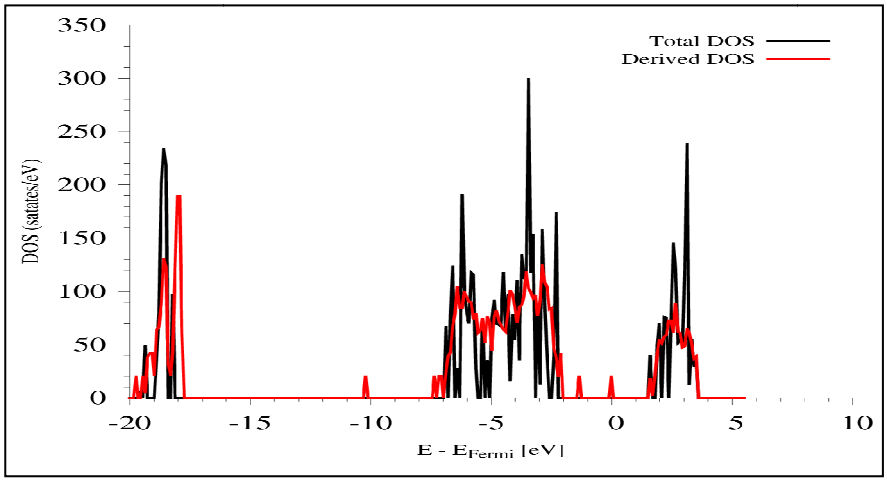

Figure 27: The total DOS of zirconia supercell with a carbon interstitial atom (derived integral DOS plot)

B-2 DOS of 96 atomic supercell with an O2 vacancy

The DOS and derived DOS of the supercell with an oxygen vacancy were presented in Figure 28. They are perfectly matched which means the derived integral DOS can well present the density of states for the supercell.

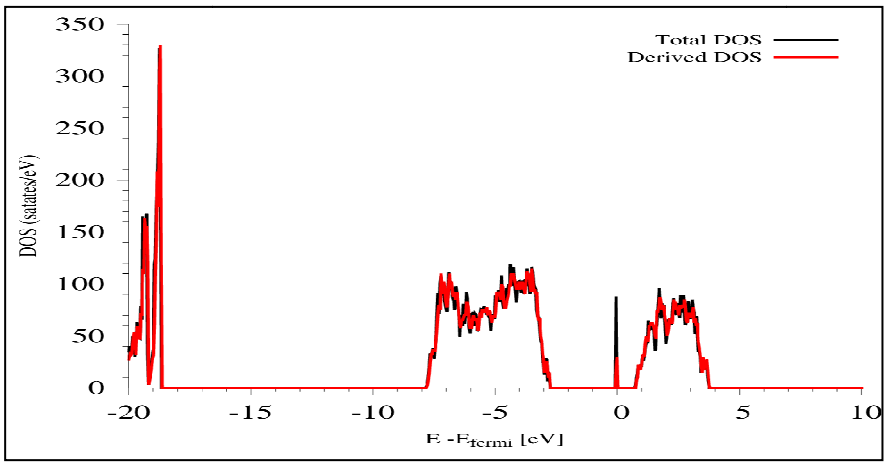

Figure 28: The total DOS of zirconia supercell with an O2 vacancy

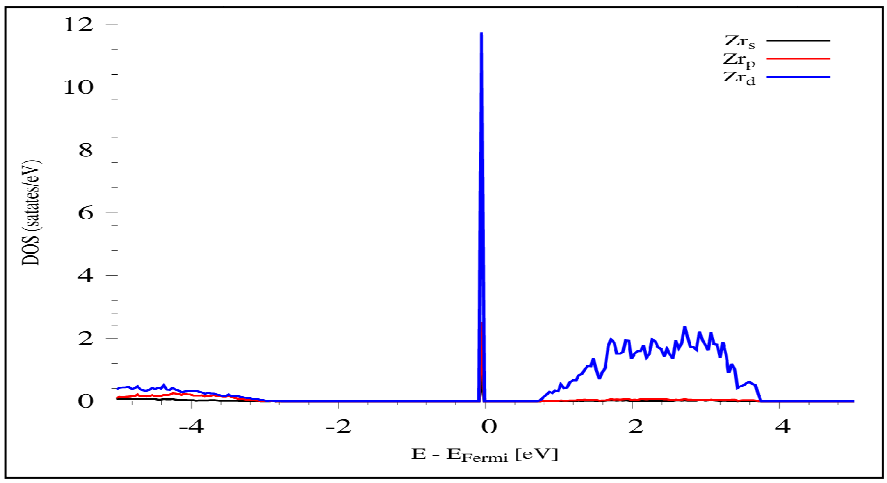

(a)

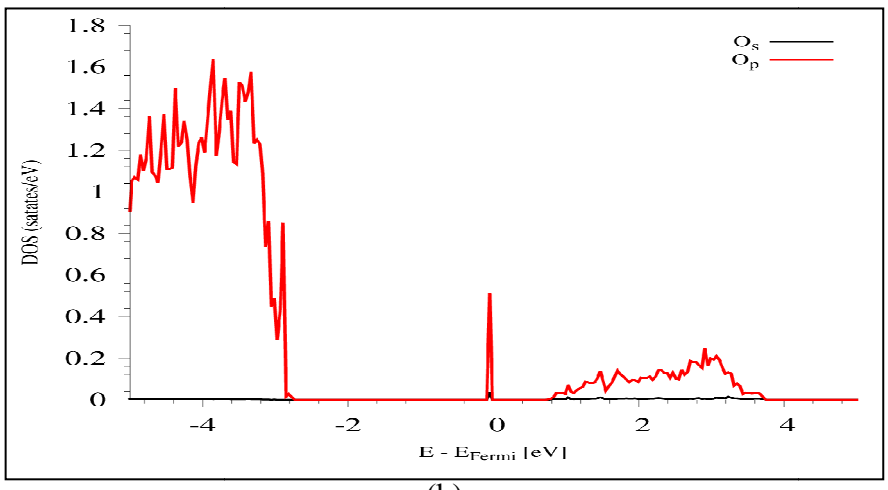

(b)

Figure 29: The partial DOS of a neighbor Zr atom (panel a) and a neighbor O atom (panel b) of the O2 vacancy

To identify the peaks, the partial DOS of Zr and O are plotted (Figure 29). It was found that the two electrons presented in Figure 28 are Zr_4d offered from the neighbor Zr atom of the vacancy.

When there is an O vacancy, the valence band was below the Fermi level. The Fermi level corresponds to the last level which was occupied by the electrons of the system. A neutral oxygen vacancy leads to the appearance of a DOS peak in the gap because in zirconia, the chemical bonds have ionic character, and the O atom was charged by two electrons. So the created vacancy was charged and the zirconia contains plus two electrons.

B-3 DOS of 96 atomic supercell with a carbon substitution in O2 position

Since a C atom is more stable in vacancy position than in an interstitial site, the DOS of supercell when there is a C in O2substitution position is calculated(Figure 30). To understand the total DOS, the partial DOS for a neighbor Zr and a neighbor O of the carbon substitution was alsoperformed(Figure 31). The compositions of different peaks caused by defects were analyzed in Table 20from the PROCAR file. The peaks at -0.15 eV and 0 eVare both composed by C_2p and Zr_4d.

Peak (eV)	-0.15	0	0.06
total	0.926	0.859	0.842
C	0.333	0.333	0.327
O	0.041	0.036	0.052
Zr	0.134	0.148	0.126

Table 20: The compositions of different peaks in DOS of supercell with a carbon atom insubstitution O2 position

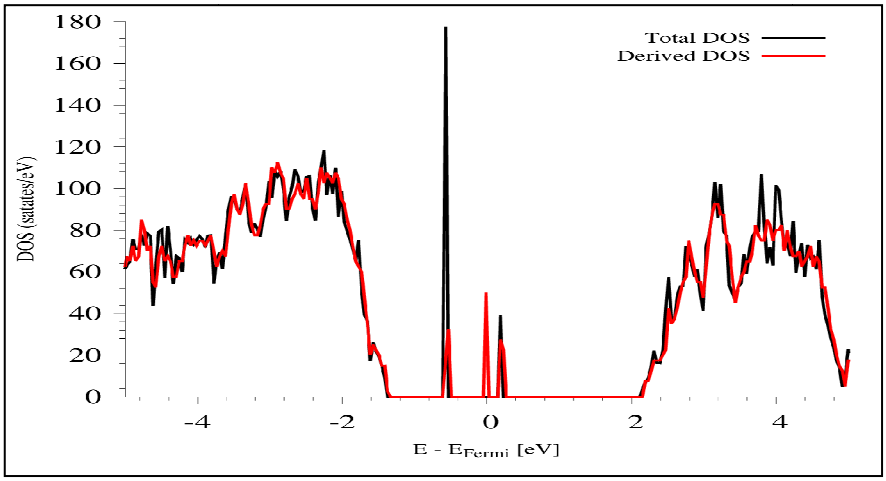

Figure 30: The total DOS of zirconia supercell with a carbon atomin O2 substitution position

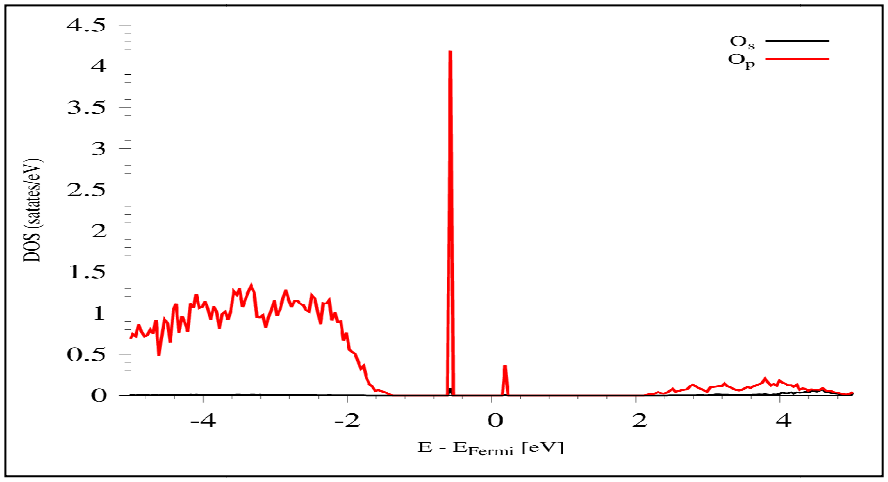

(a)

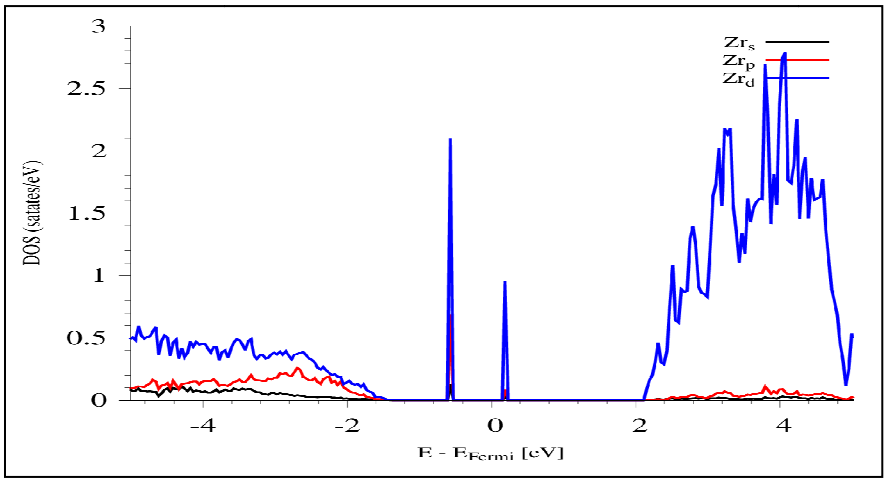

(b)

Figure 31: The partial DOS of a neighbor O atom (panel a) and a neighbor Zr atom (panel b) of the C atom in O2 substitutionposition

B-4 DOS of 96 atomic supercell with a carbon substitution in O2 position with an O vacancy

To study the vacancy effect on the substitution, an oxygen vacancy was made with a distance 3 Å, 5 Å and 7 Å from the substituted carbon. The calculations for distance 3 Å and 5 Å are performed in the 96 atomic supercell. A larger supercell of 324 atoms was built to perform the simulation of distance 7 Å (the 12 atomic supercell was expanded three times in each direction x, y and z). The total DOS for the three supercell models were similar. Here the DOS of the supercell in which the vacancy is 5 Å away from the substitutionispresented (Figure 32).

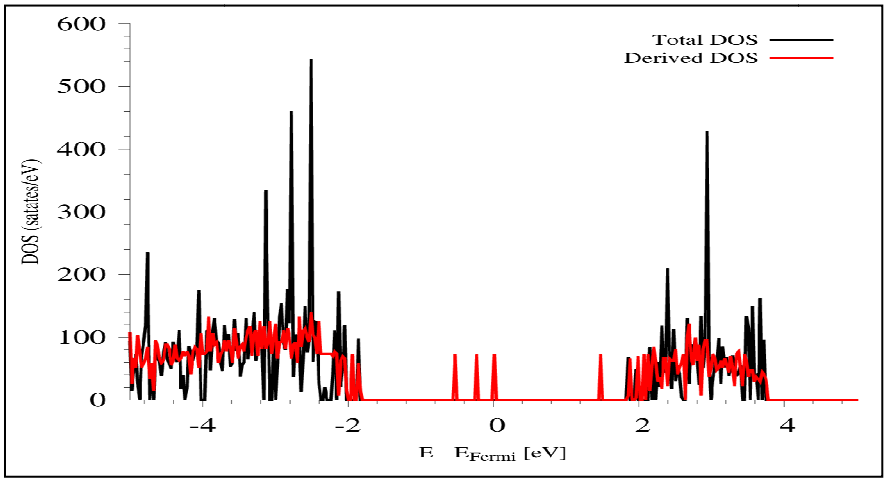

Figure 32: The total DOS of zirconia supercell with a carbon substitution and an O vacancy at 5 Åaway from the substitution(derived integral DOS plot)

The analyzed results of the different peaks using PROCARand DOSCAR is presented in Table 21. The peaks at -0.54 eV and -0.25 eV are both composed by electrons from C_2p and Zr_4d. For the peak at Fermi level energy (0 eV), it is principally from the electrons of C_2p from the substituted carbon.

Peak (eV)	-0.54	-0.25	0	1.47
total	0.874	0.839	0.759	0.693
C	0.316	0.323	0.279	0
O	0.022	0.039	0.033	0.018
Zr	0.162	0.154	0.088	0.215

Table 21: The compositions of different peaks in DOS of supercell with a carbon atom in O2 substitution position

For the supercell with distance 5 Å between carbon in substitution and the O2 vacancy, the binding energy was calculated to be 2.21 eV by Eq. 9. For distance at 3 Å and 7 Å, the binding energies calculated were 3.25 eV and 1.99 eV (cf. Table 22).

The binding energy decreased when the distance increased. However, there should not bea binding energy between vacancy and substitution when the distance is as far as 7 Å. But the calculated binding energy presented here is as large as 1.99 eV.

So to understand where 1.99 eV comes from, the binding energy was also calculated with charged vacancy. Indeed, for the 324 atomic supercell, when an oxygen vacancy is neutral, the binding energy is 1.99 eV. But if an O vacancy is charged in the calculations which means the supercell with an O vacancy loses two electrons(losing 2 electrons since one O^{2-} vacancy) the binding energy calculated for distance 7 Å is now 0.04 eV. So that means 1.99 eV comes from the neutral oxygen vacancy. There is no binding energy when the carbon atom is 7 Å far away from the vacancy.

With the same method, for distance 5 Å between the C substitution and the O vacancy, if an O vacancy is considered to be charged, the binding energy is 0.12 eV. The corrected binding energy proves that there is no vacancy effect on the carbon atom in substitution position when the vacancy is5 Å away from the substitution. So when the carbon is further than 5 Å to the vacancy, the vacancy effect on the migration of C can be neglected.

distance (Å)	3	5	7
Supercell size(atom number)	96	96	324
$E_{binding}$(eV)	3.25	2.21	1.99
$E_{binding\ corrected}$ (eV)	1.19	0.12	0.04

Table 22: The binding energies and corrected binding energies between C in different neighbor O positions and the O2 vacancy

For distance 3 Å, the corrected binding energy with the same method is 1.19 eV, so there is still interaction between the carbon substitution and the O2 vacancy. Since for anO vacancy, the neighbor positions were in radius of 3.5 Å, the energy difference 2.06 eV caused by

neutral vacancy for distance 3 Å is chosen to correct all the binding energies of the neighbor atoms to the vacancy.

The binding energies in Part II.1.C-2 are correctedand listed in Table 23 and Table 24.

Sites	34/66 (O1)	44/60 (O1)	41 (O1)	48 (O2)	45 (O2)	37 (O2)	40 (O2)
$E_{binding}$ (eV)	3.15	3.27	3.33	3.73	3.35	4.55	3.68
$E_{binding\ corrected}$(eV)	1.09	1.21	1.27	1.67	1.29	2.49	1.62

Table 22: The binding energies and corrected binding energies between C in different neighbor O positions and the O1 vacancy

Sites	35 (O1)	43 (O1)	66 (O1)	74 (O1)	45 (O2)	77 (O2)	78 (O2)	94 (O2)
$E_{binding}$ (eV)	2.34	3.44	2.54	3.34	3.45	3.45	3.62	3.30
$E_{binding\ corrected}$ (eV)	0.28	1.38	0.48	1.28	1.39	1.39	1.56	1.24

Table 23: The binding energies and corrected binding energies between C in different neighbor O positions and the O2 vacancy

By correcting binding energies presented in these two tables, the binding energies between neighbor C and O vacancy get smaller. When the binding energy is very small to be neglected, the carbon substitution has no interaction with the O vacancy, so it is more difficult to do the migration to the O vacancy.

Conclusions

Since there is oxidation reaction between zirconium and water, an oxide layer which is principally zirconia is formed (about 50 μm at the external layer). Zirconia at the storage temperature exists in monoclinic phase, so the monoclinic zirconia is chosen to do the simulations in order to study carbon behavior in it.

Density Functional Theory, in static approach, was used to evaluate the carbon behavior in the zirconia bulk. Cell models which are the smallest cells to reproduce the structure of three different structures for zirconia were built, such as cubic, tetragonal, and monoclinic. It is

proved that monoclinic phase was the most stable one of the three phases, which corresponds to the phase transitions of zirconia at different temperature.

For the monoclinic phases, the possible stable sites for carbon atoms were characterized in the perfect bulk without any vacancies. By doing the Monte Carlo simulations for C diffusion by interstitial mechanism, it was found that the carbon atom does not diffuse in the perfect monoclinic zirconia at storage condition.

To simulate more realistic conditions, the formation energies of a vacancy, a substitution, and an interstitial carbon with a vacancy were studied. According the results, it was shown that it is more favorable for carbon atoms to go to the position of vacancies as substitution than in the interstitial sites.

The migration of O, the migration of C and their competition by vacancy mechanism have been performed. Comparing with the migration of C by interstitial mechanism (without vacancies), the migration energies of the carbon atoms are comparable. However, it was shown that a neighbor carbon atom of an O vacancy increases the migration of neighbor O atomsto the vacancy, leading to a stronger competition between the oxygen migration and the carbon migration to the same vacancy.Therefore, we can say that the carbon diffusion by vacancy mechanism is more difficult than the carbon diffusion by interstitial mechanism. As at the storage temperature, it was shown that there is no carbon diffusion by interstitial mechanism, we can say that there would be no carbon diffusion by vacancy mechanism.

References

[C. Arhammar 2009] C. Arhammar, C. Moysés Araujo, Rajeev Ahuja, Phys. Rev. B 80, 115208 (2009)

[P. E. Blochl 1994] P. E. Bloch, Physical Review B, 50, 17953 (1994)

[K. Burke 1998] K. Burke, J. P. Perdew, and Y. Wang, Electronic Density Functional Theory, 81-111, Springer US, New York, (1998)

[A. S. Foster 2001] A. S. Foster, V.B. Sulimov, F.L. Gejo, A.L. Shluger, R.M. Nieminen, Phys. Rev. B 64, 224108 (2001)

[R. H. French 1994] R. H. French, S. J. Glass, F. S. Ohuchi, Y. N. Xu, and W. Ching,Phys. Rev. B 49, 5133 (1994)

[C. J. Howard 1988] C. J. Howard, R. J. Hill, and B. E. Reichert, Acta Crystallogr. Sect. B: Struct. Science. 44, 116 (1988)

[G. M. Hood 1993] G. M. Hood, Defect and Diffusion Forum, 755, 95-98 (1993)

[H. Jiang 2010] H. Jiang, R. I. Gomezabal, P. R. Rinke, and M. Scheffler, Phys. Rev. B 81, 085119 (2010)

[G. Jomard 1999] G. Jomard, T. Petit, A. Pasturel, L. Magaud, G. Kresse, J. Hafner, Phys. Rev. B 59, 4044 (1999)

[H. Josson 1998] H. Jonsson, G. Mills and K.W. Jacobsen, Classical and quantum dynamics in condensed phase simulations, World Scientific Inc, 385-404 (1998)

[C. Kittel 2005] C. Kittel.Introduction to Solid State Physics, 8th edition. Hoboken, NJ: John Wiley & Sons, Inc, 50 (2005)

[W. Kohn 1965] W. Kohn and L. J. Sham, Phys. Rev. B 140, A1133 (1965)

[G. Kresse 1996 a] G. Kresse and J. Furthmuller, Comput.Mater. Sci. 6, 15(1996)

[G. Kresse 1996 b] G. Kresse and J. Furthmuller, Phys. Rev. B 54, 11 169 (1996)

[O. Kurapova 2014] A CORRIGER DANS LE TEXTE AUSSI O. Y. Kurapova, and V. G. Konakov, Rev. Adv. Mater. Sci. 36, 177-190 (2014)

[A. Kuwabara 2005] A. Kuwabara, T. Tohei, T. Yamamoto, and I. Tanaka, Phys. Rev. B 71, 064301 (2005)

[D. W. Mccomb 1996] D. W. McComb, Phys. Rev. B 54, 7094 (1996).

[G. E. Murch 1979] G. E. Murch, Acta Metallurgica. 27, 1701- 1704 (1979)

[J. P. Perdew 1992] J. P. Perdew, J. A. Chevary, S. H. Vosko, K. A. Jackson, M. R. Pederson, D. J. Singh, and C. Fiolhais, Phys. Rev. B 46, 6671(1992)

[J. P. Perdew 1996] J. P. Perdew, K. Burke, et al., Physical review letters 77, 3865 (1996)

[G. M. Rignanese 2005] G. M. Rignanese, J. Phys. Condens. Matter 17, R357 (2005)

[K. Schwarz 1982] K. Schwarz, H. Ripplinger, A. Neckel, Cond. Matt 48, 79-87 (1982)

[G. Stapper 1999] G. Stapper, M. Bernasconi, N. Nicoloso, and M. Parrinello, Phys. Rev. B 59, 797(1999)

[E. V. Stefanovich 1994] E. V. Stefanovich, A. L. Shluger, and C. R. A. Catlow, Phys. Rev. B 49, 11 560 (1994)

[J. X. Zheng 2007] J. X. Zheng, G. Ceder, T. Maxisch, W.K. Chim, W.K. Choi, Phys. Rev. B 75, 104112 (2007)

Conclusion

To study the carbon behavior in the used fuel claddings, a multi-scale approach has been developed and performed for carbon atom in bulk zirconium and bulk monoclinic zirconia.

Behavior of a carbon atom in bulk zirconium

For the carbon atom in zirconium, first, with the DFT atomic scale simulation, a 96 atomic hcp zirconium supercell was optimized to perform the diffusion simulation. Two types of possible interstitial sites for the carbon atom were characterized: distorted Basal Tetragonal site noted as BT_d site and Octahedron site noted as O site. BT_d site is less stable than the O one by 1.45 eV. To study the atomic jump between the different neighbor interstitial sites, all the migration energies and the attempt frequencies were calculated in order to get the corresponding jump probabilities from the transition state theory for all possible atomic jumps. As a preliminary result, calculation from the DFT-NEB approach showed that the easiest migration pathway for carbon diffusion should be the successive jumps between BT_d site and O site.

In a second step, a macroscopic simulation by the Kinetic Monte-Carlo approach (KMC) was performed using jump probabilities. From the KMC simulations at different temperatures, the carbon's trajectory as well as the diffusion coefficient (as a function of temperature) were calculated. It is found that the carbon diffusion in zirconium has 2.02 eV effective activation energy, which corresponds to the lowest migration energy path: O site → BT_d site → BT_d site → BT_d site (n times) → O site → BT_d site… (compared to the O site → O site path). The carbon diffusion coefficient in perfect Zr crystal, at the storage temperature (around 50°C), is calculated to be very small ($\sim 10^{-34}$ cm^2/s). Therefore, these first investigations show it will be very difficult for a carbon atom to diffuse in a perfect Zr crystal in the range of the storage condition.

In order to investigate the vacancies effect on the carbon diffusion, DFT simulations were also performed with vacancies. It was proved that the carbon atom stability decreases when it gets closer to a Zr vacancy. Therefore, bulk zirconium with vacancies won't increase the carbon diffusion relative to interstitial diffusion mechanism without vacancies.

To summarize, this first part has pointed out that the carbon will be blocked in zirconium bulk with and without Zr vacancies.

Behavior of a carbon atom in the zirconia

For the oxide layer of the fuel claddings (about 50 μm at the external layer), it is zirconia in monoclinic phase that principally exists at the storage temperature, so it was chosen to do the simulations in order to study carbon behavior in it.

At atomic scale, using Density Functional Theory, first, an optimized bulk model was built for the three different structures for zirconia, such as cubic, tetragonal, and monoclinic. It was proved that monoclinic phase was the most stable one of the three phases which corresponded to the phase transitions of zirconia at different temperatures.

For the pure monoclinic phase, the possible interstitial sites for carbon atoms were investigated. There are eight types of different interstitial sites for carbon atoms and each type has four symmetric positions. For each interstitial site position, all the neighbor positions were identified. By studying the possible atomic jumps, it is identified that there are 28 possible atomic jumps between the different neighbor interstitial positions.

The migration energy and attempt frequency were calculated for each atomic jump to get the jump probabilities. Then, using the atomic results to do the macroscopic simulations by the Kinetic Monte Carlo approach, it was found that it is very difficult for a carbon atom to diffuse by interstitial mechanism in monoclinic zirconia structure with effective activation energy of 1.19 eV. As example, a carbon atom in the center of the oxide layer of 50 μm will need 10^{11} years to leave it.

At last, the vacancy effect on the carbon diffusion was also considered. Firstly, the binding energy between carbon atom in an interstitial position, and an O vacancy were calculated which indicated that the closer they were, the larger the binding energy was. It means that the carbon atom prefers to go near a vacancy position. So the study of the carbon diffusion by vacancy mechanism was performed. We have demonstrated that:

1) For the self-migration of oxygen atoms, the migration energies of different vacancy positions are between 1.3 eV and 3 eV, which have low jump probabilities.
2) The binding energies when a carbon atom is in different neighbor positions of an O vacancy were calculated. It was found that a carbon atom in substitution was more stable in neighbor position of an O vacancy site. So the possibility of carbon diffusion by

vacancy mechanism was calculated. The migration energies of C were calculated for all the possible atomic jumps which turned out between 0.17 eV and 2.03 eV.

3) Since there is a positive binding energy between an O vacancy and the substituted carbon atom near to the vacancy, and the substituted carbon changes the geometrical structure around the vacancy, the migration energies of neighbor O atoms would be affected. All the possible atomic migrations of O to the vacancy were recalculated with presence of a neighbor C atom. It is found that the migration energies get smaller when there is a carbon atom nearby the vacancy. The migration energies were calculated between 0.27 eV and 3.20 eV. Since the migration energies are comparable to the migration energies of C (between 0.17 eV and 2.03 eV), there is a competition between the migration of O and the migration of C.

The simulations for the migration of O, the migration of C and their competition by vacancy mechanism have been performed. Comparing the carbon diffusion by two different mechanisms, the migration energies of C by vacancy mechanism (between 0.17 eV and 2.03 eV) are comparable with the activation energy of C diffusion by interstitial mechanism (1.19 eV). The neighbor O atoms of an O vacancy have competition with the carbon atom to migrate to the vacancy, which makes the C diffusion by vacancy mechanism more difficult. In the two ways, the carbon diffusion by vacancy mechanism is proved to be also extremely limited, the same as for the carbon diffusion by interstitial mechanism. As at the storage temperature, based on our calculations, and considering a half life of 5600 years for ^{14}C, the consequences are the following:

After 100.000 years, C should have diffused on 10^{-7} μm in Zr and 0.1 μm in ZrO_2, and the activity should be reduced by 10^{-6} in the meantime.

After 200.000 years, C should have diffused on 10^{-7} μm in Zr and 0.2 μm in ZrO_2, and the activity should be reduced by 10^{-11} in the meantime.

Thus, after 100.000 or 200.000 years, and a diffusion distance on 0.1 to 0.2 μm, C should remain within the grain of zirconia (whose size should be around 1 μm size) and very few amounts may reach grain boundaries. Even if grain boundaries and micro-cracks, which were not studied in this work, are short circuits for diffusion (e.g. with very high Carbon diffusion coefficients), their impact on C release should remain small.

Consequently, when C will diffuse out of the zirconia, after several thousands or millions of years it will no more be active. Thus the release of ^{14}C should be expected to be really very small, and it should have a very limited contribution to the release of radionuclides outside.

This extremely low ^{14}C release should allow to improve the models of the container evolution in storage conditions, and contribute to reduce the cost of storage.

Perspectives

In the chapter 3, it is found that the charged O vacancy will change the binding energies between an O vacancy and neighbor C/O atoms. To see charge effect on the migration energies, the migration by charged vacancy mechanism can be simulated.

In this first step toward an understanding of the carbon behavior in the fuel claddings, it was proved that there is no carbon diffusion in bulk zirconia with and without vacancies. However, if there are some carbon atoms in the ground boundaries or cracks of the bulk, it should be interesting to simulate them.

Once the diffusion of carbon in ZrO_2 is well understood, it should be interesting to investigate the carbon form at the ZrO_2 / water interface.

ANNEXE

Migration of a neighbor O atom to the vacancy No. 48

1. With a neighbor C atom in O1 position around the vacancy

C in nearest O1 position (No. 74)	Possible jumps	35 (O1)	43 (O1)	66 (O1)	45 (O2)	77 (O2)	78 (O2)	94 (O2)
	Emig	1.31 /0.94	X	1.81 /2.33	1.36/0. 42	X	1.06 /0.05	2.28 /2.10
C in second nearest O1 position (No. 35)	Possible jumps	43 (O1)	66 (O1)	74 (O1)	45 (O2)	77 (O2)	78 (O2)	94 (O2)
	Emig/	1.54 /2.20	2.11 /3.01	0.21 /0.83	1.42 /1.62	1.13 /0.79	0.62 /0.49	1.27 /1.09
C in third nearest O1 position (No. 66)	Possible jumps	35 (O1)	43 (O1)	74 (O1)	45 (O2)	77 (O2)	78 (O2)	94 (O2)
	Emig	1.47 /2.90	2.05 /2.46	0.30 /0.86	1.62 /1.11	1.62 /1.41	0.88 /0.37	1.05 /1.17
C in fourth nearest O1 position (No. 43)	Possible jumps	35 (O1)	66 (O1)	74 (O1)	45 (O2)	77 (O2)	78 (O2)	94 (O2)
	Emig/	0.97 /1.98	1.18 /2.06	0.24 /1.39	1.94 /1.94	0.57 /0.73	0.67 /0.55	1.35 /1.79

2. With a neighbor C atom in O2 position around the vacancy

C in the nearest O2 position (No. 78)	Possible jumps	35 (O1)	43 (O1)	66 (O1)	74 (O1)	45 (O2)	77 (O2)	94 (O2)
	Emig	1.11 /1.51	2.73 /2.73	1.73 /1.73	0.44 /0.54	1.49 /0.69	1.66 /0.84	1.41 /0.78
C in seond nearest O2 position (No. 77)	Possible jumps	35 (O1)	43 (O1)	66 (O1)	74 (O1)	45 (O2)	78 (O2)	94 (O2)
	Emig	1.39 /1.67	1.90 /2.18	1.81 /2.33	0.51 /0.98	1.04 /0.67	0.65 /0.27	1.68 /1.18
C in third nearest O2 position (No. 94)	Possible jumps	35 (O1)	43 (O1)	66 (O1)	74 (O1)	45 (O2)	77 (O2)	78 (O2)
	Emig	1.28 /1.69	1,66 /2.50	1.91 /2.34	0.73 /1.22	1.31 /0.87	1.22 /0.85	0.51 /0.20

Migration of a neighbor O atom to the vacancy No. 48

1. With a neighbor C atom in O1 position around the vacancy

C in the nearest O1 position (No. 41)	Possible jumps	34 (O1)	66 (O1)	44 (O1)	60 (O1)	48 (O2)	45 (O2)	37 (O2)	40 (O2)
	Emig(eV)	1.18 /1.38	1.00 /0.32	1.19 /1.75	1.41 /0.77	1.94 /0.98	2.58 /2.31	1.02 /0.27	2.74 /1.44
C in second nearest O1 position (No. 66)	Possible jumps	34 (O1)	44 (O1)	60 (O1)	41 (O1)	48 (O2)	45 (O2)	37 (O2)	40 (O2)
	Emig(eV)	1.15 /0.04	2.11 /0.89	1.93 /1.37	X	X	2.21 /0.27	1.84 /0.25	X(large)
C in third nearest O1 position (No. 44)	Possible jumps	34 (O1)	66 (O1)	60 (O1)	41 (O1)	48 (O2)	45 (O2)	37 (O2)	40 (O2)
	Emig(eV)	0.56 /0.26	1.25 /0.65	1.16 /0.78	1.54 /1.43	2.34 /1.30	2.16 /1.34	1.19 /0.09	2.94 /1.62

2. With a neighbor C atom in O2 position around the vacancy

C in the nearest O2 position (No. 37)	Possible jumps	34 (O1)	66 (O1)	44 (O1)	60 (O1)	41 (O1)	48 (O2)	45 (O2)	40 (O2)
	Emig(eV)	1.19 /0.33	X	1.58 /0.66	1.37 /0.76	1.26 /0.83	2.26 /0.43	2.22 /0.47	3.20 /2.00
C in the second O2 position (No. 48)	Possible jumps	34 (O1)	66 (O1)	44 (O1)	60 (O1)	41 (O1)	45 (O2)	37 (O2)	40 (O2)
	Emig(eV)	0.64 /0.40	0.88 /0.87	1.23 /1.13	1.32 /1.30	1.18 /1.18	2.32 /1.80	0.99 /0.06	2.61 /1.68
C in the third O2 position (No. 45)	Possible jumps	34 (O1)	66 (O1)	44 (O1)	60 (O1)	41 (O1)	48 (O2)	37 (O2)	40 (O2)
	Emig(eV)	1.46 /1.43	0.68 /0.48	1.14 /1.51	1.41 /1.24	1.25 /1.25	1.94 /1.59	0.99 /0.09	2.51 /1.53
C in the fourth O2 position (No. 40)	Possible jumps	34 (O1)	66 (O1)	44 (O1)	60 (O1)	41 (O1)	48 (O2)	45 (O2)	37 (O2)
	Emig(eV)	0.76 /0.58	0.32 /1.19	1.19 /1.03	1.23 /1.67	1.04 /0.93	1.95 /1.07	1.76 /0.88	0.98 /0.47

université PARIS-SACLAY | ÉCOLE DOCTORALE PHENIICS

Titre : Etude de la diffusion du carbone dans le zirconium et la zircone en volume des gaines de combustible usées par simulations multi-échelles

Mots clés : DFT, coefficient de diffusion, carbone-14, Monte-Carlo cinétique

Résumé : Dans le cadre de la gestion des déchets nucléaires, les coques et embouts des gaines de combustibles sont coupées, compactées et empilés dans les colis CSD-C (Colis Standards de Déchets Compactés). Actuellement entreposés à la Hague, ces déchets seront stockés en milieu géologique profond dans des alvéoles en béton. Ces déchets MA-VL contiennent des RN d'intérêts dont le carbone-14 qui provient de l'activation neutronique de l'azote-14 et de l'oxygène-17 présents dans le Zircaloy oxydé. L'objectif de cette thèse, qui est menée en collaboration avec EDF et AREVA, est de répondre à la question du devenir et du comportement du carbone-14 dans ZrO_2 et Zr-métal.

Cette thèse consistera à utiliser la simulation numérique, au moyen de la Théorie de la Fonctionnelle de la Densité (DFT), afin de modéliser le comportement du carbone-14 dans les CSD-C.

Les simulations sont effectué avec approche multi-échelles :

1) Echelle atomique, optimisation de modèles atomiques permettant de représenter les différentes phases de ZrO_2 ; identification des différents sites d'insertion possibles pour l'atome de carbone en sites interstitiels et en substitutions à un atome d'oxygène ou de zirconium ; modélisation des différentes chemins d'énergie minimum associées à la migration d'un atome de carbone d'un site à un autre par mécanismes interstitiels et lacunaires.

2) Echelle macroscopique, détermination des coefficients de diffusion par la méthode Monte-Carlo dans ZrO_2 monoclinique pure et Zr pure.

Title : Carbon diffusion behavior in bulk zirconium and zirconia of the used fuel claddings by multi-scale simulations

Keywords : DFT, diffusion coefficient, carbon-14, Kinetic Monte-Carlo

Abstract: As part of the nuclear waste management, hulls and ends of fuel claddings are cut, compacted and put in CSD-C containers (compacted standard waste containers). Currently stored at La Hague, the waste will be stored in deep geological environment. The MA-VL waste contains RN including carbon-14, which comes from the neutron activation of nitrogen-14 and oxygen-17 present in the oxide Zircaloy. The objective of this thesis, which is taken in collaboration with EDF and AREVA, is to answer the question of the carbon-14 behavior in ZrO_2 and Zr metal.

This thesis is to perform numerical simulations, using the Theory of Density Functional (DFT) to model the behavior of carbon-14 in the CSD-C.

The simulations are performed with multi-scale approach:

1) At atomic scale, optimization of atomic models to represent the different phases of ZrO_2; identification of the insertion sites for the carbon atom in interstitial sites and substitutions of an oxygen or zirconium atom; modeling different minimum energy path for the migration of a carbon atom from one site to another by interstitial and vacancye mechanisms.

2) At macroscopic scale, determination of diffusion coefficients in pure bulk monoclinic ZrO_2 and pure bulk Zr by the Monte Carlo method.